

**COMPARATIVE ANALYSIS OF MEDIUM VOLTAGE DC AND AC NETWORK
INFRASTRUCTURE MODELS**

by

Matthew J Korytowski

Bachelor of Science in Electrical Engineering, University of Pittsburgh, 2009

Submitted to the Graduate Faculty of
Swanson School of Engineering in partial fulfillment
of the requirements for the degree of
Master of Science

University of Pittsburgh

2011

UNIVERSITY OF PITTSBURGH
SWANSON SCHOOL OF ENGINEERING

This thesis was presented

by

Matthew J Korytowski

It was defended on

April 1, 2011

and approved by

George Kusic, PhD, Associate Professor, Electrical and Computer Engineering Department

Zhi-Hong Mao, PhD, Assistant Professor, Electrical and Computer Engineering Department

William Stanchina, PhD, ECE Chairman and Professor, Electrical and Computer Engineering
Department

Thesis Advisor: Gregory F Reed, PhD, Associate Professor, Electrical and Computer
Engineering Department

Copyright © by Matthew J Korytowski

2011

COMPARATIVE ANALYSIS OF MEDIUM VOLTAGE DC AND AC NETWORK INFRASTRUCTURE MODELS

Matthew J Korytowski, M.S.

University of Pittsburgh, 2011

An increasing amount of consumer devices and end-use applications of electricity at the low voltage level that require a direct current (DC) power source have continued to advance in modern day society. At the same time the existing alternating current (AC) infrastructure that has served so well over the past century is beginning to show its age and vulnerability, leading to increased outages and reduced reliability. Also, the amount of high voltage direct current (HVDC) transmission system installations continue to increase around the world because of their proven superiority to high voltage alternating current (HVAC) in certain scenarios. However, with the widespread development and maturation in recent years of low voltage DC devices and systems, as well as large scale HVDC systems, no DC-based infrastructure or delivery system exists to efficiently connect the two together. Such an infrastructure would be developed through a medium voltage DC (MVDC) architecture. In order to properly analyze the benefits of a MVDC infrastructure for power distribution networks, a comparison between MVDC and MVAC architectures is necessary to identify advantages and disadvantages of both approaches. Investigating an architecture that would supply DC power to loads that is not much different in function to the existing AC grid system used today may bring with it increased efficiencies, therefore leading to economic operational and reliability benefits. To the author's knowledge, this thesis provides the first system scale comparative analysis of this nature comparing MVAC

and MVDC. The preliminary design for such a system to supply DC power was created in this thesis using the PSCAD software package. The system analyzed utilizes a medium voltage DC bus rated at 20kV with a set of interconnected loads and generation. The DC system, while complicated with its wide array of power electronic converters, grants the ability to control power flow into the system from the different generation sources and to the loads. While the infrastructure design created is an initial step for a larger system, it lays the foundation for the future development of a DC distribution system for real world applications.

TABLE OF CONTENTS

ACKNOWLEDGMENTS	XVI
1.0 INTRODUCTION.....	1
1.1 APPLICATIONS FOR DC DISTRIBUTION	3
1.2 THE MVDC AND MVAC SYSTEMS THAT WERE COMPARED	6
1.2.1 MVAC System.....	6
1.2.2 MVDC System.....	8
1.2.3 Process and Basis for Comparison.....	9
2.0 THEORY FOR CONVERTERS AND GENERATION SOURCES	10
2.1 AC/DC RECTIFIER	10
2.2 DC/DC CONVERTER	14
2.3 DC/AC INVERTER.....	17
2.4 WIND GENERATION SOURCE.....	22
2.5 PHOTOVOLTAIC GENERATION SOURCE	25
3.0 MODELS OF MVAC AND MVDC INFRASTRUCTURES IN PSCAD.....	33
3.1 POWER ELECTRONIC CONVERTERS MODELED IN PSCAD	34
3.1.1 Five-Level and Three-Level Diode Clamped Multilevel Inverter.....	34
3.1.2 Six-Pulse Diode Rectifier.....	43
3.1.3 Dual Active Bridge Converter (DC Transformer)	45

3.1.3.1	Buck Orientation.....	45
3.1.3.2	Boost Orientation	48
3.2	PSCAD IMPLEMENTATION OF GENERATION SOURCES	50
3.2.1	Utility	50
3.2.2	Wind Turbine.....	51
3.2.3	Photovoltaic Array	57
3.3	MVDC INFRASTRUCTURE REALIZED IN PSCAD.....	62
3.4	MVAC INFRASTRUCTURE REALIZED IN PSCAD.....	66
4.0	COMPARATIVE RESULTS OF THE SYSTEMS IN PSCAD	71
4.1	MVDC SYSTEM AT STEADY-STATE	72
4.2	MVAC SYSTEM AT STEADY-STATE	80
4.3	COMPARISON OF SYSTEMS DURING FAULTS	88
4.3.1	Loss of Generation.....	89
4.3.1.1	PV Array – MVDC System	89
4.3.1.2	PV Array – MVAC System	91
4.3.1.3	Wind Fault – MVDC System	93
4.3.1.4	Wind Fault – MVAC System	94
4.3.1.5	Utility Fault – MVDC System.....	97
4.3.1.6	Utility Fault – MVAC System.....	99
4.3.2	Load Faults.....	101
4.3.2.1	AC Load Fault – MVDC System	102
4.3.2.2	AC Load Fault – MVAC System	103
4.3.2.3	Storage Load Fault – MVDC System.....	105

4.3.2.4	Storage Load Fault – MVAC System	107
5.0	CONCLUSIONS	109
6.0	FUTURE WORK	113
	APPENDIX A	115
	BIBLIOGRAPHY	117

LIST OF TABLES

Table 2-1. Switching Table for the DCMLI [8].....	19
Table 2-2. Parameters to generate curve shown in Figure 2.8.....	24
Table 2-3. Kyocera Solar KC125G module parameters	29
Table 3-1. Parameters for Induction Machine	52
Table 3-2. Parameters for Wind Turbine block	53
Table 3-3. Parameters for Wind Turbine Governor block.....	53
Table 3-4. Comparison of Estimated and Actual Values for Wind Turbine Output	56
Table 4-1. Generation Sources and Loads	71

LIST OF FIGURES

Figure 1.1. Conceptual design of a future MVDC infrastructure	2
Figure 1.2. One-line diagram of the MVAC System created	7
Figure 1.3. One-line diagram of the MVDC system created	9
Figure 2.1. Six-pulse Diode Rectifier [8].....	11
Figure 2.2. Output voltage of the diode rectifier [8].....	13
Figure 2.3. Common arrangement widely used for DC/DC converters	14
Figure 2.4. Dual Active Bridge DC/DC Converter (DC Transformer)	15
Figure 2.5. Five Level DCMLI (showing one of three total phases).....	17
Figure 2.6. SPWM with IPD.....	18
Figure 2.7. Balancer Circuit with IGBT switch.....	21
Figure 2.8. Theoretical wind turbine output for a range of beta values.....	24
Figure 2.9. Transfer function for wind governor block	25
Figure 2.10. Equivalent circuit model of a PV module	26
Figure 2.11. Key curve coordinates of the Sandia model [22]	28
Figure 2.12. Theoretical V-I curve using calculated Sandia model values of R_s and R_{sh}	29
Figure 2.13. V-I Curve for a solar module.....	30
Figure 2.14. Effect to V-I curve from placing modules in series	31

Figure 2.15. Effect to V-I curve from placing modules in parallel.....	32
Figure 2.16. Effect to V-I curve from placing modules in series and in parallel.....	32
Figure 3.1. DCMLI Inverter as created in PSCAD.....	35
Figure 3.2. Closer look at one leg of the MLI (Phase B).....	35
Figure 3.3. PSCAD node usage in DCMLI model	36
Figure 3.4. Control for DCMLI as seen in PSCAD.....	37
Figure 3.5. Carrier Signal PSCAD Dialog Box	38
Figure 3.6. One set (Phase A) of comparators	39
Figure 3.7. Control Sequence and resulting output voltage waveform.....	40
Figure 3.8. Outputs for line-to-neutral and line-to-line voltages of the DCMLI.....	40
Figure 3.9. Capacitor Balancing Circuitry for DCMLI	41
Figure 3.10. Control for Capacitor Balancing Circuits.....	41
Figure 3.11. Three-level DCMLI Realized in PSCAD.....	42
Figure 3.12. Control, Switching Signals, Output Voltages for Three-level DCMLI.....	42
Figure 3.13. Six-Pulse Diode Rectifier Realized in PSCAD	43
Figure 3.14. Input and output (bold line) waveforms of diode rectifier without filter	44
Figure 3.15. Input and output (bold line) waveforms of diode rectifier with tuned filter	44
Figure 3.16. DAB converter oriented in buck mode.....	46
Figure 3.17. Control Blocks for DAB converter in buck mode.....	46
Figure 3.18. Measurements for DAB Converter (buck mode)	47
Figure 3.19. DAB converter oriented in boost mode.....	48
Figure 3.20. Control Blocks for DAB converter in boost mode.....	48
Figure 3.21. Measurements for DAB Converter (boost mode)	49

Figure 3.22. Utility component realized in PSCAD	50
Figure 3.23. Wind Generation realized in PSCAD.....	51
Figure 3.24. Estimation of power output for specified parameters of the wind block	54
Figure 3.25. Estimation of torque output for specified parameters of the wind block	54
Figure 3.26. PSCAD plots of wind turbine component for torque, power, beta, and speed.....	55
Figure 3.27. Zoomed-in data of Figure 3.26 at steady-state	56
Figure 3.28. Photovoltaic equivalent circuit realized in PSCAD	57
Figure 3.29. Calculations of I_{sc} , V_{oc} , resistor values, and diode voltages in PSCAD circuit.....	58
Figure 3.30. V-I curve produced in PSCAD for a single array (x-axis is volts, y-axis is amps)..	58
Figure 3.31. Comparison of V-I curves generated with different methods ($N_s=1$, $N_p=1$)	59
Figure 3.32. PSCAD V-I curve for a 250kW PV array	60
Figure 3.33. Comparison of V-I curves generated with different methods ($N_s=35$, $N_p=58$)	60
Figure 3.34. PSCAD, 3MW PV array circuit layout	61
Figure 3.35. Final PSCAD layout of MVDC infrastructure	62
Figure 3.36. Closer look from the Utility block to the main bus	63
Figure 3.37. Closer look from the PV Array block to the main bus	64
Figure 3.38. Closer look from the Wind block to the main bus.....	65
Figure 3.39. Closer look at the main bus to the AC load.....	65
Figure 3.40. Closer look at the main to the simplified storage element	66
Figure 3.41. Final PSCAD layout of MVAC infrastructure	67
Figure 3.42. Closer look at Utility to the main bus.....	68
Figure 3.43. Closer look at PV Array to the main bus.....	68
Figure 3.44. Closer look at Wind to the main bus	69

Figure 3.45. Closer look from the main bus to the AC load.....	69
Figure 3.46. Closer look from the main bus to the simplified storage model.....	70
Figure 4.1. Voltage values on bus at steady-state.....	72
Figure 4.2. Zoomed-in version of steady-state voltage on the bus.....	72
Figure 4.3. Real power flow for each section of the system.....	73
Figure 4.4. Total power generated and consumed at steady-state.....	74
Figure 4.5. Closer look at steady-state duration in Figure 4.4.....	74
Figure 4.6. Measurement of power for the AC load from the bus to the load itself.....	75
Figure 4.7. Total power flow from the main bus to the storage load.....	76
Figure 4.8. Voltage and current present at the storage load.....	76
Figure 4.9. Power flow from utility to the DC bus.....	77
Figure 4.10. Close up of Figure 4.9 from 0.6s to 1.0s.....	77
Figure 4.11. Power produced and delivered to the bus.....	78
Figure 4.12. Power from wind delivered to the main DC bus.....	79
Figure 4.13. Closer look at steady-state portion of Figure 4.12.....	79
Figure 4.14. Voltage on the AC bus during steady-state.....	80
Figure 4.15. Closer look at the peaks appearing in Figure 4.14.....	81
Figure 4.16. Power being supplied and consumed by the generation and loads individually.....	82
Figure 4.17. Total generation and load consumption for the system.....	82
Figure 4.18. Power flow from the bus to the AC load.....	83
Figure 4.19. Closer look at Figure 4.18 to emphasize small losses of transformer.....	83
Figure 4.20. Power flow from the main bus to the storage load.....	84
Figure 4.21. Voltage and current values appearing at the storage load.....	84

Figure 4.22. Closer look at the ripple present on the curves in Figure 4.21	85
Figure 4.23. Power flow from the utility to the bus.....	85
Figure 4.24. Power flow from the PV array to the bus.....	86
Figure 4.25. Power from wind source to the AC bus.....	87
Figure 4.26. Components used to apply single and three-phase faults.....	89
Figure 4.27. DC bus voltage during PV fault (MVDC).....	90
Figure 4.28. Power flow for PV array during PV fault (MVDC).....	90
Figure 4.29. Power flow of the whole system during PV fault (MVDC).....	90
Figure 4.30. Power flow for loads and sources during PV fault (MVDC).....	91
Figure 4.31. Voltage of the AC bus during PV fault (MVAC).....	91
Figure 4.32. Power flow of PV array during PV fault (MVAC)	92
Figure 4.33. Total generation and load consumption during PV fault (MVAC).....	92
Figure 4.34. Power flow of each element during the PV fault (MVAC).....	92
Figure 4.35. DC bus voltage during wind fault (MVDC).....	93
Figure 4.36. Power flow of wind source during wind fault (MVDC)	93
Figure 4.37. Total generation and load consumption during the wind fault (MVDC)	94
Figure 4.38. Individual power flows during wind fault (MVDC)	94
Figure 4.39. AC bus voltage during wind fault (MVAC).....	95
Figure 4.40. Power flow of the wind generation during wind fault (MVAC).....	95
Figure 4.41. Electrical torque of the wind induction machine during wind fault (MVAC)	96
Figure 4.42. Total generation and power consumption during wind fault (MVAC).....	96
Figure 4.43. Individual power flows during wind fault (MVAC)	96
Figure 4.44. DC bus voltage and current during utility fault (MVDC).....	97

Figure 4.45. Utility power flow during utility power fault (MVDC)	98
Figure 4.46. Wind power flow during utility fault (MVDC).....	98
Figure 4.47. Total generation and power consumption during utility fault (MVDC)	98
Figure 4.48. Individual power flows for the system during utility fault (MVDC).....	99
Figure 4.49. AC bus voltage during utility fault (MVAC)	100
Figure 4.50. Total power generated and consumed during utility fault (MVAC)	100
Figure 4.51. Individual power flows during utility fault (MVAC).....	101
Figure 4.52. Bus voltage during the AC load fault (MVDC)	102
Figure 4.53. Individual power flows during AC load fault (MVDC).....	103
Figure 4.54. Total power generation and consumption during AC load fault (MVDC)	103
Figure 4.55. Voltage on the bus during the AC load fault (MVAC)	104
Figure 4.56. Individual power flows during the AC load fault (MVAC).....	104
Figure 4.57. Total power generation and consumption during AC load fault (MVAC)	105
Figure 4.58. Voltage on the bus during the storage load fault (MVDC)	105
Figure 4.59. Individual power flows during storage load fault (MVDC).....	106
Figure 4.60. Total power generated and consumed during storage load fault (MVDC)	106
Figure 4.61. Voltage on the bus during storage load fault (MVAC)	107
Figure 4.62. Individual power flows during storage load fault (MVAC).....	108
Figure 4.63. Total power generated and consumed during storage load fault (MVAC)	108

ACKNOWLEDGMENTS

I would first and foremost like to thank my mother and father for their unending support through all of my years of university studies. They have always contributed what they could at all times and I cannot thank them both enough for that. I am also extending thanks to my brother and two sisters for making me feel welcomed home when I came to visit during holidays. It made any visits to my hometown that much better, enjoyable, and relaxing.

My adviser, Dr. Gregory Reed, has been of the utmost help with keeping deadlines, fleshing out ideas and concepts, as well as providing the motivation and passion towards the ideas investigated in this thesis. I am grateful to those on the defense committee and Dr. Joseph Hibey for providing suggestions to improve this document. I would also like to thank Manitoba HVDC Research Centre and Sandia National Laboratories for sharing documents concerning their wind and solar model development, respectively.

Special thanks for work on this thesis to my friends whom I see on a daily basis for listening to my ideas and providing critical feedback on the theory and concepts utilized throughout this document. Those individuals were Emmanuel, Bob, Brandon, Hussain, Raghav, Ray, Mircea, and Ang. Lastly, I additionally thank my friend Dan and others previously mentioned for taking the time to listen to my presentation prior to its official delivery and providing helpful suggestions and criticism.

1.0 INTRODUCTION

When electricity started to become an even more prominent commodity much later after being discovered, the preference for alternating current (AC) for distribution was chosen primarily based on its superiority to transport power over large distances much more efficiently than its direct current (DC) counterpart. The AC system has been the standard for transmission and distribution of electricity since the late 19th century and continues to be today. One goal of this thesis is to investigate whether DC has a place in distribution for certain applications where it may prove to be of benefit from an efficiency standpoint and therefore an economic standpoint [1]. There is a realization of this notion already in the form of taking advantage of the unique capabilities of High Voltage Direct Current (HVDC) transmission lines but little in the form of a medium voltage direct current system outside of shipboard applications [2].

With the advent of switching technologies like thyristors and the more recent insulated gate bipolar transistor (IGBT), the ability to alter DC voltage levels has become a much more efficient process. The approach today is to always change from AC to DC for use, and this conversion, as will be discussed, is not as efficient as going from DC to DC. A shift toward having a supply of DC for specific loads could alleviate demand from the grid and result in better performance and increased efficiencies across the board. There are many applications that would see a benefit in implementing DC as a main feed of power that will be discussed.

The model developed in this thesis is an initial step toward determining whether DC is a viable approach for certain applications or if it still needs some time for other technologies to arise or mature. A first step toward determining the feasibility of a DC distribution infrastructure would be to make a comparison against the same equivalent infrastructure using AC. This first step is what this thesis sets out to accomplish. The ultimate goal would be to have a system similar to the one shown in Figure 1.1. The final system would have full integration of renewable generation with other forms of generation like fuel cells and energy storage with loads such as variable frequency drives, data centers, and industrial facilities.

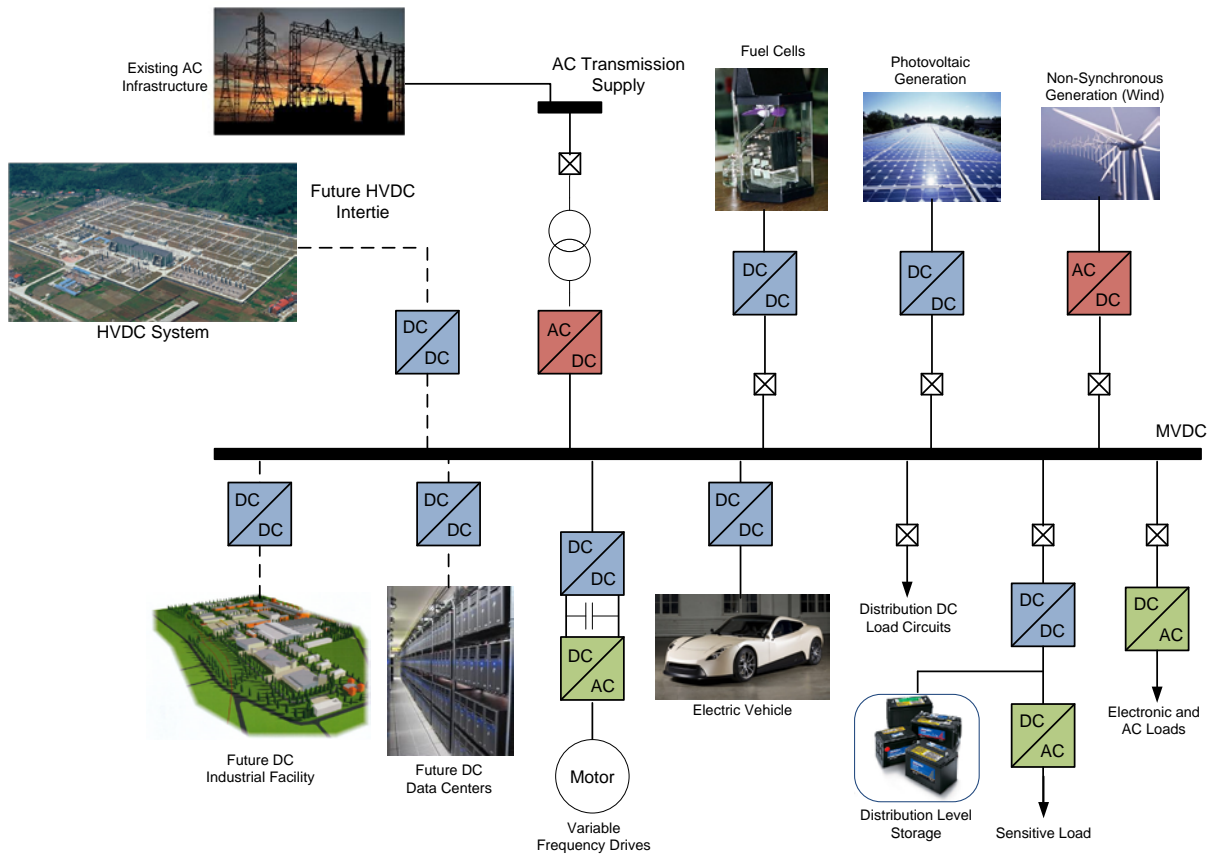


Figure 1.1. Conceptual design of a future MVDC infrastructure

A key component to the successful operation of a DC distribution system is the use of power electronic converters for transformation between electricity types. These converters

appear in flavors of AC/DC rectifiers, DC/AC inverters, and DC/DC converters. All three types appear in the Medium Voltage DC (MVDC) system that was constructed. The future development of power electronic devices will bring with it greater efficiencies, less losses, and therefore a better overall system in terms of DC conversions.

1.1 APPLICATIONS FOR DC DISTRIBUTION

There is an array of benefits for utilizing a DC supply for certain applications over the traditional AC supply. The result is often increased efficiency and a less complicated system. This would lead further to less maintenance, lower operating costs, and increased longevity of the system [1]. With the demand to construct more and more renewable forms of generation, direct usage of DC would be beneficial. For wind turbines, it still makes sense to continue using the traditional approach of an AC interconnect to the grid but for photovoltaic and solar generation, which produces its power in DC at the source, a tie using a DC infrastructure would possibly be superior. With the expanding production and development of hybrid vehicles that use batteries for power and for that matter, storage technologies in general, a connection with DC would sidestep the need for conversion from DC to AC and even possibly back again to DC depending on the end use of the power. An option in the future for consumers to have some independence from the main grid connection by use of energy storage technologies would provide further support towards a form of DC distribution on a smaller scale because a wide range of consumer electronic loads require a DC power source.

An already abundant use of DC on the grid is present in the form of HVDC transmission lines. With the dawn of switching devices for efficient conversion from AC to DC and back

again to AC, HVDC has proven to be a better option in applications where a long transmission distance is called for. There are a few main economic considerations for using an HVDC line versus an AC line. Depending upon the distance of an overhead transmission line, a breakeven point exists for HVDC where it becomes cheaper per unit of length. The HVDC terminal points also have less environmental impact because it has a smaller footprint and the electric and magnetic fields generated cause less disruption. When considering underground and submarine cables, the breakeven point is much less due to less lines being necessary to transmit DC. Attempts at constructing new transmission lines to feed areas with an increase in power demand often results in “not in my backyard” complaints from the public resulting in delays and possible rejection of overhead power lines. Underground high power delivery would be an attractive option because the power demand could be handled while eliminating the unsightly placement of poles for power lines. Systems that may be operating at different frequencies (i.e., 60Hz and 50Hz) cannot be connected together because of this asynchronous mismatch. Since the conversion to DC is independent of frequency, a HVDC interconnection would allow these two different frequency systems to share power between them and therefore assist with stability and power balancing. While a lot of advantages for HVDC are based upon its application, others such as tying two asynchronous systems together cannot be achieved as easily using only AC. The MVDC architecture also possesses advantages in certain applications, which will be discussed next [3].

Naturally, equipment that uses DC power for operation would be the most viable option for integration into a system that supplies DC power to begin with. These forms of equipment would include switched mode power supplies (SMPS), water heating units, LED lighting, adjustable speed motor drives, and uninterruptable power supplies (UPS) [1]. By supplying

directly from a DC source, the conversion step necessary to change AC into DC would be avoided leading to efficiency gains. A DC to DC conversion would still be necessary but this form of conversion is greater than 95% efficient in optimum conditions [4].

For SMPS, typical external converters like those used for laptop computers range between 30% and 40% efficient and internal converters are 65% to 70% efficient. In 2004, it was found that electricity flowing through power supplies accounted for about 6% of national electric usage. An improvement in the power supplies used in electronic equipment would net significant gain in energy savings. It is also possible in some cases to supply DC power directly to existing AC-DC power supplies and have it function properly [5]. With this in mind, to utilize a DC source, new power supply designs would not have to be immediately manufactured but could be integrated at a slower pace. A prime market for this form of DC integration would be in data centers since they have such a large load that is computer-centric and must have DC to operate.

Any device utilizing a passive heating element in the form of a resistor may be operated using DC since the only requirement is to actually generate heat losses. Issues lie in protection schemes that would require the ability to interrupt DC power flow, which proves to be more difficult than AC since there is no zero crossing in DC. A UPS already has the capability to run on DC power since internally a DC bus exists for the battery storage within the device. Currently, an inverter is used to convert the AC from an electric outlet to feed into the UPS. This inverter stage can simply be removed and, depending on voltage levels, replaced with a direct connection to a DC source if a DC/DC conversion is not required.

In industry application, approximately two-thirds of total power used comes from motors. Unfortunately, motors require the unique properties of AC power to achieve flux and magnetic

fields resulting in rotation of the motor shaft. This is where variable frequency drives (VFDs) come into play. The VFD is fed with an AC input that is first converted to DC. This DC is then controlled by means of IGBT switches in order to create a varying frequency and voltage in AC once more. This variable frequency and voltage grants control of motor speed so that more options are available besides being completely on or off [6]. The initial feed of AC into the VFD can simply be replaced with a DC input, again avoiding a conversion stage from AC to DC and thus leading to increased efficiency [1].

With an adoption of supplying the discussed devices and equipment with DC instead of AC, a range of benefits is available for energy savings leading ultimately to economic savings. An about-face change to DC from AC is absolutely not necessary, but a slow, steady change for certain applications would carve out a path for the future and the benefits will eventually be abundant and the technology easier to integrate.

1.2 THE MVDC AND MVAC SYSTEMS THAT WERE COMPARED

A brief overview of the MVAC and MVDC systems will be discussed to establish how the systems look and operate and the reason for choosing the different loads and generation sources. The systems will be presented in the form of one-line diagrams for ease of visualization.

1.2.1 MVAC System

A one-line diagram of the MVAC system may be seen in Figure 1.2. The bus in the center was chosen to be 20kV. Three forms of generation were chosen, which appear on the left side of the

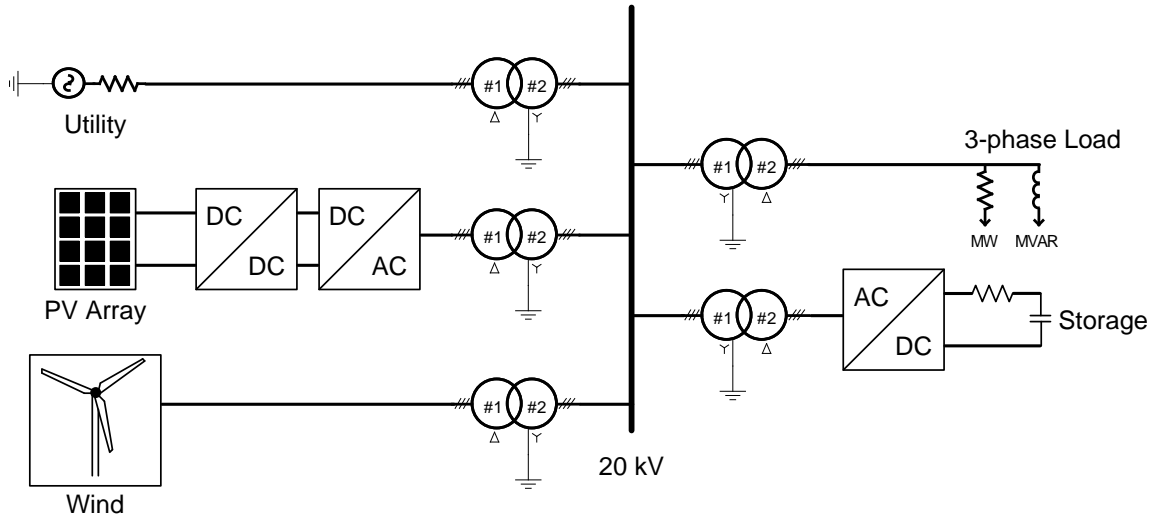


Figure 1.2. One-line diagram of the MVAC System created

one-line. Two sources are renewables in the form of a PV array and a wind turbine. The PV array was rated to have a maximum output of 3MW. The wind turbine was set to deliver 2.135MW during normal operation. The last generation source, the utility, provides the remaining power that is not supplied from the renewable sources. Also, in the simulation, a fourth generation source exists inside of the wind block that is essentially another grid or utility connection. It has the capability of supplying any power necessary for the system. This exists in the wind block because the induction machine connected to the turbine requires an external connection to maintain its voltage output and be supplied with reactive power. All of the generation sources will be discussed in more detail later.

Two types of loads were chosen for simulation with one being AC and the other being DC. The AC load was rated at 10MW with a power factor of 0.9 resulting in a reactive component of 4.8432Mvar. The AC load was modeled as a resistive and inductive, passive, three-phase load with a voltage of 4kV. The DC load was created to simulate what will later be replaced by a more complex model for battery storage. For all intents and purposes, it will simply be referred to as a storage load from here forward. By having the two forms of loads

being AC and DC, different converters were necessary to connect them in either system. This allowed for investigation as to how the loads were affected by changes in the system.

The approach taken for the conversion processes was simply to get the voltages in the right type of current, DC or AC, and at the correct voltage level. The entire system was open loop with no feedback to make adjustments in the converters themselves. The assumption was that the voltages for the inputs and outputs were known and the control was created for the converter to accommodate them. There were three main converters implemented, which included a DC/DC dual active bridge (DAB) converter, DC/AC diode clamped multilevel inverter (DCMLI), and AC/DC six-pulse diode rectifier. The DAB was chosen based on its high power rating and bi-directional capability. The DCMLI was chosen also for its high power rating, redundant switching scheme, and use in industry. In this initial development of the system model, the diode rectifier was chosen because of its passive nature requiring no control scheme to function properly. Lastly, the transformer orientations were chosen to be delta-wye for the generation sources [7] and a wye-delta configuration for both loads.

1.2.2 MVDC System

The MVDC infrastructure was made to be as similar as possible to the MVAC infrastructure but utilizing DC instead of AC on the common bus. All of the generation discussed for the MVAC system was exactly the same as in the MVDC system. The only difference between the two systems was the conversion schemes necessary for the bus to be 20kV DC instead of 20kV AC. A DCMLI was needed for conversion from DC to AC for one of the loads while for the storage load a DAB in a bucking configuration was used. The PV array was also connected using a

DAB converter but in this case it is in a boosting configuration because the PV output voltage is lower. A one-line diagram of the system is shown in Figure 1.3.

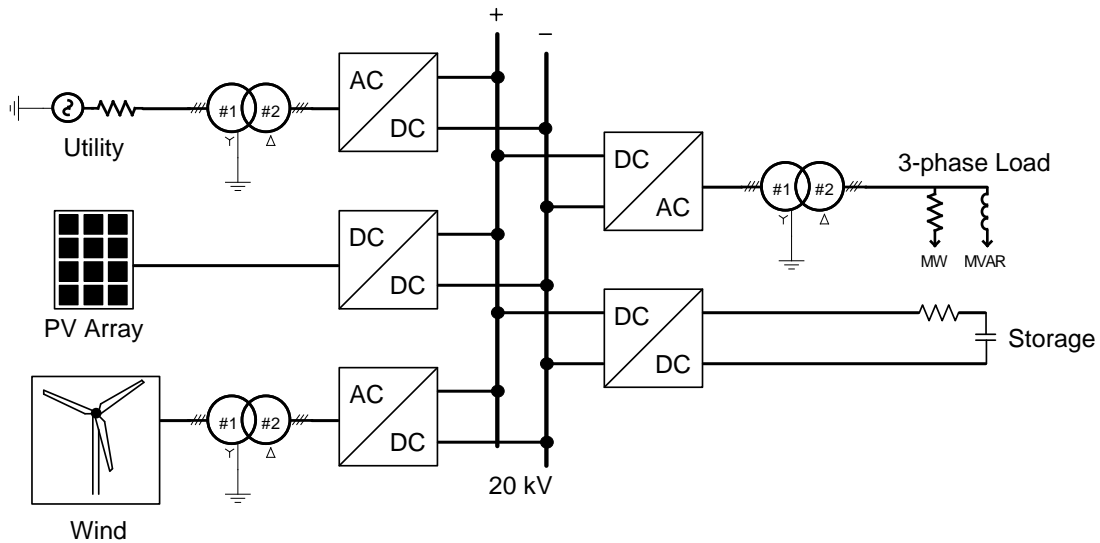


Figure 1.3. One-line diagram of the MVDC system created

1.2.3 Process and Basis for Comparison

Because of the lack of complexity and feedback control with the initial development of both system models, two forms of tests were carried on the completed systems that seemed relevant. The first test of faults was to remove one generation source and observe how the others reacted to compensate for power flow to the loads. The other was to apply a fault to ground directly before each load. The AC load received a line-to-ground, single-phase fault on phase A and the storage load received a fault tying the positive terminal of the DC output to the negative terminal therefore shorting them. The power flows for the entire system and also each individual branch were measured and also the voltage on the main bus was monitored in each case.

2.0 THEORY FOR CONVERTERS AND GENERATION SOURCES

As discussed in earlier sections, there are three different types of converters being utilized in the system. There is a converter for almost every combination of AC and DC. That is, AC/DC, DC/DC, and DC/AC. The only conversion that does not require a power electronics converter is going from one level of AC to another. This is handled by a transformer and hence requires no power electronic switches. This section will outline the theory and operation characteristics of the three different converters.

2.1 AC/DC RECTIFIER

The AC/DC rectifier chosen for the models in PSCAD was a six-pulse diode rectifier (DR). The six-pulse structure is extended by means of transformer phase shifts to topologies that reach 24-pulses. The six-pulse structure was chosen for its simplicity to avoid complications with control and analysis.

The six-pulse diode rectifier has a topology layout as seen in Figure 2.1. The entire structure is comprised of the main AC inputs, six diodes for the rectification stage, and finally a LC filter to smooth out the output DC waveform. All diodes are assumed to be ideal for analysis and have no losses or voltage drops from conduction.

The voltages at the utility source on the left side of the circuit diagram are

$$V_{an} = V_{rms} \cos(\omega t)$$

$$V_{bn} = V_{rms} \cos(\omega t - 120^\circ)$$

$$V_{cn} = V_{rms} \cos(\omega t + 120^\circ)$$

Based on the operation of the circuit, line-to-line voltages will be necessary and are

$$V_{ab} = V_{an} - V_{bn} = \sqrt{3} V_{rms} \cos(\omega t + 30^\circ)$$

$$V_{bc} = V_{bn} - V_{cn} = \sqrt{3} V_{rms} \cos(\omega t - 90^\circ)$$

$$V_{ca} = V_{cn} - V_{an} = \sqrt{3} V_{rms} \cos(\omega t + 150^\circ)$$

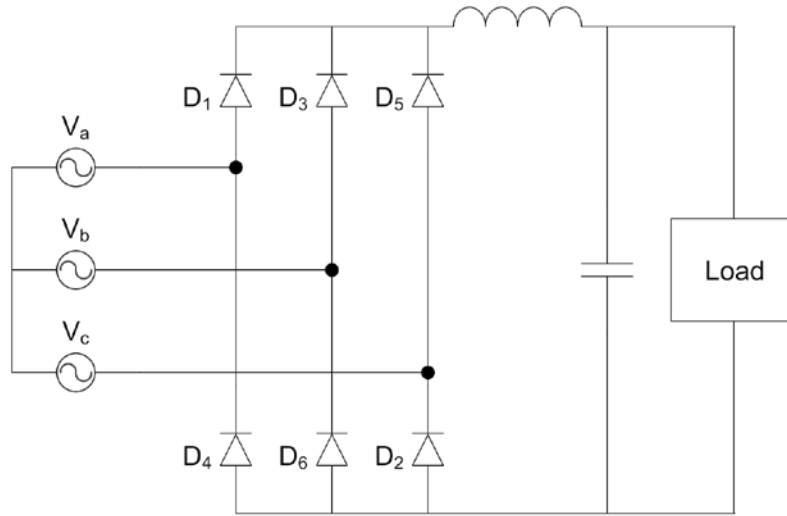


Figure 2.1. Six-pulse Diode Rectifier [8]

The diodes conduct in such a way that when one of the three phase voltages is greater in magnitude than the others, the corresponding diode will then conduct. Figure 2.2 shows the input voltages (line-to-ground), followed by their equivalent line-to-line values, and finally how the rectified signal corresponds to the line-to-line voltages resulting in the pulse-like nature.

Assuming the system is already operating at steady state, Diode 6 would already be conducting at point 0° . At 30° V_a is greater than V_b and V_c , thus Diode 1 will conduct. Diodes 3 and 5 do not conduct since the potential is greater at the cathode than at the anode. With Diodes 6 and 1

conducting, this results in the line-to-line voltage V_{ab} appearing at the load starting at 30° . Diode 1 will continue to conduct so long as V_a is greater than the other two voltages. This applies also to Diode 6 but it must remain the most negative in value rather than positive. At the point of 30° once more, V_a is still the most positive voltage but V_b is surpassed as the greatest negative voltage by V_c . Now Diode 6 is reverse bias and no longer is conducting. Diode 2 is now conducting and applies the voltage of V_c to the load's negative terminal. The line-to-line voltage of V_{ac} is now present across the load. The operation explained has covered the space between 0° to 120° .

Let us now take a look at what occurs from 120° to 240° . At the point 120° , V_b becomes the most positive voltage and V_c remains the most negative. Diode 1 no longer conducts, Diode 2 continues to conduct, and Diode 3 begins conducting. The line-to-line voltage is now V_{bc} . At 180° , V_b remains the most positive and V_a becomes the most negative. Diode 2 no longer conducts, Diode 3 continues to conduct, and Diode 4 begins conducting. The voltage at the load is therefore V_{ba} .

To complete one period, let us examine what occurs between 240° and 360° . At the point 240° , V_c becomes the most positive voltage and V_a remains the most negative. This translates to Diode 3 no longer conducting whereas Diodes 4 and 5 do. V_{ca} appears at the load. At 300° , V_c stays the most positive and V_b is the most negative. Diode 4 ceases to conduct and Diodes 5 and 6 do conduct. At the load, a voltage of V_{cb} is present. This concludes one period of operation and the process will begin again and continue at 30° in the next period.

Looking at the middle graph in Figure 2.2, six "pulses" of voltage can be seen to create the rectification of the AC sources into a DC output. The final DC output in terms of voltage will result in a value of $1.35V_{LL}$ (rms) [8][9].

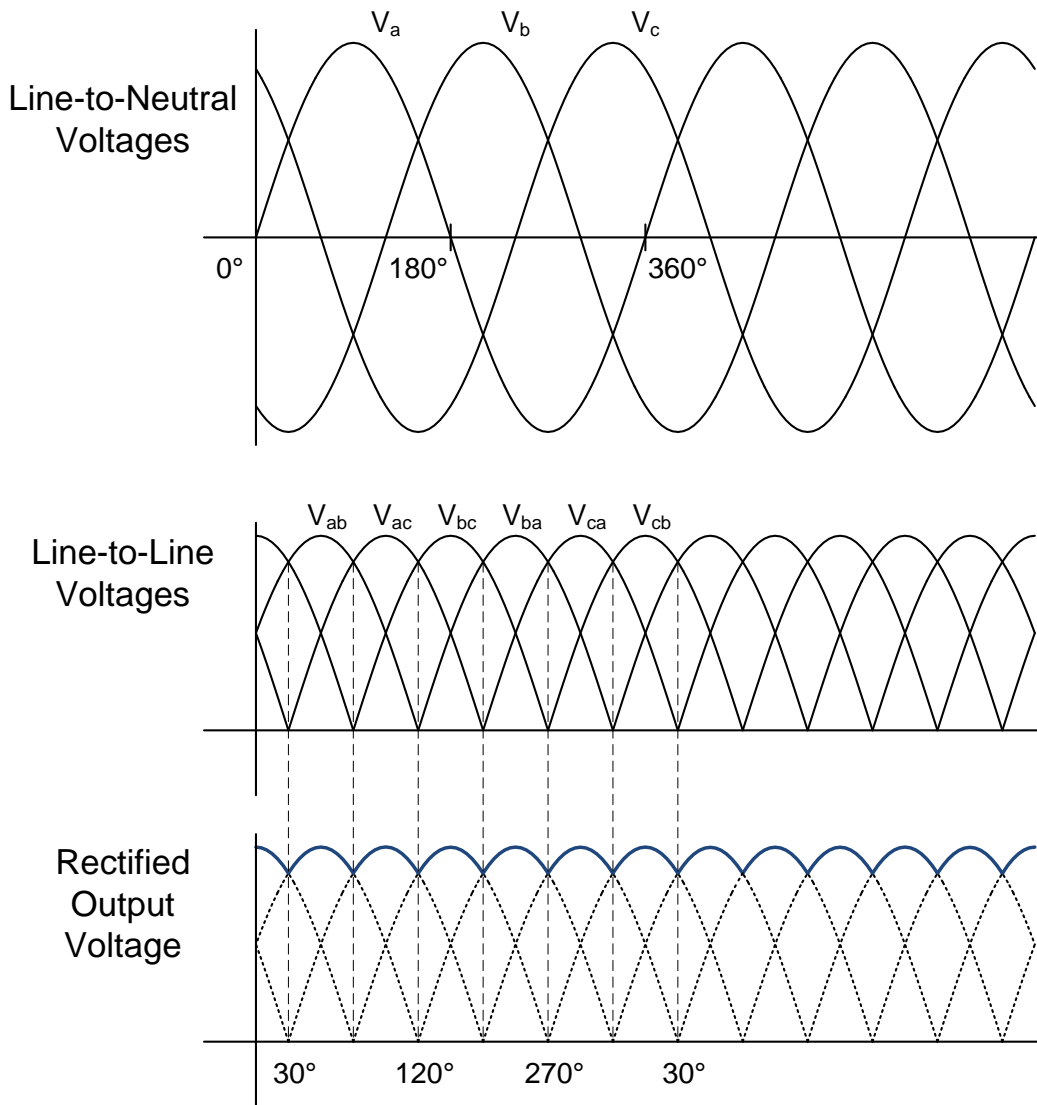


Figure 2.2. Output voltage of the diode rectifier [8]

Between the two diodes connected to each phase of the utility source, only one is ever conducting at one time. This means that any current being provided by one phase will have it through the load by another. As depicted in Figure 2.2 between the interval of 30° and 150° , when V_a is the most positive voltage of the three phases, it provides the positive current flowing through the load whereas whatever voltage source is the most negative will be providing the negative, return current. From the perspective of the load, it sees a steady, positive ripple of

current identical in shape to the output voltage with a magnitude determined by the Ohm's Law relationship.

2.2 DC/DC CONVERTER

In a DC-centric system a converter for changing between two DC voltage levels is an absolute requirement. The DC/DC converter is the equivalent to a transformer in an AC system to change AC voltage levels. Coincidentally, the concept behind the DC/DC converter used in the system model for this thesis centers on taking advantage of the inherent voltage altering abilities of the transformer for AC signals and applying it to the DC realm. Before investigating this, let us look at the most common types of DC/DC converters and how they are unfortunately not suitable for high power applications.

The three configurations used most widely for DC/DC conversion are the boost, buck, and buck-boost topologies. Each involves taking advantage of the characteristics of an inductor. These configurations utilize the charging and storing of energy in the inductor in order to transfer and alter voltage values depending on the duration it is exposed to current flow. The three different circuits can be seen in Figure 2.3. Since all three are based around similar principles, let us only analyze the buck converter.

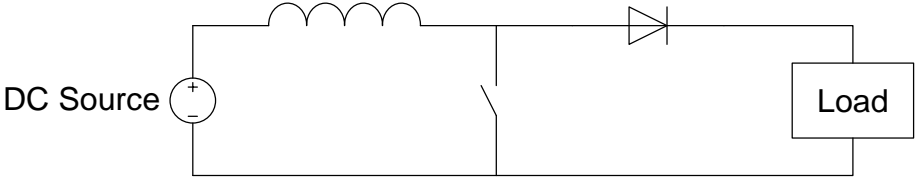


Figure 2.3. Common arrangement widely used for DC/DC converters

Each circuit has two states, one for when the switch is open and the other for when it is closed. For the buck configuration, when the switch is closed there is a voltage drop across the inductor and the output voltage is

$$V_o = V_i - V_L$$

The inductor is storing energy from the source and thus the current begins to rise. In the open state, the inductor voltage is the negative of the output voltage and is dissipating its stored energy from the previous state and the current through it begins to decrease [10].

The voltage gain of this type of circuit is limited and therefore not a viable option in high gain or high power environments. The operation of the circuit is dependent on the ratings of the switch, diode, and inductor used. These components would have to be rated at a high power with large currents and voltages. This approach, while it may be possible if many switches were placed in parallel and series to split the voltage and current to each individual switch, and the same approach goes for the other components, is not realistic, therefore a different type of topology is used for the high power application necessary in this thesis.

The dual active bridge or DC transformer seen in Figure 2.4 was the topology chosen to accomplish this task of providing a high power DC/DC converter. The circuit works by

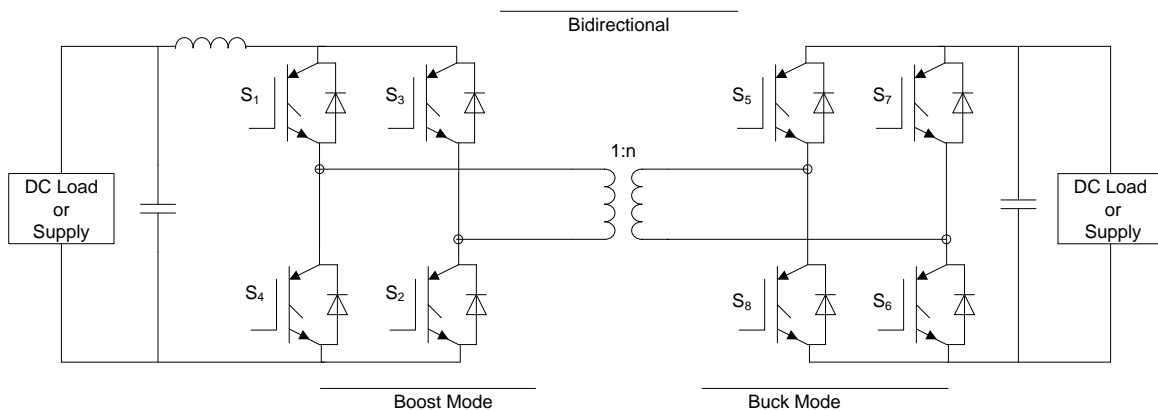


Figure 2.4. Dual Active Bridge DC/DC Converter (DC Transformer)

alternately switching the polarity of the DC voltage applied to the transformer. This is accomplished by switches at the input and output of the transformer. The switching scheme is such that switches S_1 and S_2 connect at the same time as do switches S_3 and S_4 . By varying the duty cycle of either switching pair, the constant DC input is made to look more AC in nature, more specifically similar to a square wave, so that the transformer sees an alternating current through it. Another way of describing this process is to say that the switches are “chopping” the DC input so that the transformer is able to see a positive and negative current flowing through it and therefore able to function as a transformer normally would. The output is then rectified by the freewheeling diodes in parallel with the output switches on the other side of the transformer. No switching action is needed on the output side of the transformer [11][12].

If the DC transformer is utilized only to provide power in one direction, the switches on the output of the circuitry are unnecessary and can be substituted with diodes. This would be useful in a situation such as with photovoltaic generation. The panels are generating power to be supplied to the system and require no input power from the electrical grid. A situation that would be ideal for a bi-directional DC transformer would be for electrical storage. The DC transformer would be in a “bucking mode” for charging and sending power to the storage device. For discharging, the DC transformer would transition to a “boosting mode” so the storage would therefore be feeding power back to the grid system. By developing a proper control scheme for the different operational states of the switches, sensors would detect whether the storage needs to be charged or discharged depending on its state and the control would fire the corresponding switches to operate in a buck mode or in a boost mode.

2.3 DC/AC INVERTER

Due to the large amount of power that is required through a distribution network system, a multilevel inverter was employed for conversion between DC to AC. Specifically, a five level, neutral-point diode clamped multi-level inverter (DCMLI) was used. This structure is shown in Figure 2.5. The NPC was chosen based on two main advantages it has over other inverters. The control system is very simple to implement and is a derivative method of sinusoidal pulse width modulation. The control scheme will be discussed in detail in this section. The other advantage is that with enough levels implemented, the harmonic content in the output is minimized and the need for a filter may not be required. The overall topology also involves diodes, which are relatively smaller in size compared to other structures that require larger components such as capacitors [13].

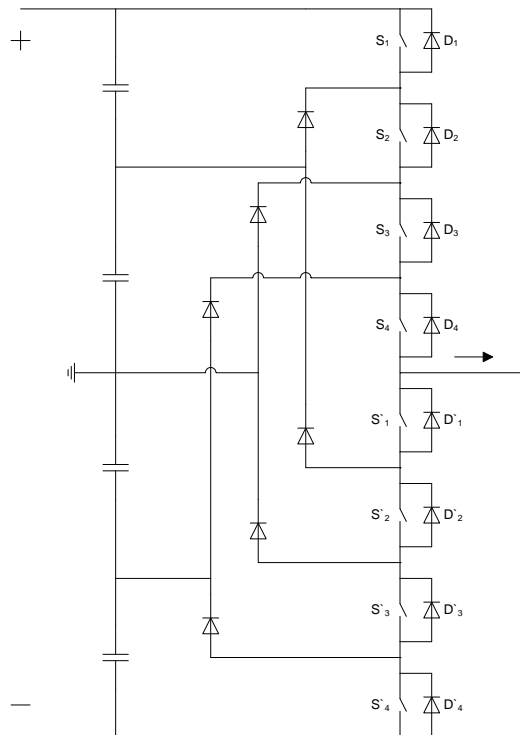


Figure 2.5. Five Level DCMLI (showing one of three total phases)

The control scheme utilized for the operation of the DCMLI was a carrier based pulse width modulation with an in-phase disposition scheme. This control method was chosen primarily on its ease of implementation as well as its output resulting in relatively low THD. The concept of sinusoidal pulse width modulation is pretty simple when stated in a straightforward manner. There are two signals present, a sinusoidal reference and a triangular carrier, and when one is greater than the other, a switch is turned on and when the same signal is less than the other the same switch is turned off. The switches are set up in pairs so when one is on, the other is off. Due to the DCMLI structure and it being a three-phase system, there are three reference signals that are required, separated from each other by 120° to emulate a three phase system. There are four sets of switches in the five-level topology and therefore four carrier signals, one to govern each set, are necessary. The carrier signals and reference signals can be seen in Figure 2.6.

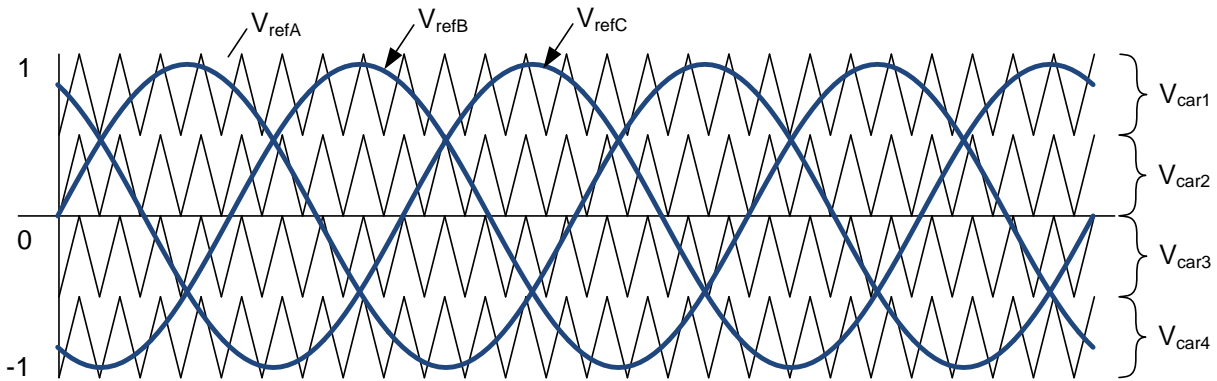


Figure 2.6. SPWM with IPD

The states shown in Table 2-1 depict what switch combinations correspond to what output voltages. It can be noted that adjacent rows in Table 2-1 only have one pair of switches changing states between them.

Table 2-1. Switching Table for the DCMLI [8]

S_1	S_2	S_3	S_4	S'_1	S'_2	S'_3	S'_4	$ V_a $
1	1	1	1	0	0	0	0	$2V_{cap}$
0	1	1	1	1	0	0	0	V_{cap}
0	0	1	1	1	1	0	0	0
0	0	0	1	1	1	1	0	$-V_{cap}$
0	0	0	0	1	1	1	1	$-2V_{cap}$

By altering the amplitude of the reference signal relative to the amplitude of the carrier signal, the voltage output magnitude of the inverter can be controlled to some degree. The magnitude of the reference signal is determined by an amplitude modulation ratio, m_a , while the frequency is set as the desired frequency of the output AC wave. The amplitude modulation ratio is defined as

$$m_a = \frac{V_{ref}}{V_{carrier}}$$

where V_{ref} is the peak amplitude of the reference signal and $V_{carrier}$ is the peak amplitude of the carrier signal.

If only one carrier existed, the peak amplitude would be kept at some constant value. In the case of a five-level DCMLI, there are four stacked carriers. Therefore this constant amplitude will be split into four. An offset is then placed on each carrier signal so they do not overlap. For example, if constant amplitude of 1.0 were chosen, each carrier would initially

oscillate between 0.25 and -0.25. A signal would then need an offset of 0.75 so it would be between 1.00 and 0.50 whereas another would need an offset of 0.50 placing it between 0.50 and 0.00. The remaining two signals would then have an offset of -0.75, and the other -0.50, placing one between -0.50 and -1.00, and the other between 0.00 and -0.50, respectively. This can be more easily seen in Figure 2.6. The frequency of each carrier is determined by a modulation frequency ratio, m_f , defined as

$$m_f = \frac{f_{carrier}}{f_{ref}}$$

where $f_{carrier}$ is the frequency of the carrier signal and f_{ref} is the frequency of the reference signal. By utilizing a high $f_{carrier}$, the harmonic content of the output can be pushed toward higher frequencies and be filtered out more easily due to the increased proximity to the fundamental. However, the losses in each switch increase proportionally with switching frequency. It is therefore best to choose an optimal frequency that yields a desirable output yet keeps losses to a minimum. As a basic rule, m_f is chosen as an odd integer because it results in automatically eliminating all even harmonics from the output signal [14].

One major drawback to the DCMLI is the tendency of the capacitor voltages to drift from their ideal value. For example, if an input of 20 kV was to be used, the voltage present on each individual capacitor is ideally 5 kV. The drifting is dependent on the load attached and therefore additional circuitry is desired in order to keep the voltages as balanced between the capacitors as possible. In the case of a five-level configuration, the top and bottom (C_1 and C_4) capacitors increase in voltage and the middle two (C_2 and C_3) decrease in voltage. The middle capacitors experience a voltage drop since they are discharging more often than the top and bottom capacitors. This then leads to a voltage increase across the top and bottom capacitors in order to keep a split balance of the voltage input. Based upon the operation of the DCMLI, the voltage

levels present at the output will reflect these skewed values that appear on each capacitor. The output will then appear less sinusoidal, have a higher harmonic content, and the conversion will have a lower efficiency. To compensate for this issue, a buck-boost balancer circuit is added to the set of capacitors. There are three components to the complete circuit, a switch, inductor, and diode. The components are situated in the layout in Figure 2.7. For the lower two capacitors, the same circuitry will be present.

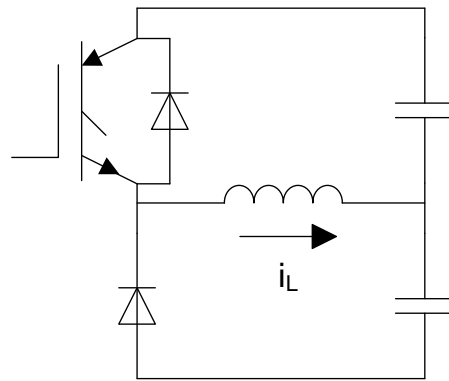


Figure 2.7. Balancer Circuit with IGBT switch

The concept behind the balancing is to transfer energy between the two capacitors by use of an inductor as a mediator. Assuming an imbalance occurs and C_1 has a larger voltage than C_2 , the switch S_1 will close and energy will then be exchanged between C_1 providing current to the inductor. Once C_1 reaches the desired voltage, the switch S_1 will then open to stop energy transfer between C_1 and the inductor. With the switch closed, a current loop is formed by the diode, inductor, and capacitor C_2 . This causes current to charge C_2 , increasing its voltage to the desired level. This see-sawing exchange of energy continues in order to keep the voltages close to a desired voltage point [15].

2.4 WIND GENERATION SOURCE

The wind generation source will be operating at steady-state and shall therefore not be analyzed in great detail. An existing PSCAD wind simulation was integrated into the main MVDC and MVAC systems rather than designing it from the ground up. The model itself will be outlined in a later section. Some of the theory of how each block functions and how the blocks interact between one another will be discussed in this section. All the components were derived from [16].

The model consists of four main components, with those being the induction machine acting as a generator, the wind turbine, a wind source, and a wind turbine governor. The induction utilized was a simple wound rotor configuration as the machine dynamics and efficiency were not of interest. The wind source output is generated from the sum of four wind components. The equation is defined as

$$V_W = V_{WB} + V_{WG} + V_{WR} + V_{WN}$$

where V_{WB} = base wind velocity V_{WR} = ramp wind component
 V_{WG} = gust wind component V_{WN} = noise wind component.

Each of these four components is governed by a set of parameters depending on the time with the exception of the base wind velocity, which is constant. The ramp is a linear increase from a starting point to a chosen final state. The gust is a two cycle sinusoid placed over the base wind velocity value with a chosen amplitude and period. Lastly, the noise places a random variance on the output. Further details regarding each component of the total wind output can be seen in [16].

The wind turbine itself is governed by a set of three equations from [16] and are

$$\gamma = \frac{V_W}{\omega_B}$$

$$C_p = \frac{1}{2}(\gamma - 0.022\beta^2 - 5.6)e^{-0.17\gamma}$$

$$P_W = \frac{1}{2} \cdot \rho \cdot A \cdot \omega_B \cdot C_p \cdot \gamma \cdot V_W^2$$

where V_W = wind velocity, mi/h C_p = power coefficient, (dimensionless)
 ω_B = blade angular velocity, mech rad/s ρ = air density, lb-f/ft³
 γ = tip speed ratio, (mi-h)/(rad/s) A = blade impact area, ft²
 β = blade pitch angle, degrees

These equations were adapted by employees at Manitoba HVDC Research Centre for use in the PSCAD wind turbine block [17] and are

$$\omega_H = \frac{\omega_M}{GR} \left(\frac{rad}{s} \right)$$

$$\gamma = \frac{V_W}{\omega_H} \left(\frac{m}{s} \right) \left(\frac{3600s}{1h} \right) \left(\frac{1mi}{1609.344m} \right) = \frac{2.237V_W}{\omega_H} \left(\frac{mi}{h} \right)$$

$$C_p = \frac{1}{2}(\gamma - 0.022\beta^2 - 5.6)e^{-0.17\gamma}$$

$$P_W = \frac{\frac{1}{2} \cdot \rho \cdot A \cdot \omega_B \cdot C_p \cdot V_W^3 \cdot G_{eff}}{1000000 \cdot G_{MVA}}$$

$$T = \frac{P \cdot \omega_{Mrat}}{\omega_M}$$

where ω_H = hub speed G_{eff} = gear box efficiency
 ω_M = machine mechanical speed in rad/s G_{MVA} = Machine rated MVA
 GR = gear ratio ω_{Mrat} = Rated mech speed of machine.

Utilizing a custom MATLAB script, the equations above were implemented with the necessary parameters, and the torque and power curves were generated for a range of different beta values ranging from the topmost curve with a $\beta = 2$ to the bottom curve with a $\beta = 20$. An example of such curves may be seen in Figure 2.8. The parameters used for these particular curves are shown in Table 2-2. The mechanical speed was varied from 0 to 200 rad/s.

Table 2-2. Parameters to generate curve shown in Figure 2.8

$V_w = 15 \text{ m/s}$	$\omega_{\text{rat}} = 376.99/3 = 126.667 \text{ rad/s}$
$GR = 55$	$A = 7854 \text{ m}^2$
$R = 50 \text{ m}$	$G_{\text{eff}} = 0.97$
$\rho = 1.229$	$GMVA = 3.0$

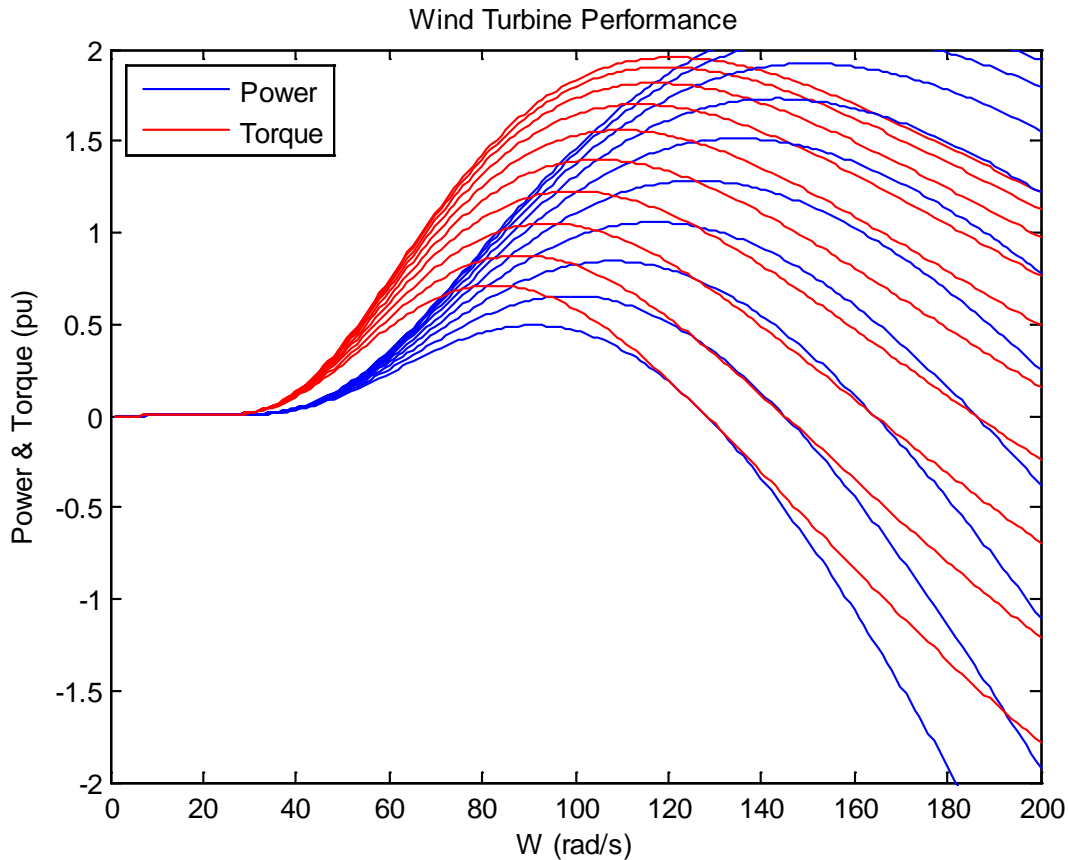


Figure 2.8. Theoretical wind turbine output for a range of beta values

Lastly, the wind governor follows the transfer function outlined in PSCAD as depicted in Figure 2.9.

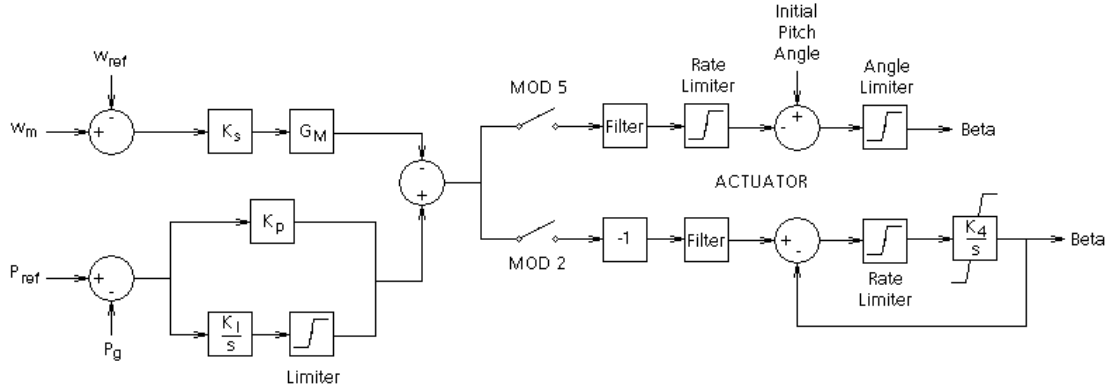


Figure 2.9. Transfer function for wind governor block

This transfer function adjusts the value of Beta so the wind turbine generates the correct amount of torque to match the demanded power based on the current mechanical speed of the machine. Adjusting the pitch angle has a direct impact on the power generated and thus the torque generated as well. The K constants present in the transfer function of Figure 2.9 are chosen by the user in the PSCAD block.

The general theory behind the overall PSCAD wind component was discussed in this section whereas the actual blocks themselves can be seen in Section 3.2.2 of this thesis.

2.5 PHOTOVOLTAIC GENERATION SOURCE

The modeling of a photovoltaic (PV) source proved to be rather challenging due to the nonlinear characteristics of the equations for the equivalent circuit model. However, by following the technique outlined in [18], the V-I curve of a PV array was recreated in PSCAD with relative ease. The model itself created in PSCAD can be seen with explanation of components in the

modeling Section 3.2.3. The V-I curve of a PV module will be discussed in this section as well as how placing modules in series and/or parallel changes the curve shape.

A PV module is accurately represented by a current source in parallel with a diode and resistance followed by another resistance in series as shown in Figure 2.10 [19]. Another more mathematically accurate model has also been development in [20] but this type of accuracy was not necessary in the analysis carried out in this thesis. This advanced model involves another diode in parallel in the circuit present in Figure 2.10. The technique utilized to implement this circuitry into PSCAD was actually an approximation of the mathematical curve, so more accuracy was not required.

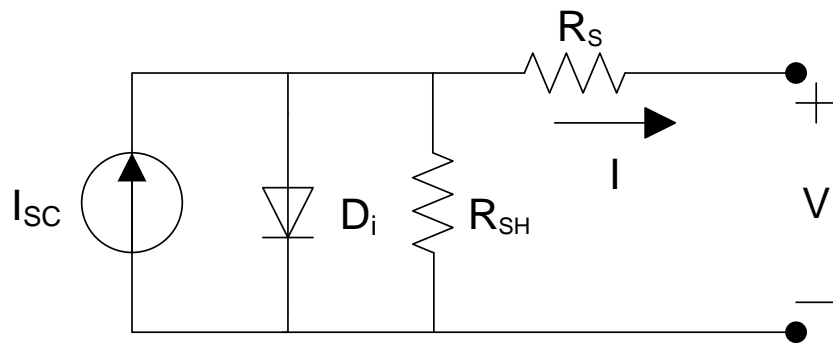


Figure 2.10. Equivalent circuit model of a PV module

Again, for the purposes of the analysis to be carried out on the MVAC and MVDC systems, the only requirement was to extract maximum real power from the PV system. The solar module thus was assumed to be operating at ideal conditions. This implies the irradiance is always at a constant 1000 W/m^2 and the operating temperature is 25°C . By doing so, the result was simpler equations to determine the V-I curve of the chosen PV module. By operating at ideal conditions, only a DC/DC converter was necessary in order to control what impedance from the rest of the system was being seen by the PV array.

The equations themselves simplify to the following based on ideal conditions [21]

$$I = I_{sc} - I_s \left[e^{\left(\frac{q(V+I \cdot R_s)}{k \cdot T \cdot A \cdot N_{sbase}} \right)} - 1 \right] - \frac{V + I \cdot R_s}{R_{sh}} \quad (1)$$

$$I_s = \frac{I_{sc}}{e^{\left(\frac{q \cdot V_{oc}}{k \cdot T \cdot A \cdot N_{sbase}} \right)} - 1} \quad (2)$$

where I = output current of PV module

I_{sc} = short circuit rating

I_s = cell saturation of dark current

q = electrical charge on the electron ($1.602176487 \times 10^{-19}$ C)

k = Boltzman constant ($1.3806504 \times 10^{-23}$ J/K)

T = operating temperature (in Kelvin)

A = diode factor

N_{sbase} = number of modules in series to get V_{oc}

V = output voltage of PV module

R_s = series resistance

R_{sh} = shunt resistance.

As mentioned previously, implementing the equations for the PV array proved to be rather difficult and thus a circuit-based approach was implemented per [18]. In this paper, a suggested technique that takes advantage of data gathered by the Sandia National Laboratories was chosen to create the PV module for this thesis. The idea of the technique is to take key points outlined by the Sandia model to create an approximation of the actual V-I curve of the manufactured PV module that can then be matched using a layout of diodes and resistors. These key curve points may be seen in Figure 2.11.

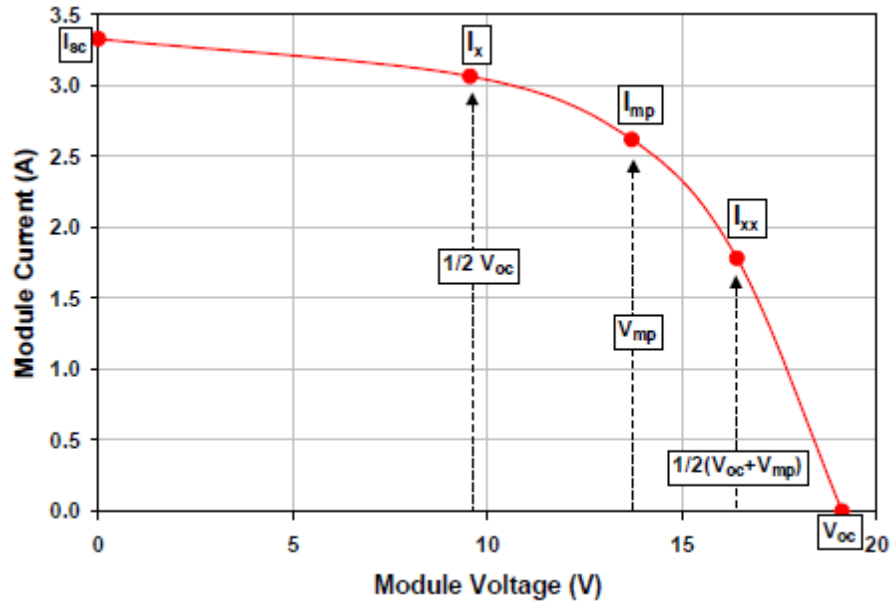


Figure 2.11. Key curve coordinates of the Sandia model [22]

The key points outlined in Figure 2.11 were provided by the Sandia database [23]. From the database, a Kyocera Solar KC125G module was chosen. The relevant parameters taken from the database are repeated here in Table 2-3. Again, following the equations outlined in [18], the values for R_s and R_{sh} were found for the Sandia Model approach using the values from the Sandia module database. These resistance values are included in Table 2-3 to keep all the parameters together in one location. The parameters in Table 2-3 were all used in the PSCAD model to simulate a PV module, however different resistance values had to be found to graph the actual V-I curve. This was due to the Sandia model being an estimation of the actual curve where R_{sh} governs the slope of the first portion of the curve and R_s governs the slope of the fourth portion. In reality, R_s has a greater effect on the entire V-I curve and not only the final portion.

Table 2-3. Kyocera Solar KC125G module parameters

Short-circuit current	$I_{sc} = 8.0 \text{ A}$
Current at $0.5V_{oc}$	$I_x = 7.86 \text{ A}$
Current for maximum power point	$I_{mp} = 7.2 \text{ A}$
Current at $0.5(V_{oc} + V_{mp})$	$I_{xx} = 5.1 \text{ A}$
Open-circuit Voltage	$V_{oc} = 21.7 \text{ V}$
Voltage for maximum power point	$V_{mp} = 17.4 \text{ V}$
Number of modules in series to get V_{oc}	$N_{sbase} = 36$
Series resistance of the Sandia model	$R_s = 0.4216\Omega$
Shunt resistance of the Sandia model	$R_{sh} = 77.5\Omega$

In the case of the theoretical curve, the values for the resistances calculated per [18] cause the curve to be unstable and oscillate near V_{oc} . This is illustrated in Figure 2.12.

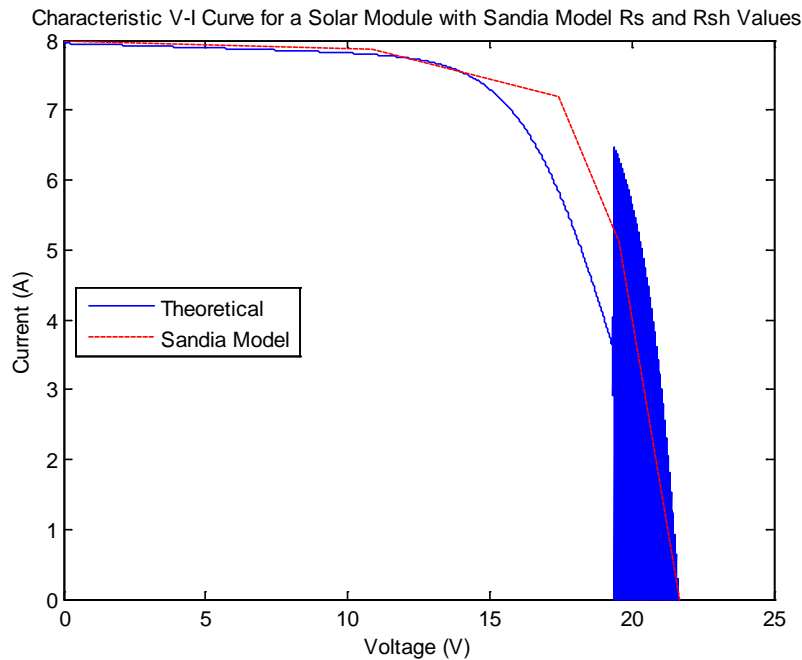


Figure 2.12. Theoretical V-I curve using calculated Sandia model values of R_s and R_{sh}

Therefore, using the equations (1) and (2) along with the current and voltage parameters from the Sandia module database, the values of R_s and R_{sh} were adjusted to fit the key points outlined in Figure 2.11. Appropriate values of R_s and R_{sh} were found to be 0.1385Ω and 87.5Ω , respectively. Ultimately, a V-I curve was able to be constructed using a MATLAB script that can be seen in Appendix A. The curve itself is shown in Figure 2.13. The locations of I_x , I_{mp} , and I_{xx} are shown on the curve.

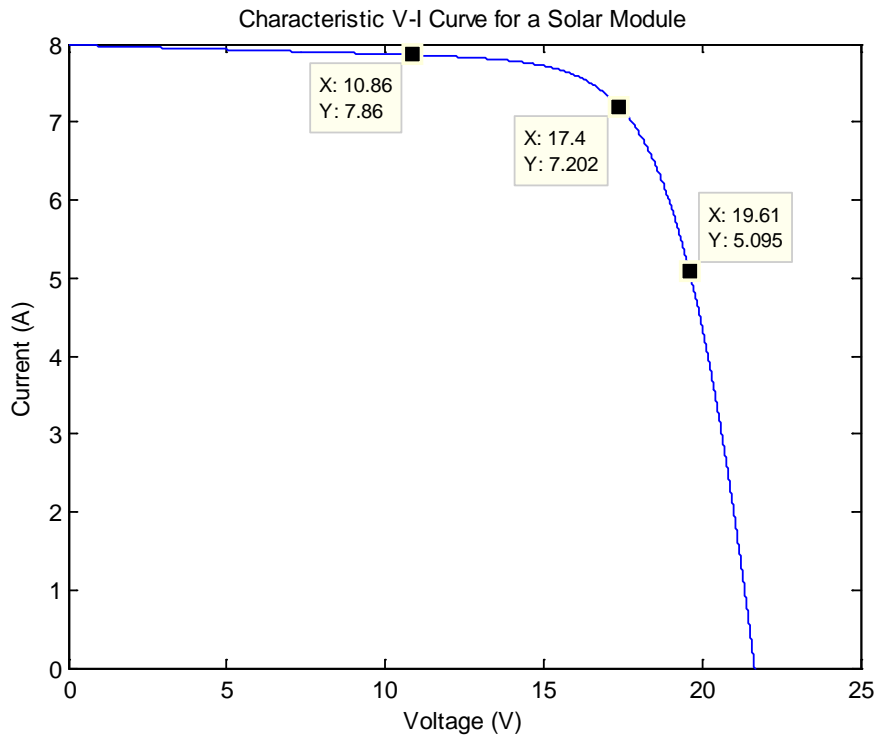


Figure 2.13. V-I Curve for a solar module

With a curve that accurately reflects the locations of key points of voltage and current values per [22], multipliers were added to the equations to account for modules in series and parallel combinations [21]. Equations (1) and (2) were altered to those shown below in (3) and (4). Note that N_{sbase} and N_s can be combined into one variable since N_{sbase} is always set to 36. The two were separated to more easily distinguish between the number of modules in series to acquire the original I_{sc} and V_{oc} versus modules in series to create an array and increase the

original V_{oc} value. For example, by placing two modules in series, V_{oc} is doubled to 43.4V and the number of modules is doubled as well to 72.

$$I = N_p \cdot I_{sc} - N_p \cdot I_s \left[e^{\left(\frac{q(V + I \cdot R_s \cdot \frac{N_s}{N_p})}{k \cdot T \cdot A \cdot N_{sbase} \cdot N_s} \right)} - 1 \right] - \frac{V + I \cdot R_s \cdot \frac{N_s}{N_p}}{R_{sh} \cdot \frac{N_s}{N_p}} \quad (3)$$

$$I_s = \frac{I_{sc}}{e^{\left(\frac{q \cdot V_{oc}}{k \cdot T \cdot A \cdot N_{sbase} \cdot N_s} \right)} - 1} \quad (4)$$

where N_s = modules connected in series

N_p = modules connected in parallel.

A selection of graphs is shown in Figure 2.14, Figure 2.15, and Figure 2.16 depicting the effect that placing modules in series, parallel, and series-parallel combinations has on the V-I curve in Figure 2.13. A value of $N_s = 2$ results in 72 modules, $N_s = 3$ yields 108 and so on. A value of $N_p = 2$ places two sets of 36 modules in parallel resulting in a total of 72 modules. Lastly, a value of $N_{sp} = 2$ requires 144 modules ($2 \times 2 \times 36$) for the desired V_{oc} and I_{sc} values.

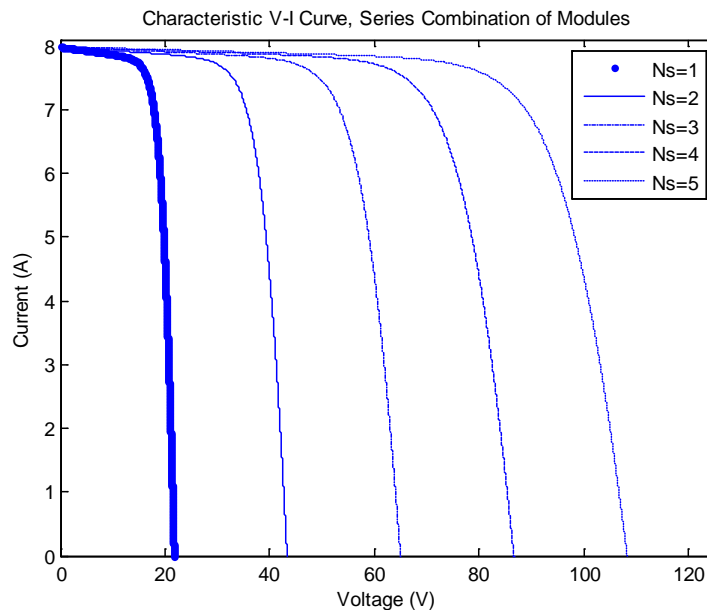


Figure 2.14. Effect to V-I curve from placing modules in series

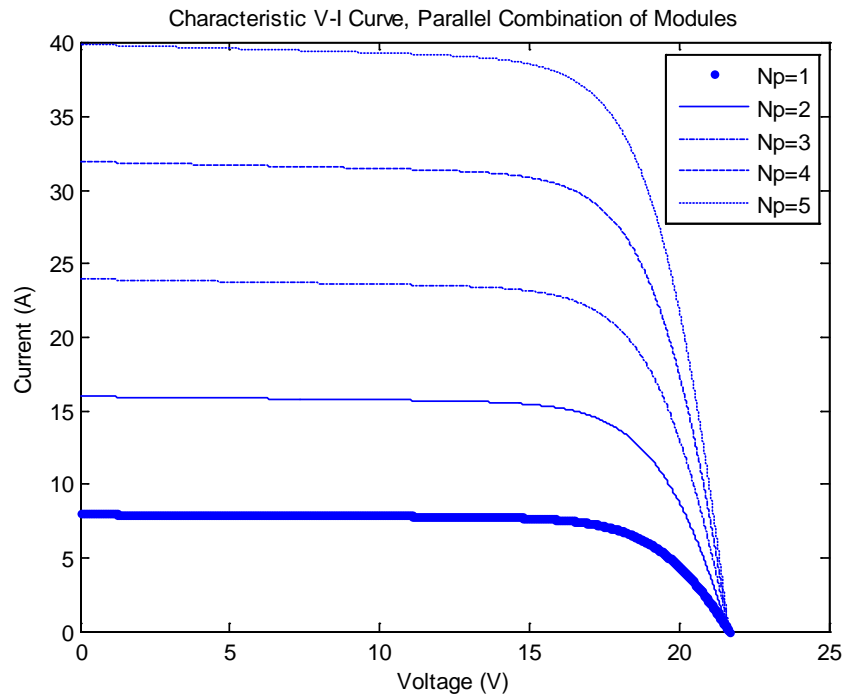


Figure 2.15. Effect to V-I curve from placing modules in parallel

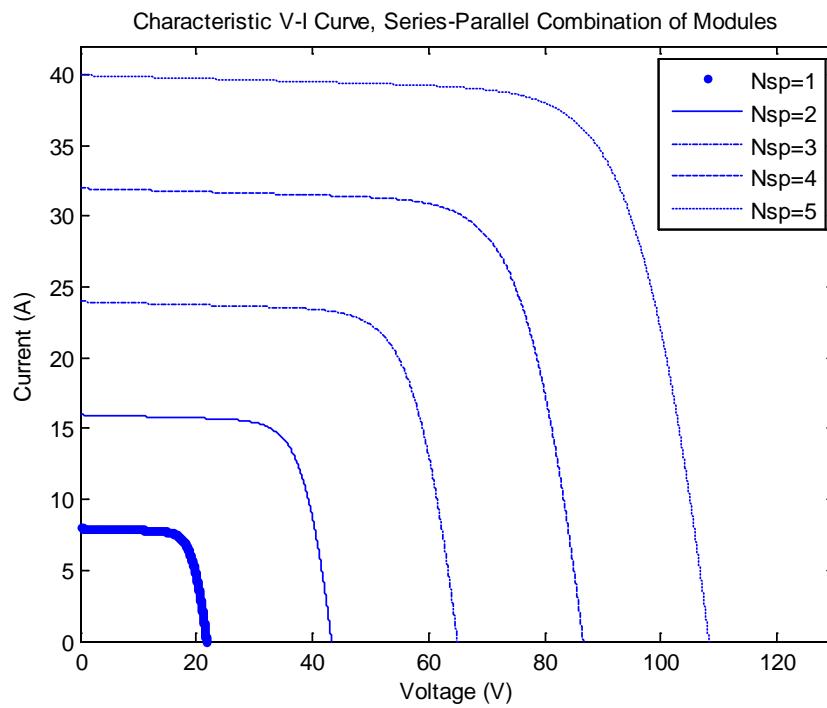


Figure 2.16. Effect to V-I curve from placing modules in series and in parallel

3.0 MODELS OF MVAC AND MVDC INFRASTRUCTURES IN PSCAD

The theoretical systems outlined previously in the section entitled “The MVDC and MVAC Systems that were Compared” were created in their ideal forms using the software PSCAD. The PSCAD software package was chosen due to its ability to simulate the transient nature that would be necessary when comparing two systems containing many power electronic devices. The layout also lends itself well to a circuit diagram making the analysis more intuitive and easier to visualize. The entirety of the system was split into separate model blocks with corresponding inputs and outputs to the central bus. The blocks containing the power electronic converters and generation sources have been contained within their own spaces due to the complexity of connections and control needed. Above all else, this approach makes it more pleasing to the eye and therefore easier to analyze the main bus structure connecting the converters to each other.

In this section, each block will be described and explained how it was realized in PSCAD with graphical and numerical analysis to prove that it is functioning as expected with different known parameters. The assumption is that if the blocks are tested with known input and output parameters while in an isolated state from any system dynamics, once placed into the real system the block should operate as expected. Each of the power converters was validated in such a manner before being connected to one another in order to form the overall system structure. The power converters were placed one by one starting from the utility source and connecting a basic

AC resistive load initially. The blocks for the solar and wind generation were then connected to the main bus by their designated power converters and the power flows and voltages were checked once more for correctness. Lastly, the storage component and DC load were attached and a base case, steady state operation was found.

3.1 POWER ELECTRONIC CONVERTERS MODELED IN PSCAD

All the power electronic converters and generation sources were realized in PSCAD using the default library components in the software. That is to say, no custom components were created using FORTRAN programming, but topologies were created by taking existing components in PSCAD and combining them to construct the desired overall model.

3.1.1 Five-Level and Three-Level Diode Clamped Multilevel Inverter

The neutral point diode clamped multilevel inverter (DCMLI) was realized in PSCAD using the default library components in the software. The diodes and IGBT switches are unaltered from their default state values. More specifically, these values include the turn on and turn off resistances, voltage drop, forward breakover voltage, and reverse withstand voltage. The interest of this analysis resides on the inverter as a whole, but these values were kept to include a more realistic model without having to conduct addition research to verify or change the default values present. The circuit used in the system can be seen in Figure 3.1. For testing purposes, there is an ideal DC voltage source as an input with a resistive load output (load not shown). The circuitry directly following the input source is the buck-boost converters to assist in balancing

the four separate capacitor voltage values. The value chosen for the four capacitors was $4000 \mu\text{F}$ [24].

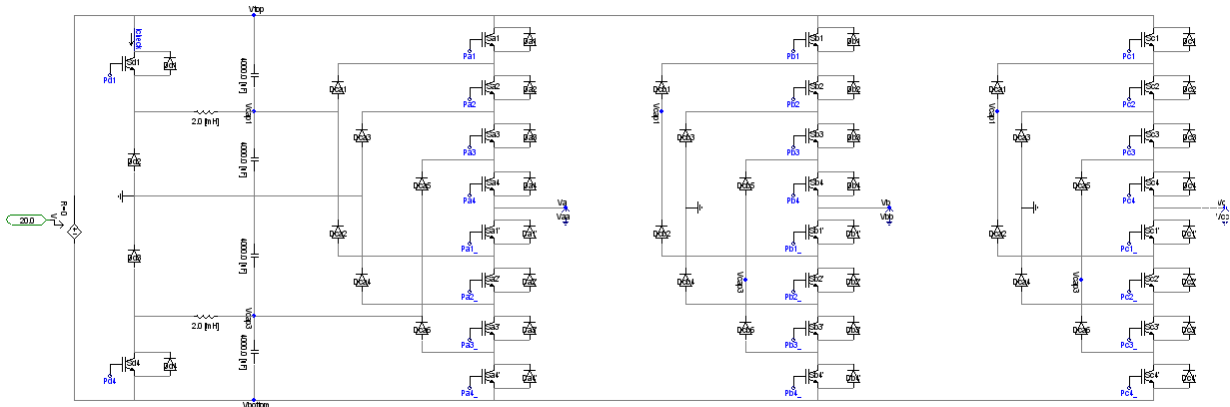


Figure 3.1. DCMLI Inverter as created in PSCAD

Taking a closer look at a single leg of the multilevel inverter, it can be more easily seen what components comprise the overall structure. As seen in Figure 3.2, one leg looks identical in its PSCAD modeled form as it does shown earlier in the layout of Figure 2.5.

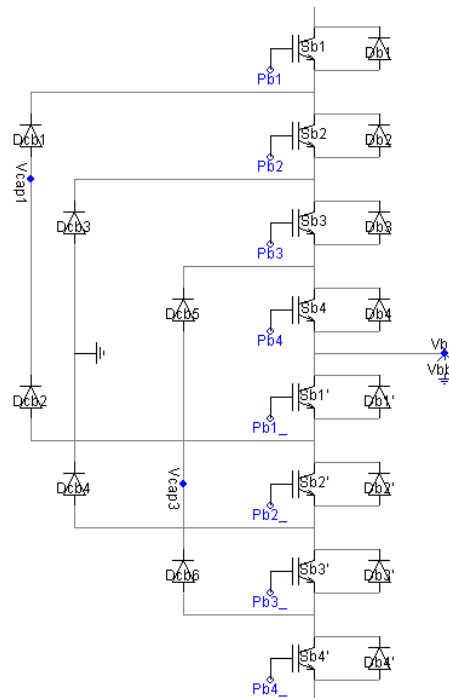


Figure 3.2. Closer look at one leg of the MLI (Phase B)

In order to remove unsightly but necessary wire connections from the MLI, nodes can be seen utilized in Figure 3.2. The node "Vcap1" is treated as the same point as the point between the first and second capacitors at the input of the MLI. The same can be said of "Vcap3" but it corresponds to the point between the third and fourth capacitors. An illustration of the nodes is shown in Figure 3.3. The nodes are treated as the exact same point electrically, therefore cleaning up the overall model but not affecting its functionality in any way. All of the legs are identical to each other in terms of component placement.

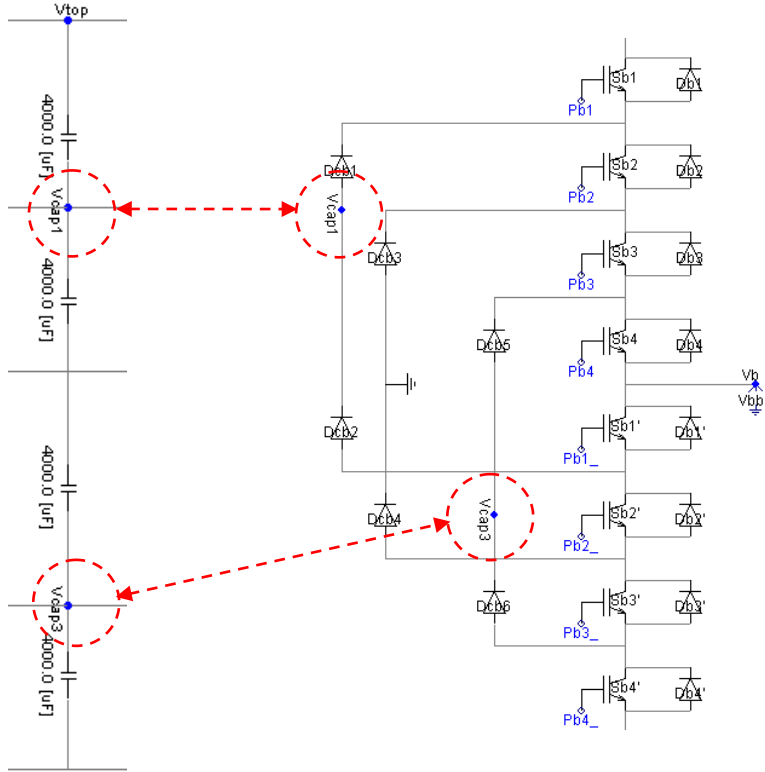


Figure 3.3. PSCAD node usage in DCMLI model

As discussed in the previous chapter, the control strategy chosen for the MLI was the carrier based pulse width modulation with an in-phase disposition. This scheme was implemented by using the PSCAD setup shown in Figure 3.4.

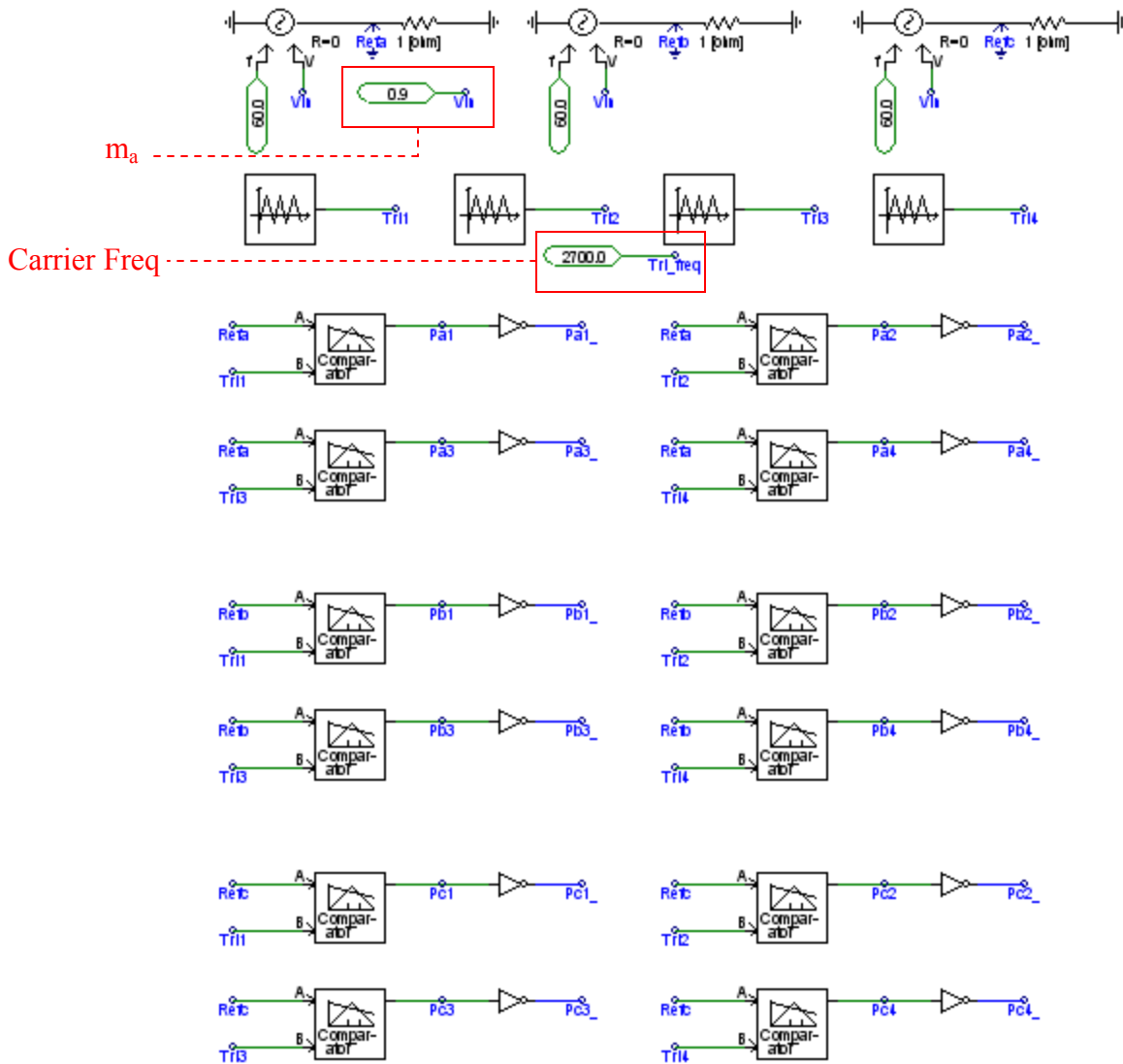


Figure 3.4. Control for DCMLI as seen in PSCAD

Working from the top of Figure 3.4 moving down, each component and its function in implementing the control scheme will be discussed. The three voltage sources serve as the reference signals for each phase. The sources differ only by a phase shift of 120° from each other. Phase B is 120° from Phase A and Phase C is 240° from Phase A. The amplitude of each reference sinusoidal waveform is governed by an external constant that can be adjusted depending on the desired MLI output. The carrier signals, to be discussed in a moment, are setup in such a way to be based on a maximum amplitude of 1.0, corresponding to an amplitude

modulation ratio of 1.0. Therefore, the external constant that governs each reference source is actually the amplitude modulation ratio. For example, if a value of 0.8 is used for the external constant of the reference sources, this would cause them to output a sine wave of 60Hz with amplitude 0.8. The carrier signals vary from -1.0 to 1.0, so comparing the amplitude of the reference signals to the carrier signals, it can be seen that the ratio is 0.8 to 1.0, the same as the value for the external constant controlling the reference sources.

The next four blocks correspond to the carrier signals in the form of a triangular wave generator. The frequency of each is the same and can easily be changed by an external constant. The max and min amplitudes of each of the four triangular wave generators are adjusted to accomplish the desired stacked structure discussed in Section 2.3. The parameters for each block are in the form shown in Figure 3.5. This particular dialog box shown is for the first, leftmost triangular wave generator. The maximum output level is set to 1.0 and the minimum output level is set to 0.5. These parameters thus limit the triangular wave to oscillate between 0.5 and 1.0 at the specified frequency. The other three triangular generators are set as 0 to 0.5, -0.5 to 0, and -1.0 and -0.5. Doing so results in four triangular waves stacked from -1.0 and 1.0.

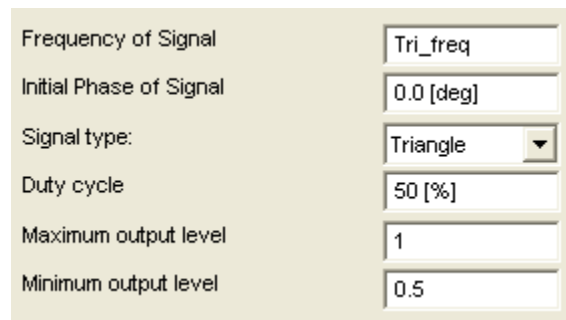


Figure 3.5. Carrier Signal PSCAD Dialog Box

The rest of Figure 3.4 is comprised of comparators to determine when a switch is to be fired. Each three sets of four comparators correspond to each leg in the MLI structure. Each of the four comparators per set controls when the eight switches on each leg fire. Let us examine

one set of comparators as seen below in Figure 3.6. This set of four controls the switches present on the MLI for Phase A of the output. The two inputs for each comparator are the reference signal for Phase A (60Hz, no phase delay) and one of four carrier waves. When the reference signal is greater than the carrier wave, the output is a '1' thus firing off the switch. In the opposite case when the reference is less than the carrier the output is a '0', preventing the switch from conducting current. Since the switch on the lower half of the structure is complementary to the same numbered switch on the upper half, the output signal of each comparator is negated for the respective switch signal. The other sets of comparators govern the switching for Phases B and C and differ by having their respective reference signals.

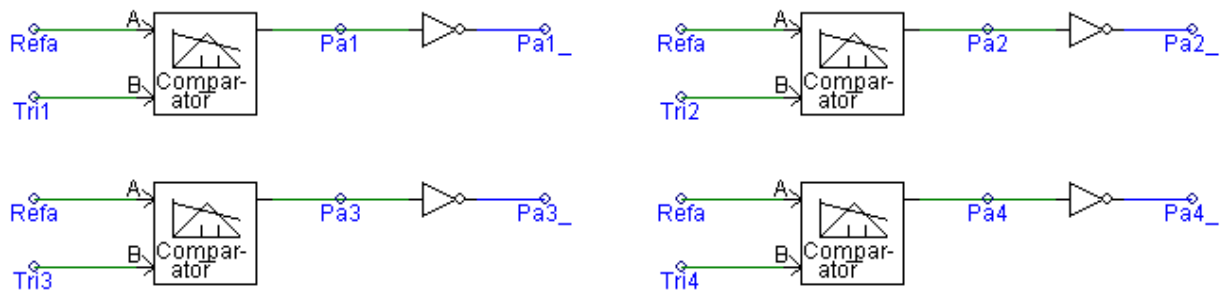


Figure 3.6. One set (Phase A) of comparators

To show that the structure and the control scheme are functioning as expected when compared to the theoretical results, a set of graphs was taken from PSCAD and are shown in Figure 3.7 and Figure 3.8. Figure 3.7 depicts how the reference and carrier signals interact (amplitude modulation ratio of 0.9 and frequency modulation ratio of 45) to create the switching signals in the middle graph and finally the resultant voltage output waveform in the last graph. The voltage shown is the line-to-neutral, peak for Phase A. It can be seen that there are five levels to this output voltage, as expected from the theory. The waveforms in Figure 3.8 correspond to voltage outputs (peak) for all three phases both line-to-neutral and line-to-line.

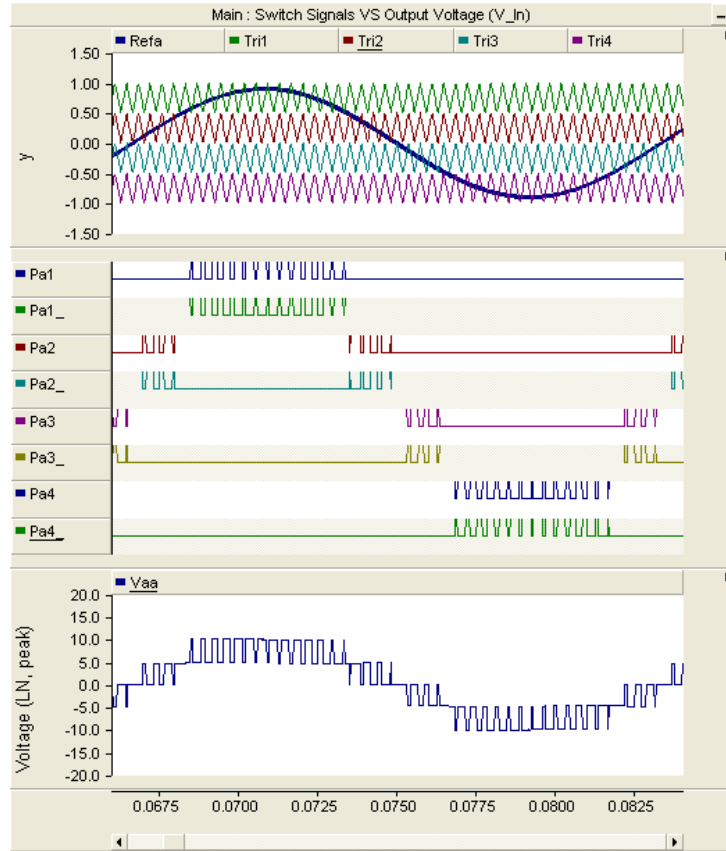


Figure 3.7. Control Sequence and resulting output voltage waveform

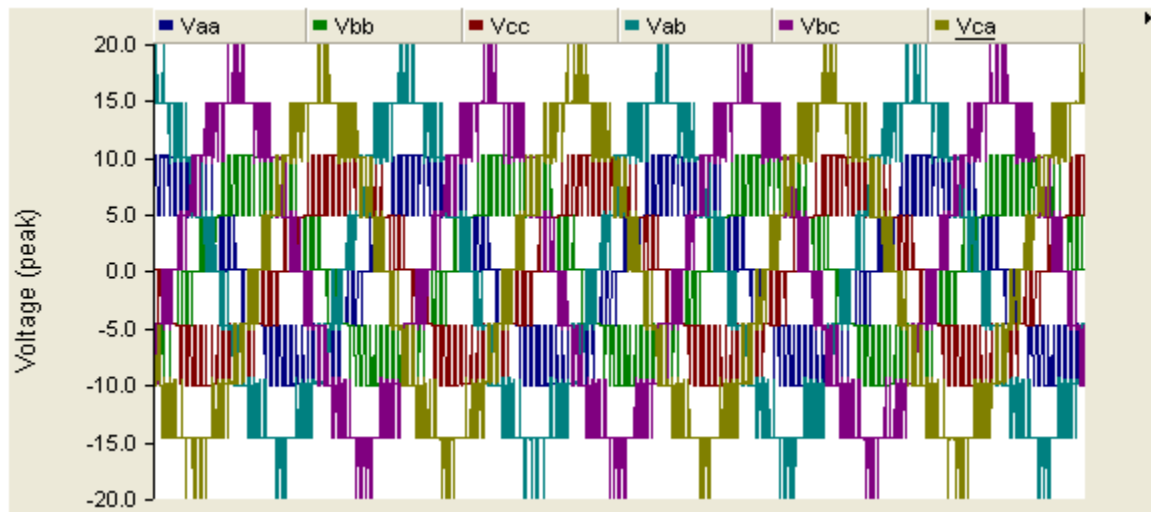


Figure 3.8. Outputs for line-to-neutral and line-to-line voltages of the DCMLI

The control circuitry for capacitor balancing can be seen in Figure 3.9. The circuit serves to transfer energy from the top capacitor to the second thus maintaining a balance of voltages between them. There is also another circuit for the lower two capacitors serving to transfer energy from the bottom capacitor to the third capacitor. The control depicted in Figure 3.10 is very simple. The voltage across the second capacitor is subtracted from the first and, if the result is less than zero, the switch is closed and energy is transferred from the top capacitor to the inductor. Once the voltage is brought down so the voltages match across the capacitors, the switch is opened and the energy stored in the inductor is transferred to the second capacitor by path of the diode, "Dd2".

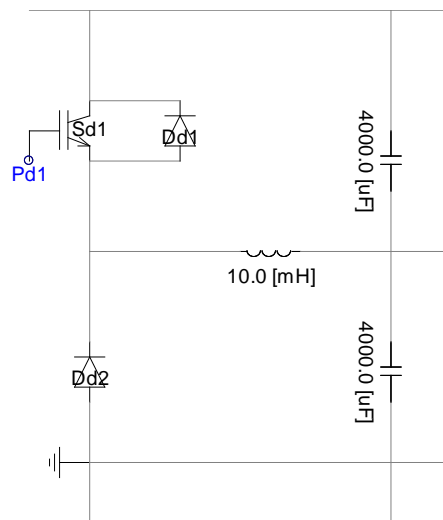


Figure 3.9. Capacitor Balancing Circuitry for DCMLI

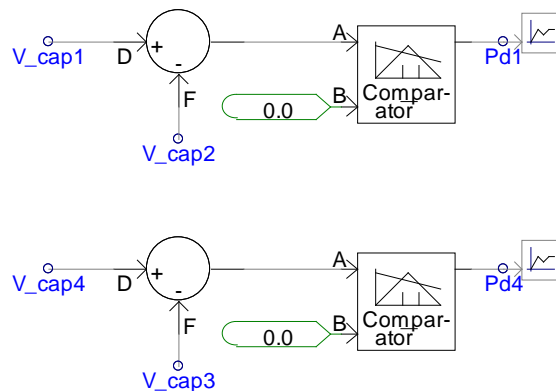


Figure 3.10. Control for Capacitor Balancing Circuits

The three-level diode clamped multilevel inverter functions in exactly the same way as outlined for the five-level version. The only exception is it only requires two carrier signals since there are only four switches total (two complimentary sets of two). Otherwise, the control for the structure itself is unchanged. Also, no balancing circuitry is present on the three-level version of the multilevel inverter. The structure, switching control outputs, and resulting waveforms can be seen in the following two figures, Figure 3.11 and Figure 3.12.

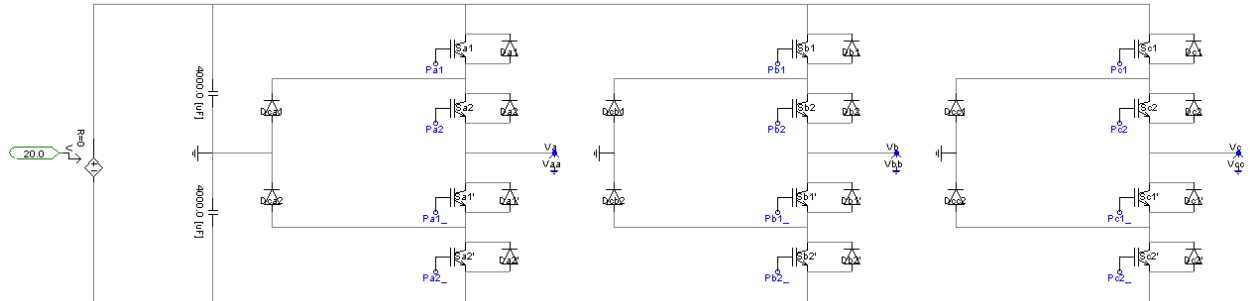


Figure 3.11. Three-level DCMLI Realized in PSCAD

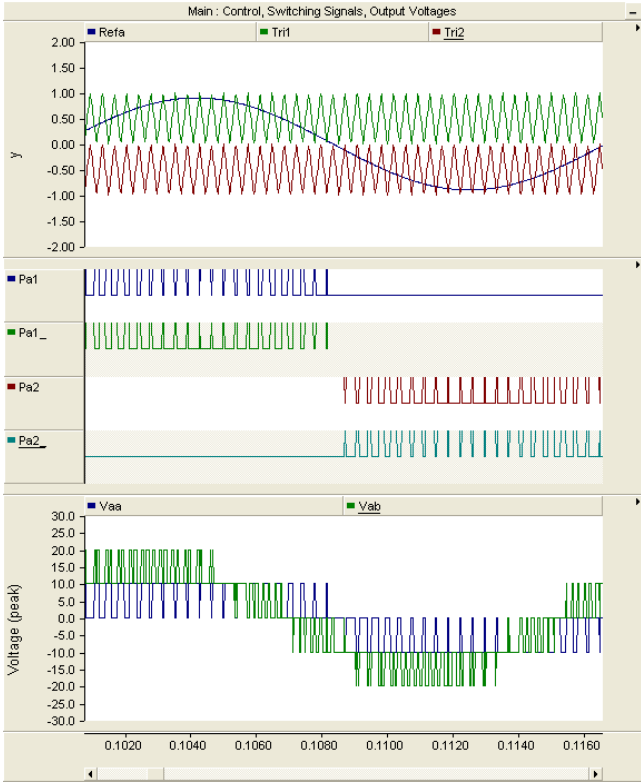


Figure 3.12. Control, Switching Signals, Output Voltages for Three-level DCMLI

3.1.2 Six-Pulse Diode Rectifier

The six-pulse diode rectifier is a simple but effective way of converting an AC signal to DC. In Figure 3.13, the rectifier can be seen with a passive output filter constructed in PSCAD. The rectifier itself is six diodes attached to the three-phase source acting as the utility. The diodes are unchanged from their PSCAD default values and the source is 14.815 kV_{rms} . The chosen input value would result in having 20 kV on the load, ignoring losses, using the output equation discussed in the theory section.

$$1.35 \cdot V_{LL_{rms}} = (1.35)(14.815 \text{ kV}_{rms}) = 20 \text{ kV}$$

No separate control scheme is necessary to operate the rectifier and so the entire structure is depicted in Figure 3.13. The input and output waveforms without the filter attached can be seen in Figure 3.14. Similarly, the same waveforms are shown in Figure 3.15 but with a tuned passive filter attached as in Figure 3.13.

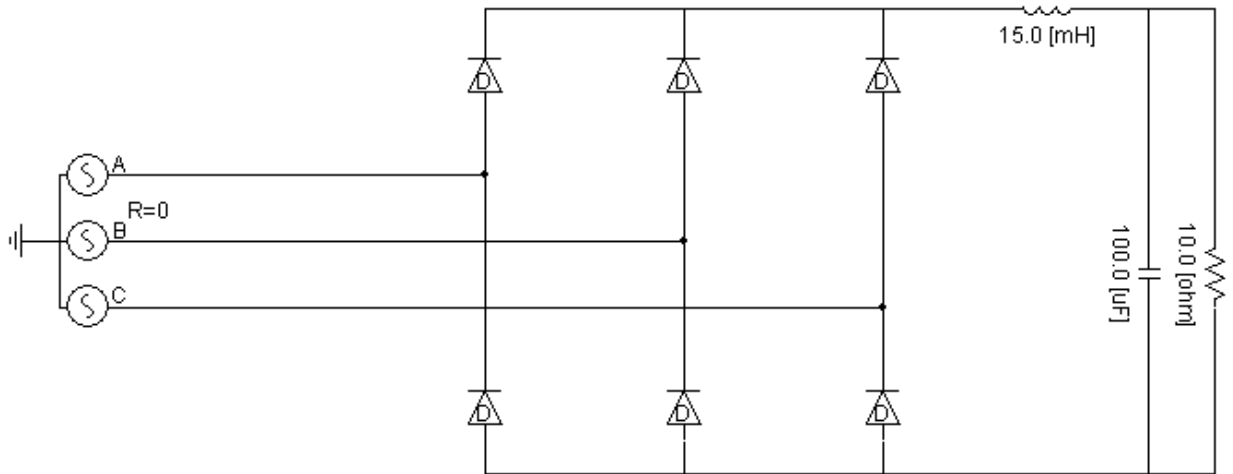


Figure 3.13. Six-Pulse Diode Rectifier Realized in PSCAD

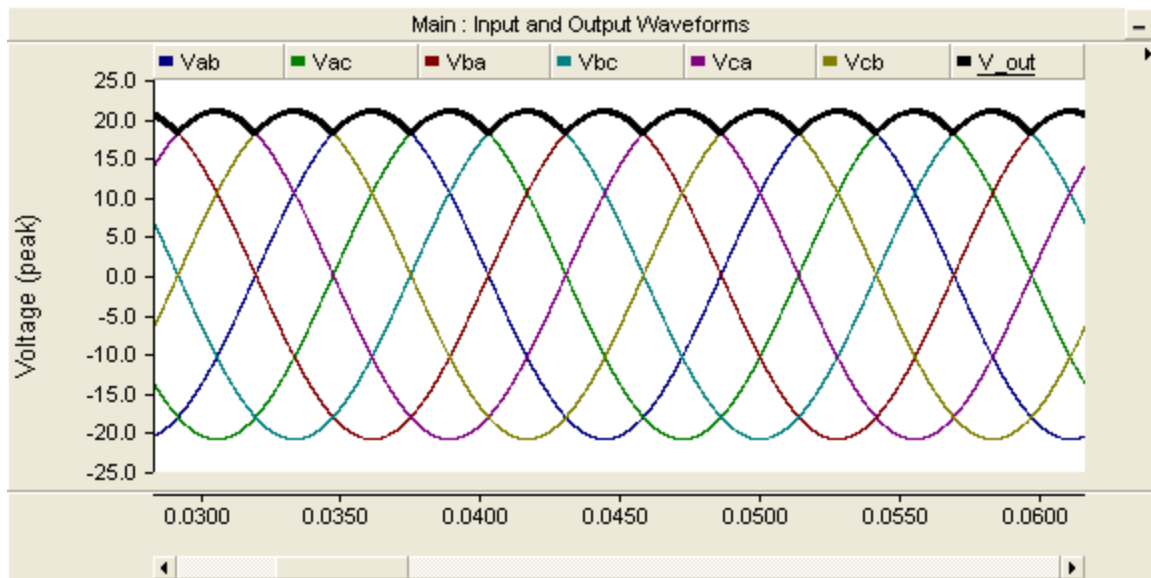


Figure 3.14. Input and output (bold line) waveforms of diode rectifier without filter

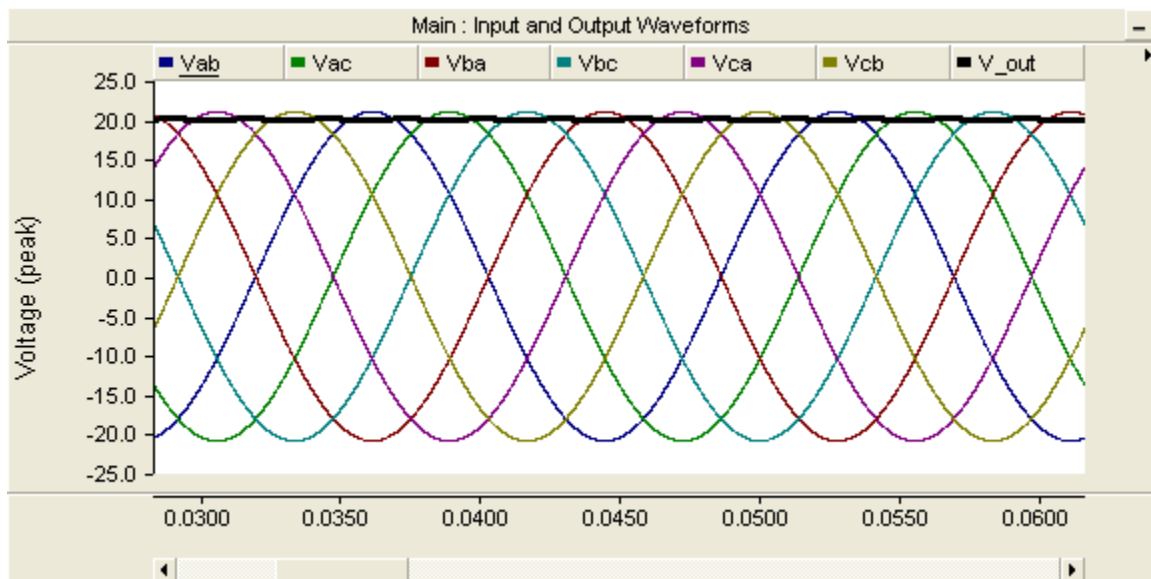


Figure 3.15. Input and output (bold line) waveforms of diode rectifier with tuned filter

3.1.3 Dual Active Bridge Converter (DC Transformer)

The Dual Active Bridge (DAB) converter was implemented to eventually be used in a bidirectional state, but in this thesis it was used in two separate locations, one as a boost converter and the other as a buck. This approach, while taking advantage of the bidirectional nature in one situation, shows the device was utilized in both environments successfully. The buck will be presented first followed by the boost orientation.

3.1.3.1 Buck Orientation

The DAB converter operated in buck mode is depicted in Figure 3.16. The switching devices are IGBTs and there are smoothing capacitors on both the high and low voltage side. A choke inductor is present as well on the low voltage side. The smoothing capacitors filter the voltage so it appears as flat as desired regardless of the orientation the converter is being operated in. This guarantees the voltage input and output of the converter is as ripple free as possible for the load or bus being supplied. The choke inductor serves to limit the current and therefore the power as well that flows through the switches and transformer. The capacitors and inductor have been tuned for the load present and may need adjustment depending on what is present on the output. The transformer in the middle of the DAB converter was set with a turns ratio of 1:5 (taking 20kV to 4kV) and a leakage reactance of 0.01pu.

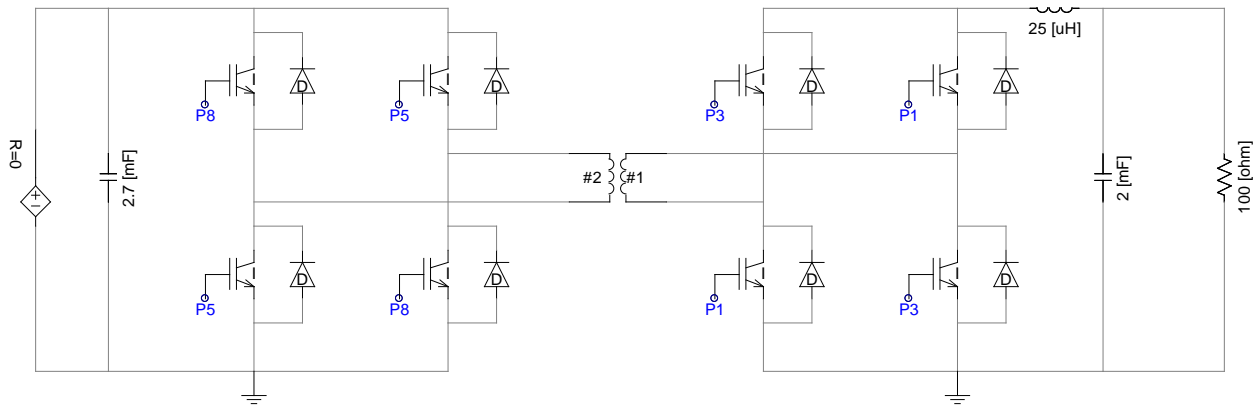


Figure 3.16. DAB converter oriented in buck mode

The controls used to operate the DAB converter are quite similar whether running in buck or boost mode. The only difference is in the duty cycle of the switching pulse. In the case of the buck converter shown in Figure 3.16, the duty cycle is set to 50.0% at a switching frequency of 1000Hz. The control blocks implemented into PSCAD are in Figure 3.17. This control implementation represents a primitive way of controlling the DAB converter when conditions are known with no disturbances. The switching signals (P5 and P8) for the switches on the high voltage side receive the control signals while the low voltage switches are set to remain open with constant zero values as their switching control inputs. The freewheeling diodes on the low voltage side switches handle the rectification, which is then filtered by the smoothing capacitor.

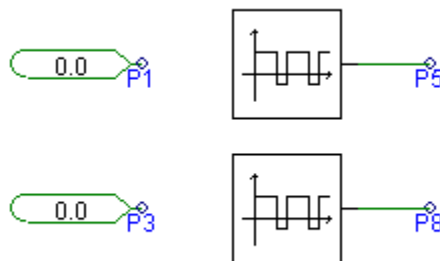


Figure 3.17. Control Blocks for DAB converter in buck mode

The results showing the input and output currents and voltages, switching signals, and voltage and current across both sides of the transformer are in Figure 3.18.

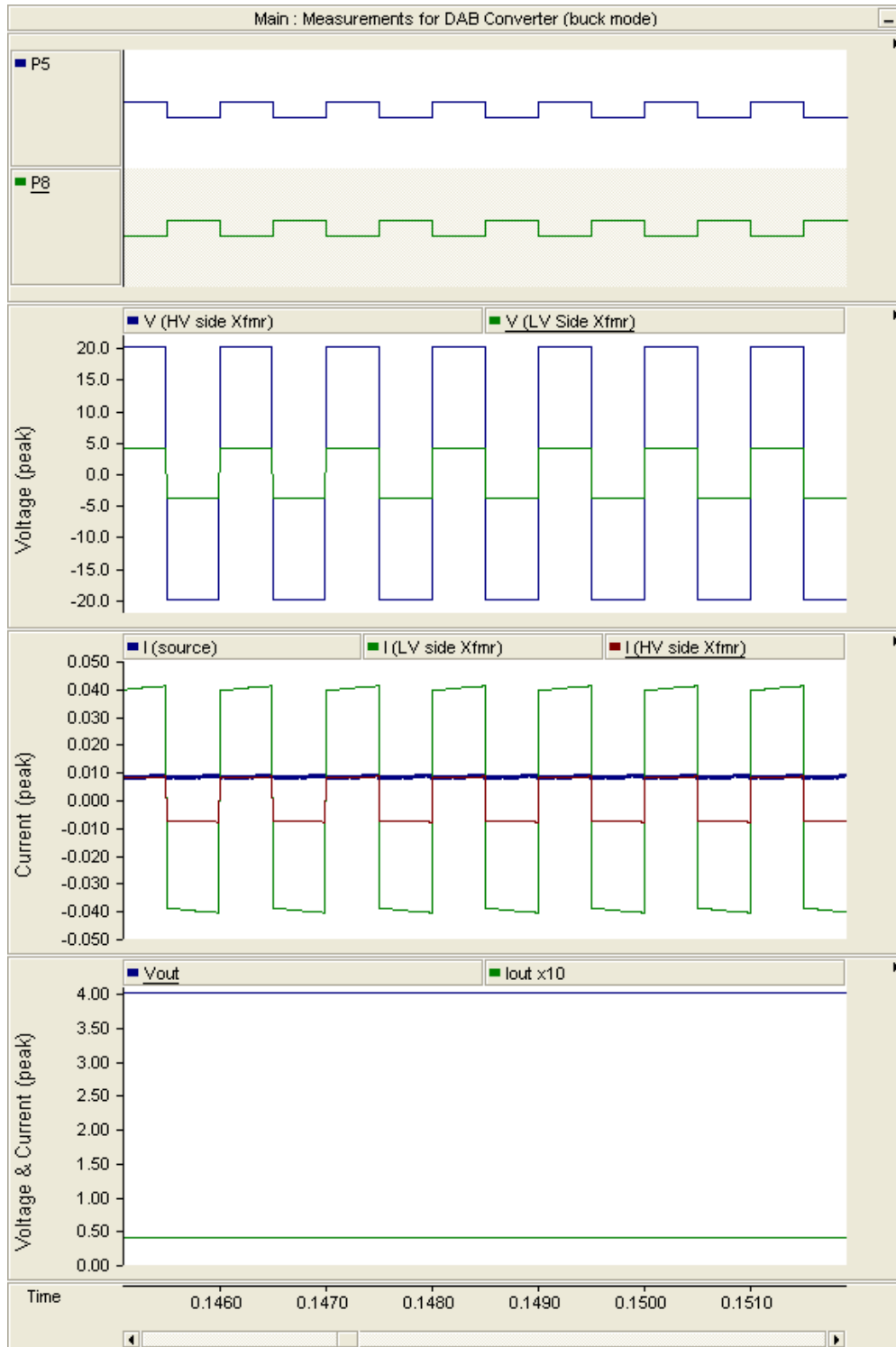


Figure 3.18. Measurements for DAB Converter (buck mode)

3.1.3.2 Boost Orientation

Next, a description and validation of the DAB converter acting in boost mode will be presented. The boost mode configuration is that shown in Figure 3.19. The control blocks used are in Figure 3.20. The only difference from the boost mode is the control signals are sent to different switches (P1 and P3 versus P5 and P8 for the buck). The duty cycle was set to 50% and the switching frequency was 1000Hz. The resulting waveforms from the boost mode are shown in Figure 3.21. All of the voltages and currents are virtually identical to the buck mode results. This makes sense because the boost mode has the same control signals as the buck mode but the turns ratio is now 5:1. Therefore the only difference between Figure 3.18 and Figure 3.21 are the output waveforms for the voltage and current.

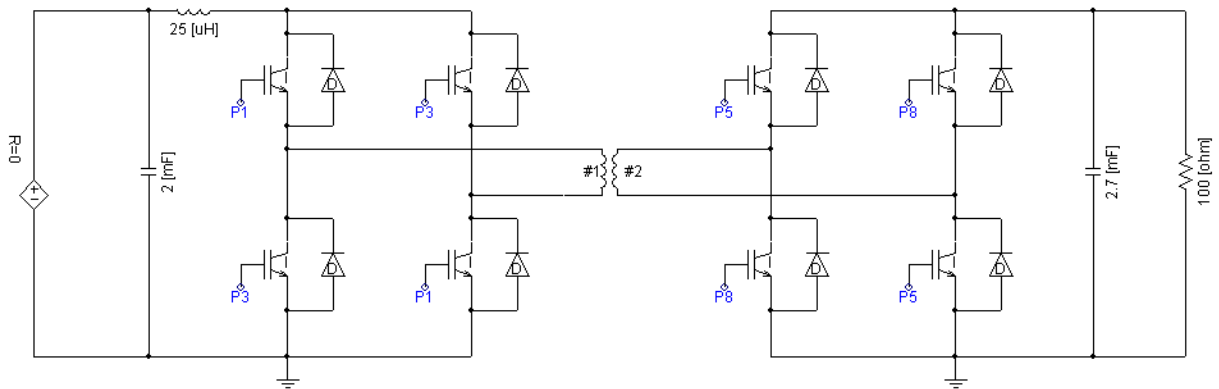


Figure 3.19. DAB converter oriented in boost mode

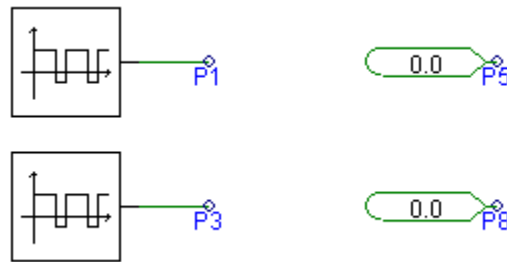


Figure 3.20. Control Blocks for DAB converter in boost mode

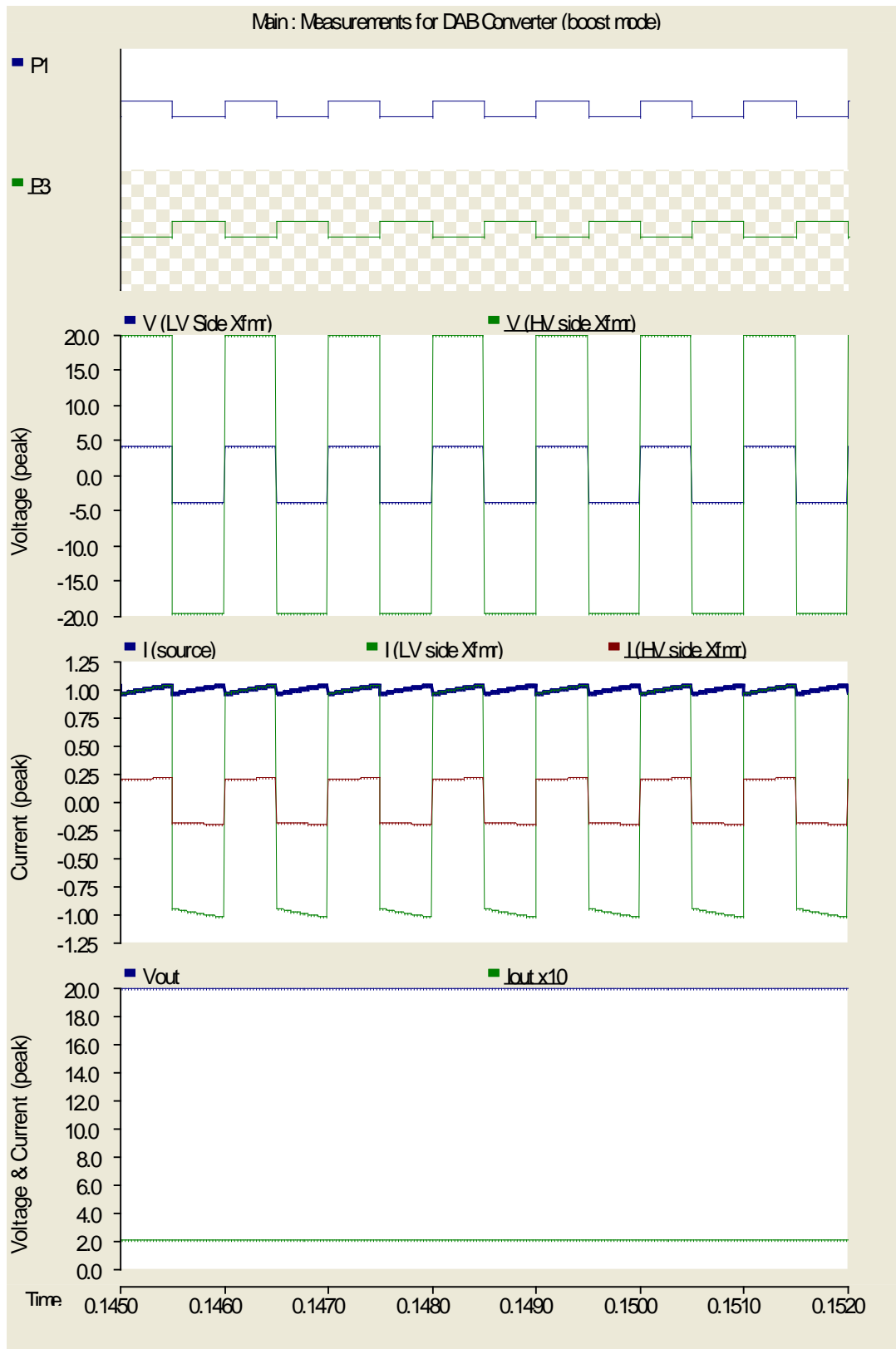


Figure 3.21. Measurements for DAB Converter (boost mode)

3.2 PSCAD IMPLEMENTATION OF GENERATION SOURCES

There are three total generation sources in each model for the MVAC and MVDC systems. These three include two renewable resources, photovoltaic (PV) and wind, while the remaining represents the rest of the system or, as it will be referred to in this thesis, the utility. The utility will be discussed first since it is the simplest, followed by the wind and finally the PV. Each generation source is identical in either system, the only differences being how they are tied to the main bus and ultimately connected to the loads. The PV and wind models were created using data from real PV modules and wind turbines. This information was gathered from Kyocera for PV and GE for the wind. The implementation of both models was created to be adaptive, so if in the future other data from a differing manufacturer wanted to be implemented, this would be more straightforward for the user.

3.2.1 Utility

The implementation of the utility source in PSCAD was the simplest between the three since its main purpose is to supply power to the loads that the renewable sources were unable to. With this key goal in mind, the utility was modeled as an ideal voltage source with a small resistance acting as a source impedance. The component is presented below in Figure 3.22. The source is actually three phases but was used in its "single-line" display form due to simplicity and ease of measurements. The component itself is set to 230kV, 60Hz, with a source resistance of 0.01 Ω .



Figure 3.22. Utility component realized in PSCAD

3.2.2 Wind Turbine

The model to simulate a wind generation source was adapted from an already existing PSCAD example file [25]. The altered model used in this thesis can be seen in Figure 3.23. All parameters that were altered from the default example file will be discussed. If a value is not mentioned, it can be assumed that it was left at the default.

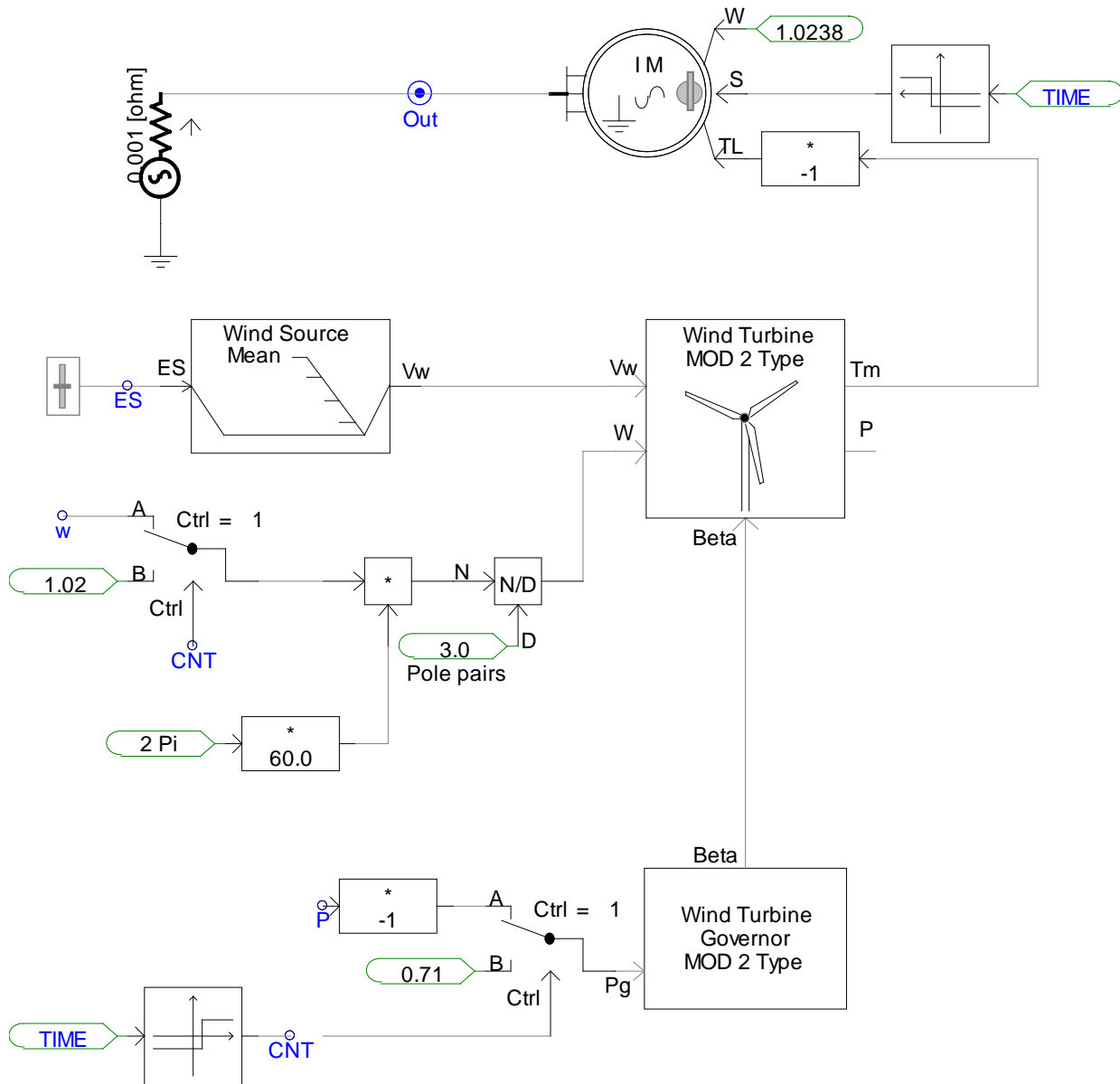


Figure 3.23. Wind Generation realized in PSCAD

The machine that was used to produce power from the torque generated from the wind turbine itself was an induction machine operating as a generator. Important parameters for the machine are shown in Table 3-1 [26]. A voltage source with a series resistance of 0.001Ω , simulating what would be in the real-world a connection from the grid system, was attached to the output of the induction machine to provide it with reactive power and to keep its terminal voltage at a constant value. The induction machine initially starts under speed control and is changed to torque control at 0.2s into the simulation. A speed of 1.0224 pu was chosen as the startup speed because this is very close to the speed the machine will be operating at when switched to torque control and providing power to the system.

Table 3-1. Parameters for Induction Machine

Motor Name	WR	Stator Resistance	0.025 [p.u.]
Rated Power	3.0 [MVA]	Wound rotor resistance	0.03 [p.u.]
Rated Voltage (L-L)	575 [V]		
Base Angular Frequency	376.99 [rad/s]	Magnetizing inductance	1.4 [p.u.]
Stator / Rotor Turns Ratio	1	Stator leakage inductance	0.1 [p.u.]
Angular Moment of Inertia (J=2H)	2	Wound rotor leakage inductance	0.1 [p.u.]
Mechanical Damping	0.00 [p.u.]		
Graphics Display	Single line vie		

The wind turbine block has the parameters shown in Table 3-2. The rotor radius and area were based off of the General Electric TC2 2.5-100 wind turbine [27]. The air density and gear box efficiency were left at their default values. The wind source block currently only serves to feed the wind turbine with a constant 15 m/s wind velocity. As discussed in the theory section, the wind source block may be used for gusts, ramps, and noise, but for this analysis the wind is left at a constant velocity to therefore supply a constant torque and power output.

Table 3-2. Parameters for Wind Turbine block

Generator Rated MVA	3.0 [MVA]	Air density	1.225 [kg/m ³]
Machine rated angular mech. speed	125.667 [rad/s]	Gear box efficiency	0.97 [pu]
Rotor Radius	50 [m]	Gear Ratio - Machine/turbine	GR
Rotor Area	7854 [m ² m]	Equation for power coefficient	MOD 2

The wind turbine governor parameters were altered to those shown in Table 3-3. The initial value for beta, the pitch angle of the turbine blades, was set to 16 degrees. These values were found by applying the theory discussed in Section 2.4. The graphs created to estimate the values necessary for a smooth, steady-state output of the wind turbine as a whole unit can be seen in Figure 3.24. These curves are an isolated case from Figure 2.8 for the value of $\beta = 16$. The values highlighted in Figure 3.24 give a fairly accurate estimation of the power produced at different speeds. The per-unit value of power being demanded from the induction machine was 0.7105 pu or 2.1351 MW. According to the graph, the speed should be within the range of 128 to 130 rad/s in terms of mechanical speed. Observing the data in Figure 3.25, a similar estimation was made for the torque required. In the same range of mechanical speed, 128 to 130 rad/s, a torque between 0.71 pu and 0.6754 pu should be necessary. Running the wind turbine components to steady-state confirms these numbers for torque, power, beta, and speed. The data appear in Figure 3.26 and Figure 3.27.

Table 3-3. Parameters for Wind Turbine Governor block

Variable pitch control	Enabled	Governor Type	MOD2
Type of Generator	Induction	Gear Ratio: machine/turbine	GR
Rated electrical frequency of the machine	60 [Hz]	Power Demand -Pref [MW]	2.1351 [MW]
Turbine Rated Power	2.5 [MW]	Reference speed -Wref	376.99 [rad/s]
Machine Rated Power	3.0 [MVA]		

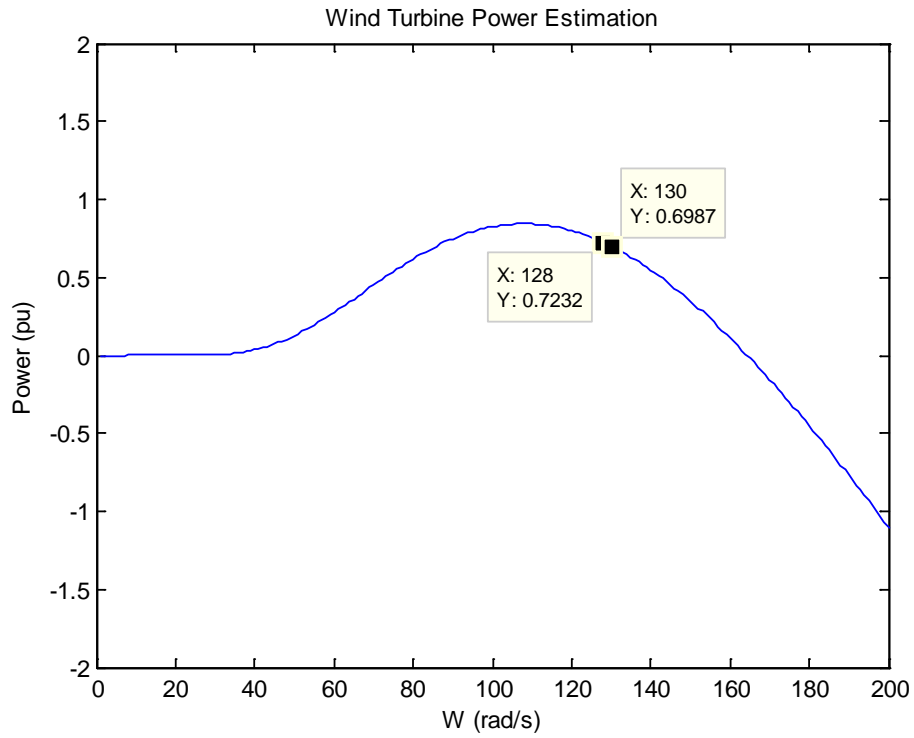


Figure 3.24. Estimation of power output for specified parameters of the wind block

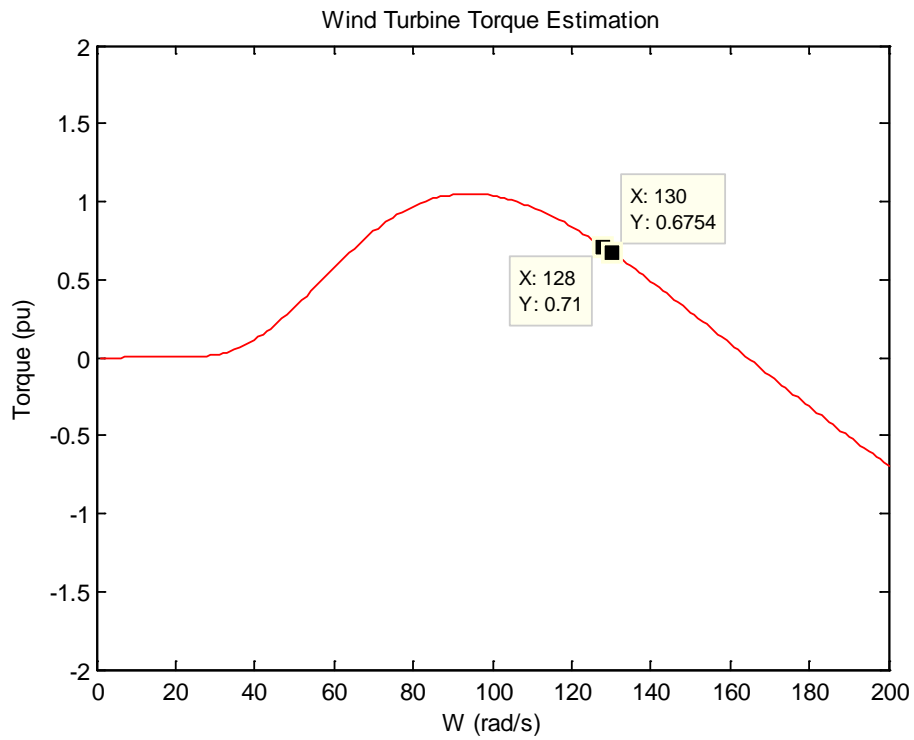


Figure 3.25. Estimation of torque output for specified parameters of the wind block

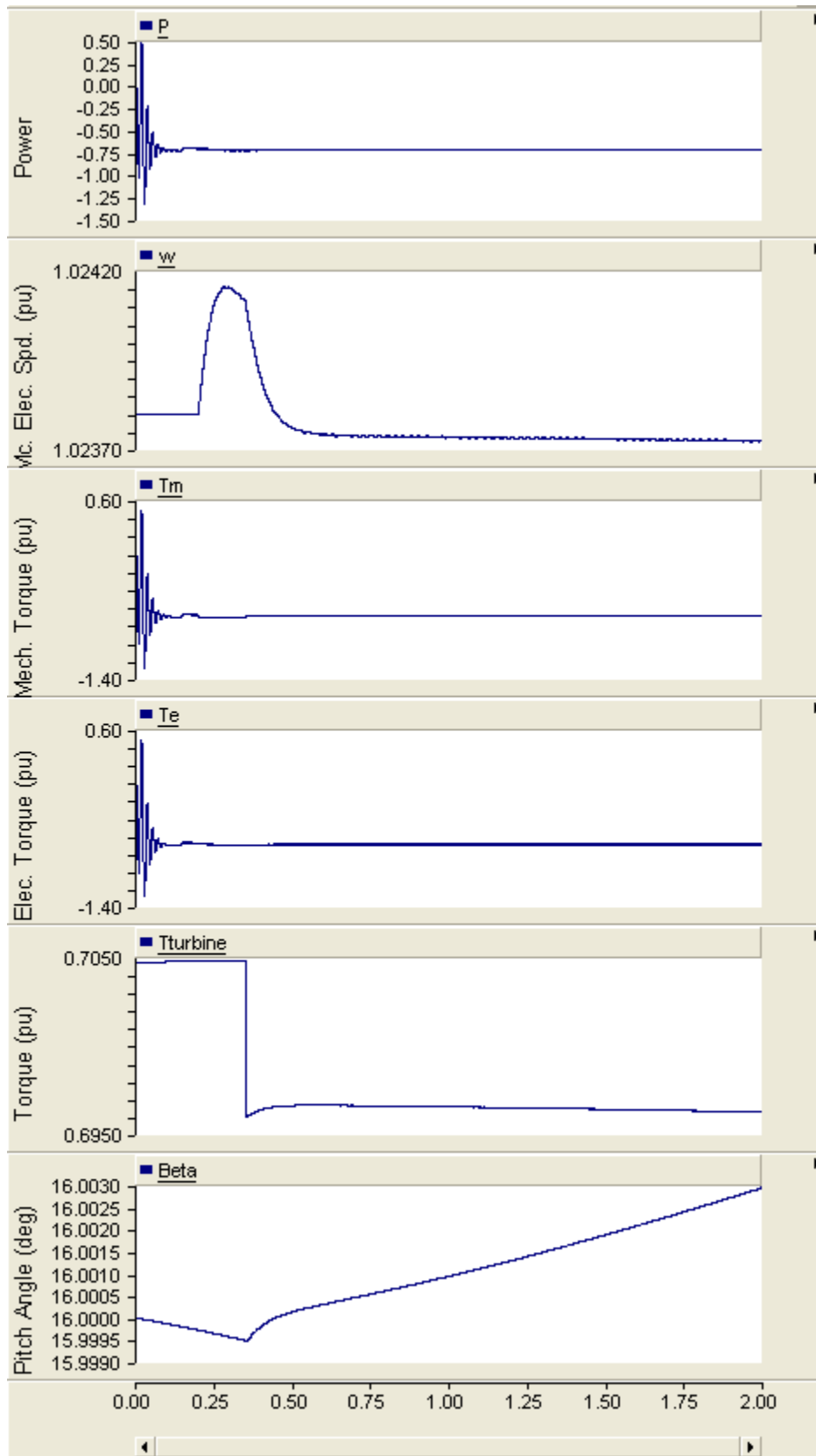


Figure 3.26. PSCAD plots of wind turbine component for torque, power, beta, and speed

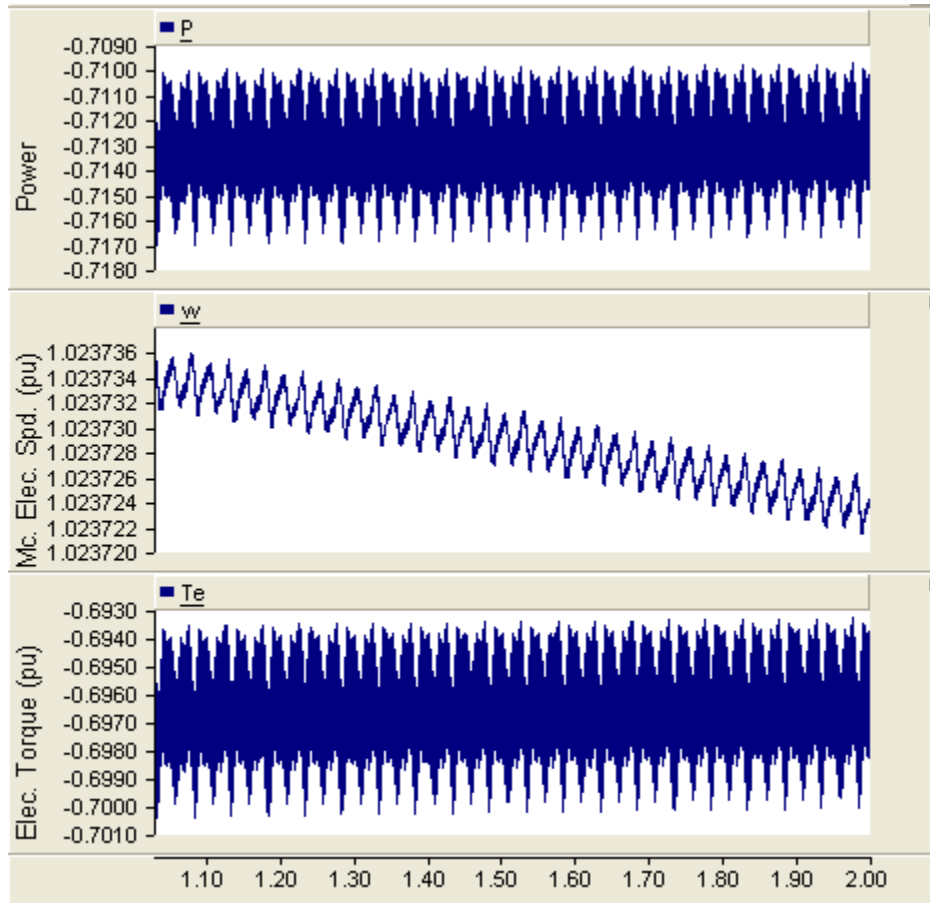


Figure 3.27. Zoomed-in data of Figure 3.26 at steady-state

Examining the data from Figure 3.27, a comparison to the estimated values in Figure 3.24 and Figure 3.25 may be carried out. The compared data appear in Table 3-4 for ease of reference. The actual values from the model fit well between the approximations made with the theoretical equations.

Table 3-4. Comparison of Estimated and Actual Values for Wind Turbine Output

	Speed	Power	Torque
Estimated	128-130 rad/s	0.7232-0.6987 pu	0.71-0.6754 pu
Actual	128.65 rad/s	0.71375 pu	0.69675 pu

3.2.3 Photovoltaic Array

The model implemented in PSCAD to act as the photovoltaic power source was designed such that the number of modules in series and/or parallel could be changed as easily and quickly as possible. The circuitry layout itself is shown in Figure 3.28. In order to allow the model to dynamically change depending on the constant chosen for the number of series/parallel combinations, variable resistors and a variable current source were used with calculations that took place at the start of the simulation. The calculations and blocks used to determine these values appear in Figure 3.29. The calculated resistor values correspond to those of the same name that appear in Figure 3.28. The voltages of V_{top} , V_{mid} , and V_{bot} are those used for the forward voltage drops of the respective diodes. Unfortunately, these voltage values cannot be variable inputs to the diode models in PSCAD and require that they be re-entered to the model parameters whenever the series (N_s) and parallel (N_p) combinations are changed.

The initial values for I_{sc} and V_{oc} were taken from the Sandia module database [23] while the remaining values initial values for resistors and diode voltages were calculated per the equations outlined in [18]. This implementation allows for the PV array circuitry to be altered with relative ease depending on the desired output power.

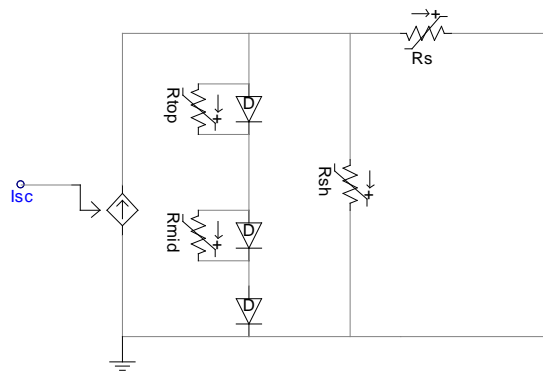


Figure 3.28. Photovoltaic equivalent circuit realized in PSCAD

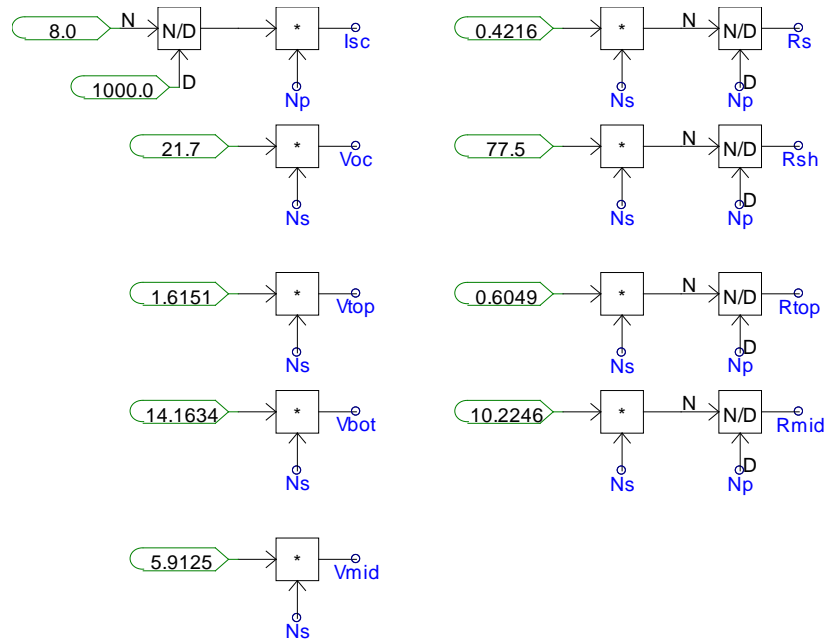


Figure 3.29. Calculations of I_{sc} , V_{oc} , resistor values, and diode voltages in PSCAD circuit

For a single array of 36 modules in series and none in parallel ($N_{sbase} = 36$, $N_s = 1$, $N_p = 1$), the V-I curve produced from PSCAD may be seen in Figure 3.30. This data were extracted from the program and also graphed in MATLAB alongside the Sandia model as well as the accurate curve from the theoretical equations. These graphs are present in Figure 3.31.

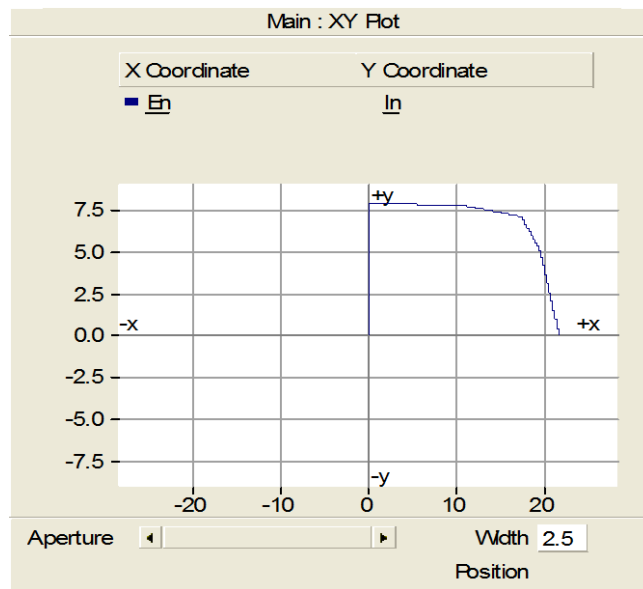


Figure 3.30. V-I curve produced in PSCAD for a single array (x-axis is volts, y-axis is amps)

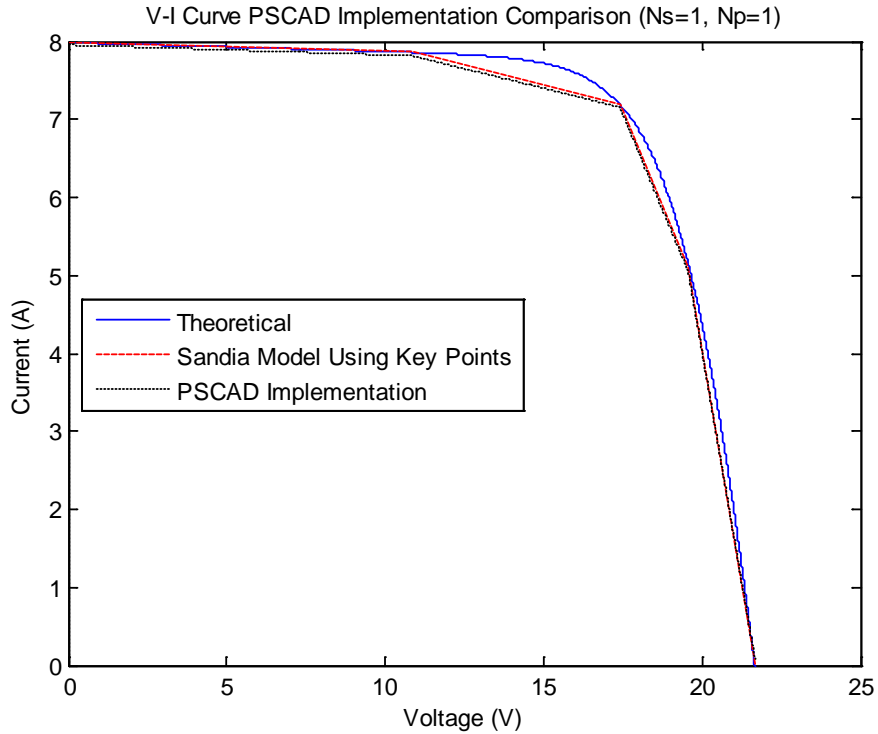


Figure 3.31. Comparison of V-I curves generated with different methods ($N_s=1$, $N_p=1$)

It can be seen by Figure 3.31 that the PSCAD circuitry used to estimate the V-I curve and especially the Sandia model was very accurate. By adjusting the values of N_s and N_p , the PV array was able to achieve a desired output of about 250kW. This was found by first choosing a voltage level, in this case 600V was chosen, and then sequentially performing the following calculations,

$$\frac{\text{Voltage level chosen}}{V_{mp}} = \frac{600V}{17.4V} \approx N_s = 35$$

$$\frac{\text{Desired power output}}{N_s \cdot V_{mp}} = \frac{250kW}{(17.4V * 35)} = 410.509A$$

$$\frac{\text{Current required}}{I_{mp}} = \frac{410.509A}{7.2A} \approx N_p = 58$$

Therefore, with a value of $N_s = 35$ and $N_p = 58$, the theoretical maximum power output of the PV array would be 254.32kW. By changing the N_s and N_p values in PSCAD, a new curve

was produced and can be seen in Figure 3.32. The data from PSCAD was once again plotted against the Sandia and theoretical model to verify it was functioning as expected. The results of the comparison are shown in Figure 3.33.

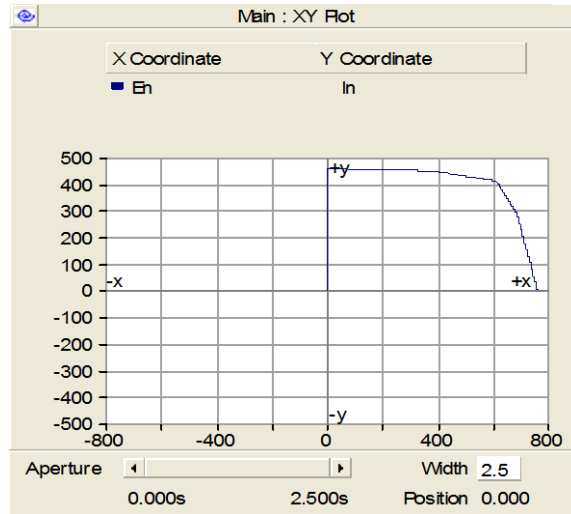


Figure 3.32. PSCAD V-I curve for a 250kW PV array

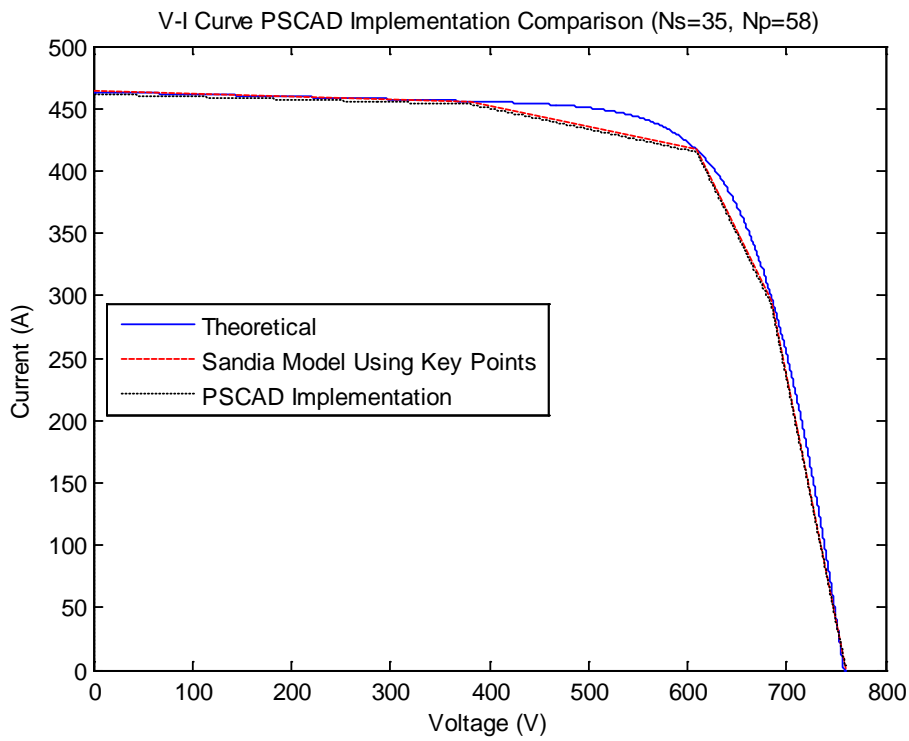


Figure 3.33. Comparison of V-I curves generated with different methods ($N_s=35$, $N_p=58$)

The last step to achieve the desired result of a 3MW output power from the PV array was to place the circuitry that resulted in a 250kW output in parallel with each other. This required that 12 separate circuits be placed in parallel to get a 3MW power output. This was accomplished by placing voltage nodes on the positive and negative terminals of each PV circuit ultimately leading to a single positive and negative terminal as seen in Figure 3.34. A single equivalent circuit may have been utilized to produce the 3MW but the option to have separate, parallel connected arrays was implemented for future applications.

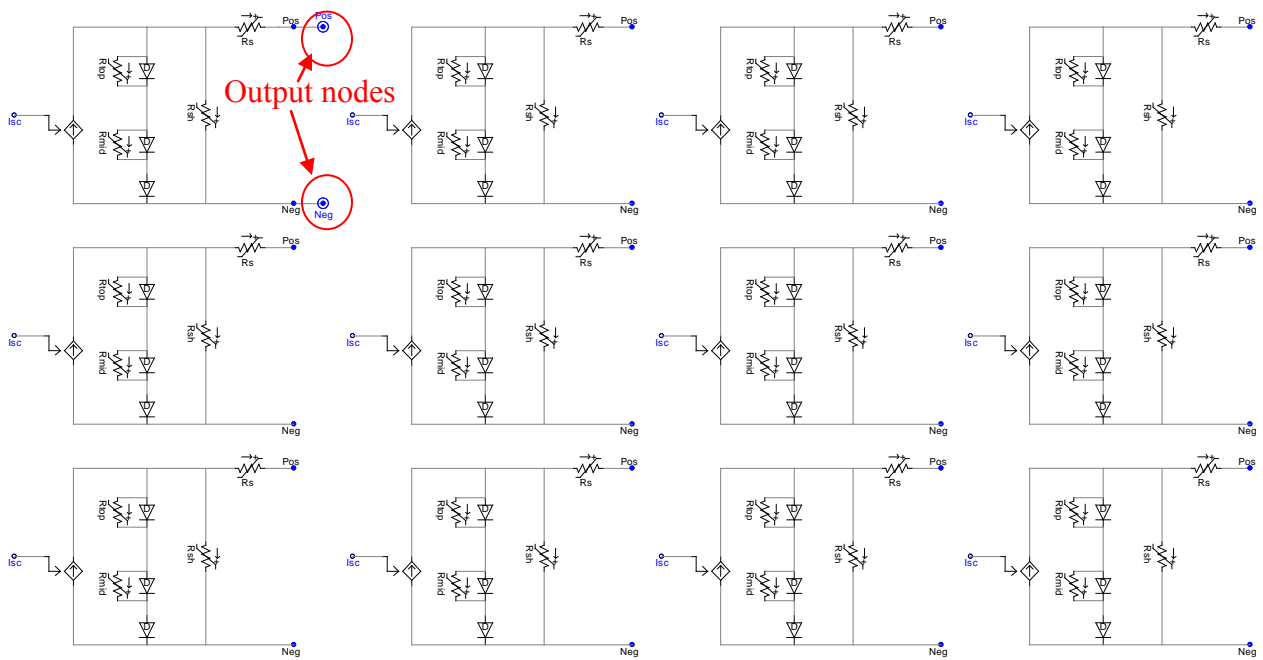


Figure 3.34. PSCAD, 3MW PV array circuit layout

3.3 MVDC INFRASTRUCTURE REALIZED IN PSCAD

The final MVDC infrastructure layout in PSCAD is shown in Figure 3.35. Each generation source and power electronic converter was housed inside of its own page module so measurements could be made more easily as well as allowing individual pieces to be identified more easily. The middle of the infrastructure represents the main bus with the positive and negative polarities necessary for DC power flow. A small resistance was added to each line connected to the bus to simulate losses the connections and to provide some damping for the passive LC filters on the outputs of the two rectifiers. Each block in Figure 3.35 will be looked at more closely.

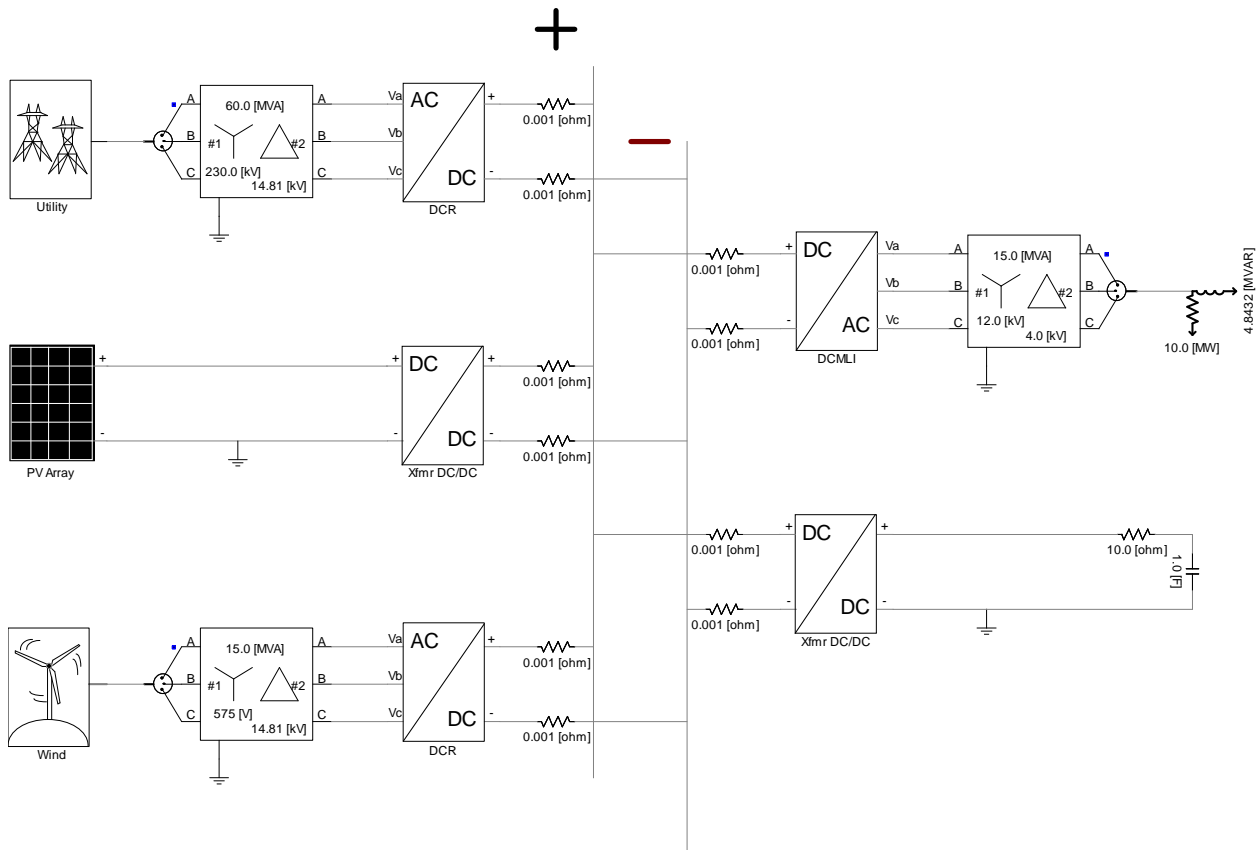


Figure 3.35. Final PSCAD layout of MVDC infrastructure

Starting at the Utility block, the voltage source with a source resistance discussed in Section 3.2.1 was placed into a page module and given an appropriate graphic to easily identify it from everything else. The block has a single output that contains a three dimensional vector with corresponding electrical characteristics for each phase of the AC feed. The three phases collapsed into one line is known as the "single-line view" in PSCAD nomenclature and allows for a simplified diagram and three phase power flow measurements. The parameters for the transformer in Figure 3.36 were a turns ratio of 15.53:1 (230kV to 14.81kV), a leakage reactance of 0.01pu, and an MVA rating of 60MVA. While not entirely realistic, this ratio was chosen because of the lack of control in the diode rectifier utilized in the analysis. A wye-to-delta connection was used because the diode rectifier does not contain a ground and will therefore have feedback current to the transformer causing a large loss of power if a ground wye connection were used. An ungrounded wye connection also works in place of a delta. The components in the DCR block are similar to what was shown in Figure 3.13 but with a different filter and input/output nodes instead of a source. The setup of the diodes and filter is the same as discussed in Section 3.1.2 with an inductance of 0.1H and capacitance of 100 μ F.

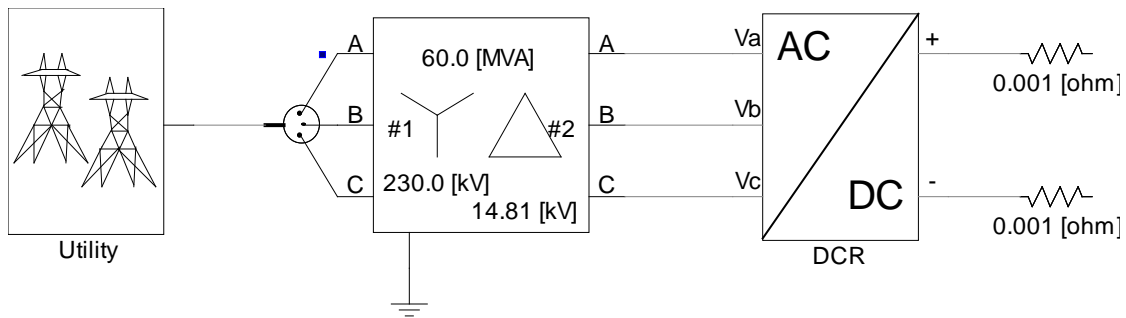


Figure 3.36. Closer look from the Utility block to the main bus

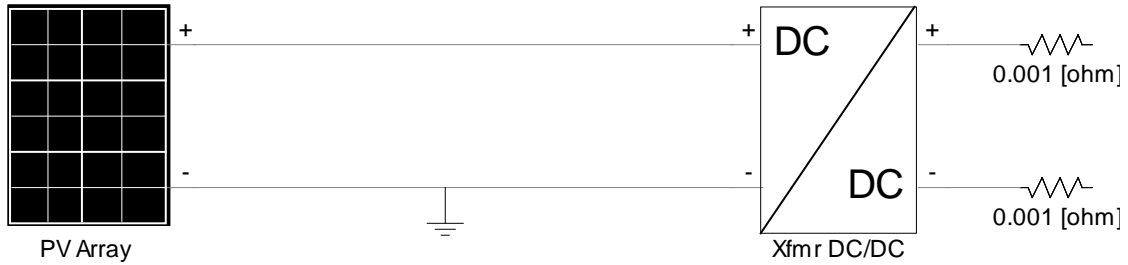


Figure 3.37. Closer look from the PV Array block to the main bus

The DC/DC converter in Figure 3.37 was oriented in a boost mode control scheme and the transformer has a turns ratio of 1:40 (500V to 20kV), 0.01pu leakage reactance, base operating frequency of 1kHz, and 15MVA rating. The turns ratio was found by trial and error until the PV array saw an input impedance of

$$\left(\frac{V_{out-250kW}}{I_{out-250kW}}\right) \cdot \left(\frac{\# \text{ in parallel}}{\# \text{ in series}}\right) = \left(\frac{600V}{417A}\right) \cdot \left(\frac{58}{35 \cdot 36}\right) = 0.0662\Omega$$

This impedance grants the PV array the ability to provide very close to its maximum amount of power. The maximum power output impedance for this particular module can be found by

$$\frac{V_{mp}/N_{sbase}}{I_{mp}} = \frac{17.4V/35}{7.2A} = 0.069\Omega$$

The rest of the DC/DC block is the same as discussed earlier in Figure 3.19.

Contained within the wind block page module are the components that were discussed in Figure 3.23. The parameters for the transformer are a turns ratio of 1:25.76 or 575V:14.81kV, leakage reactance of 0.01pu, and an MVA rating of 15. The block labeled AC/DC (DCR) contains the circuitry for a diode rectifier, which has already been discussed multiple times throughout this thesis.

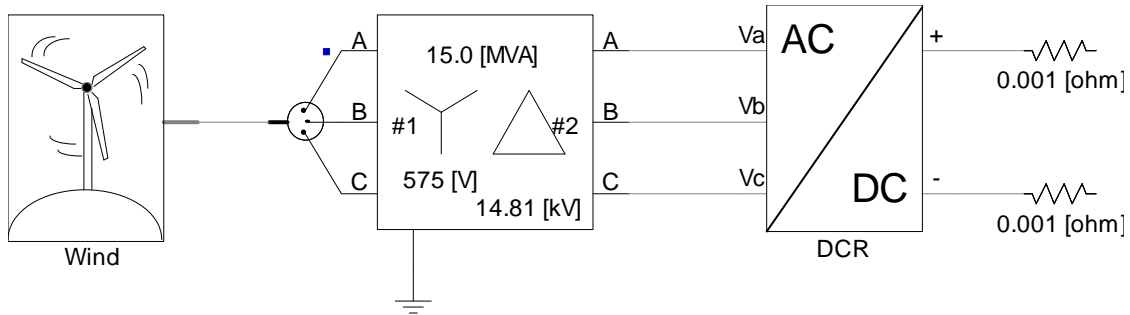


Figure 3.38. Closer look from the Wind block to the main bus

The generation sources located on the left side of the MVDC main bus infrastructure have been discussed thus far, so next the two loads will be outlined. The first load is simply an AC load of 10MW with a 0.9 power factor. This results in a reactive power load of 4.8432Mvar. The second load simulates what would be an electric storage facility. The storage was simplified to only a resistance in series with a moderately large capacitance.

The DC/AC (DCMLI) block shown in Figure 3.39 is a five-level diode clamped multilevel inverter per the discussion in Section 3.1.1. The transformer has a turns ratio of 3:1 or 12kV to 4kV, leakage reactance of 0.01pu, and rating of 15MVA. Ideally the output of the DCMLI should be 14.14kV (20kV divided by 1.4142) but due to losses and a primitive control scheme the output hovers around 11kV and therefore the first winding of the transformer was set to 12kV. Finally, the loads are in a wye configuration and have a three phase load of the values shown (10MW and 4.8432Mvar).

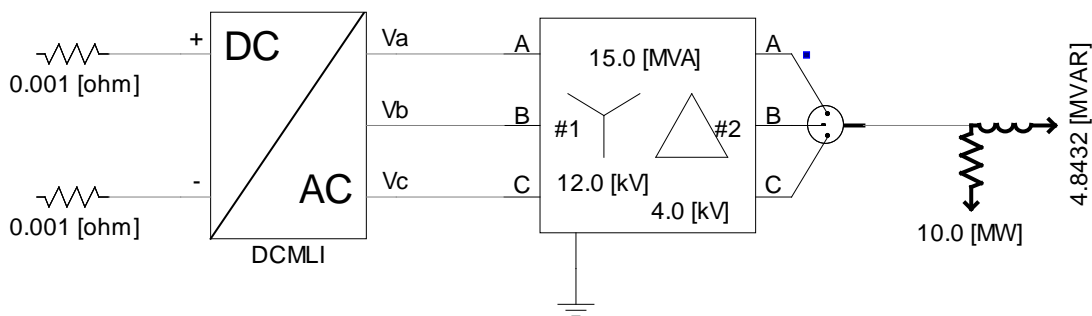


Figure 3.39. Closer look at the main bus to the AC load

The DC/DC converter in Figure 3.40 was setup in a buck orientation as discussed in Section 3.1.3.1. The transformer used in the topology has a 5:1 (20kV to 4kV) turns ratio, 0.01pu leakage reactance, base operating frequency of 2kHz, and 15MVA rating.

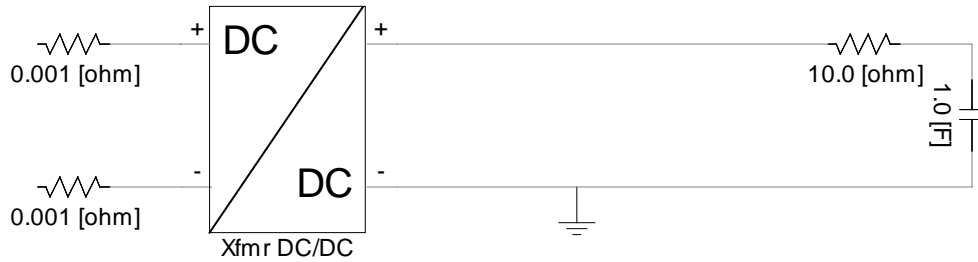


Figure 3.40. Closer look at the main to the simplified storage element

All of these pieces together make up the entirety of the MVDC infrastructure. A simulation of all the components operating with the central bus will be reported in Section 4.0 . The purpose of this section was simply to provide a more in-depth insight to how the components were tied together in the PSCAD environment.

3.4 MVAC INFRASTRUCTURE REALIZED IN PSCAD

The layout in PSCAD for the MVAC infrastructure is depicted in Figure 3.41. The first detail to be noticed is that there are fewer power electronic converters necessary to attach all of the generation sources and loads to the main AC bus. However, at every point a transformer is needed as a connector between the different AC voltage levels. A second detail of note is the equipment required to attach the PV array to the main AC bus. A DC/DC converter, DC/AC inverter, and finally a transformer is all that is required to convert the original DC power to its final form as AC power on the main AC bus. In the analysis performed in Section 4.0 it will also

be seen that a large amount of power is lost across these three conversion processes. This is largely due to the types of converters chosen and will certainly be a point to investigate in the future development of this infrastructure. As in the MVDC discussion section, each section from source to bus or bus to load will be looked at more closely.

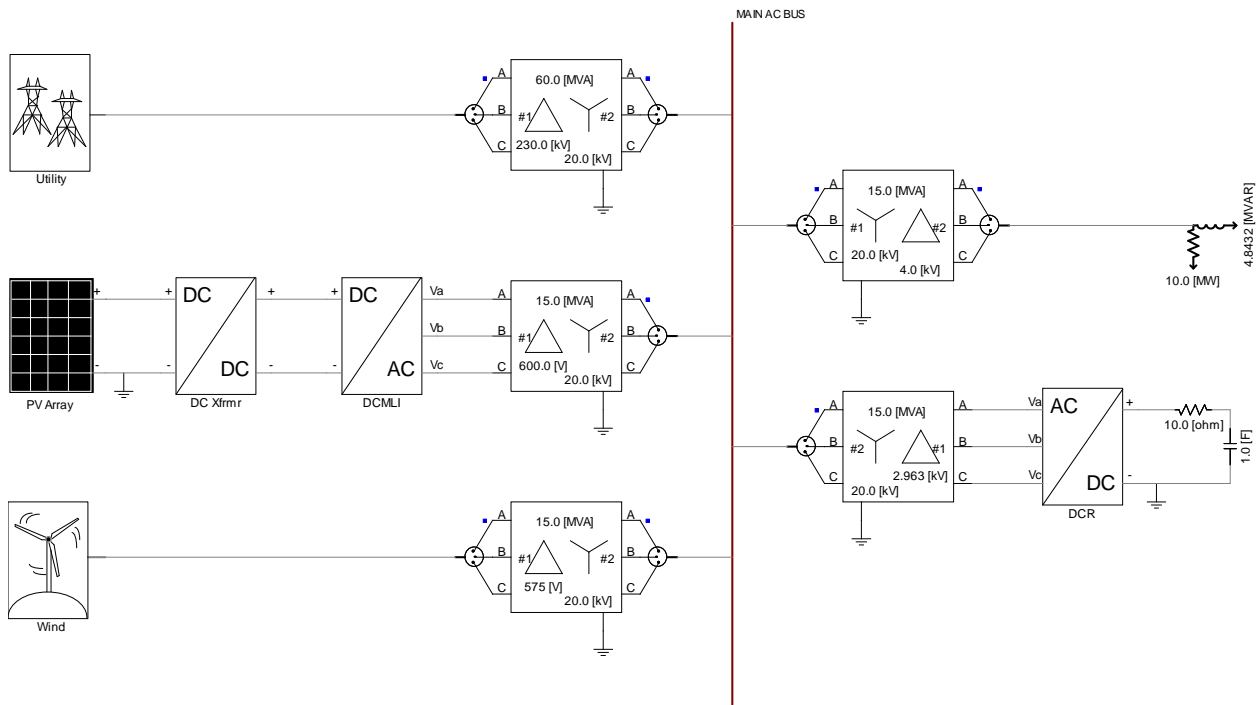


Figure 3.41. Final PSCAD layout of MVAC infrastructure

To prevent a large amount of repetition, all of the sources and loads used in the MVAC infrastructure are identical to those discussed previously in the MVDC infrastructure in the previous section. The only differences are how those sources and loads are attached to the main bus, which is now AC. Also, all of the transformers contained in the figures between Figure 3.42 to Figure 3.46 are 60Hz and have a leakage impedance of 0.01pu. The differences lie in turns ratios and MVA ratings, which can be seen in the figures, but will be repeated in text if the parameters happen to appear illegible and difficult to read.

Starting with the connection from the utility to the main AC bus in Figure 3.42, the transformer has a rating of 60MVA and a turns ratio of 11.5:1 or 230kV to 20kV. The transformer was configured in a delta-wye connection.

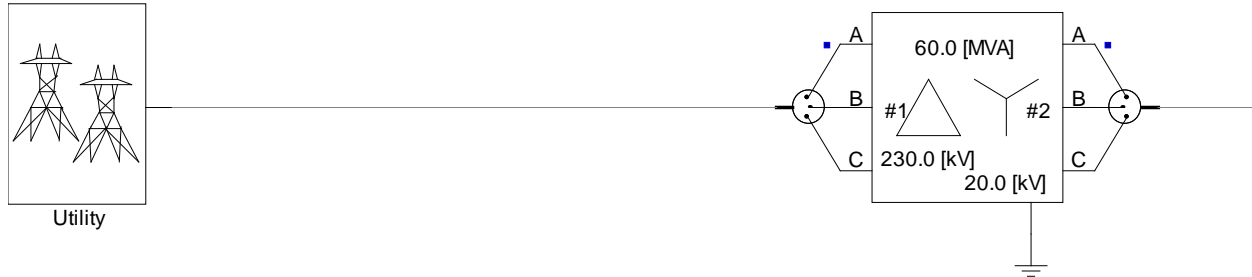


Figure 3.42. Closer look at Utility to the main bus

The PV array, as mentioned earlier, proved to be difficult to connect to the main AC bus. The problem lied in the DC/AC inverter portion of Figure 3.43. The DC/DC converter attached to the PV array itself was similar to that used in the MVDC setting with the only difference being a turns ratio of 1:2.5 (8kV to 20kV) due to the different output impedance that the converter saw.

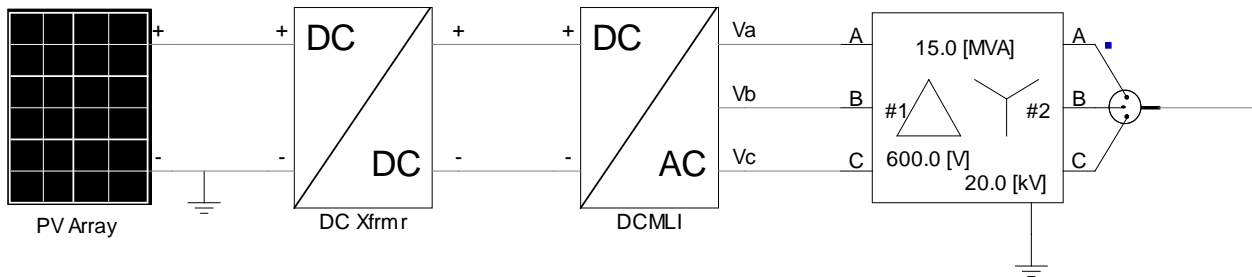


Figure 3.43. Closer look at PV Array to the main bus

Because of the lower amount of power being delivered by the PV array, a three-level diode clamped multilevel inverter was implemented in this setting instead of a five-level as used in the MVDC infrastructure. Also, a balancing circuit similar to that used on the five-level version was unnecessary since there are only two total capacitors in the three-level structure. It seemed that there was a large amount of interference to the inverter from the AC bus that caused a large disturbance and loss of power being delivered. A more in-depth analysis will be provided

in Section 4.2. Otherwise, the three-level DCMLI contained in the page module was the one discussed in Section 3.1.1. The transformer at the main bus tie-in had a 15MVA rating and a 1:33.33 or 600V to 20kV turns ratio. The configuration used for the transformer was a delta-wye.

In order to connect the wind generation source to the AC bus, only a transformer was necessary as seen in Figure 3.44. The transformer stepped-up the wind voltage level and matched it to the 20kV of the bus. The turns ratio was 1:34.78 (575V to 20kV), the rating was 15MVA, and lastly a configuration of delta-wye was employed.



Figure 3.44. Closer look at Wind to the main bus

As was the case for attaching the wind source to the bus, the AC load only required a step-down transformer to match the chosen voltage level at the load shown in Figure 3.45. The rating of the transformer was 15MVA, a wye-delta connection was used, and the turns ratio was 5:1 (20kV to 4kV).

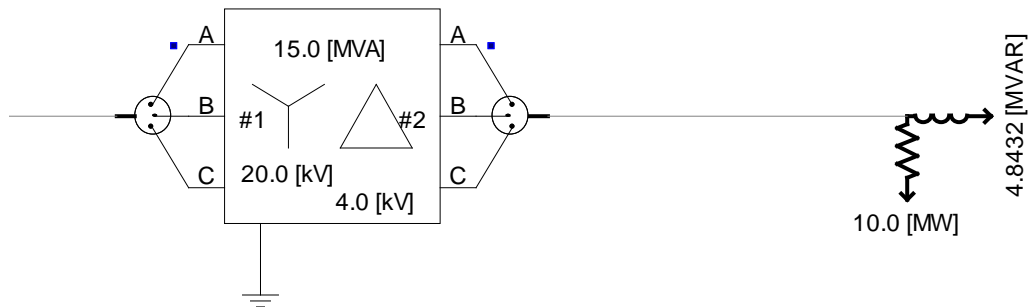


Figure 3.45. Closer look from the main bus to the AC load

As for the last remaining piece, the simplified storage model, a transformer and AC/DC rectifier seen in Figure 3.46 were required to provide power to it from the main bus. The rectifier is the same as that used in the MVDC case whereas the transformer had a rating of 15MVA, wye-delta connection, and a turns ratio of 1:6.75 (20kV to 2.963kV). The 2.963kV was needed to get a 4kV output from the rectifier seeing as the DC output is $1.35V_{LL}$.

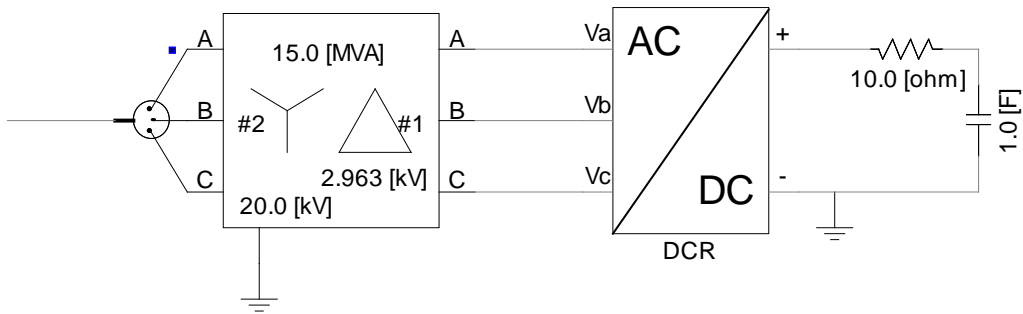


Figure 3.46. Closer look from the main bus to the simplified storage model

4.0 COMPARATIVE RESULTS OF THE SYSTEMS IN PSCAD

A base case for both the MVDC and MVAC systems are presented to use for comparison for various system faults. The fault cases themselves will then be analyzed and compared to determine the effects that occur and how the system responds. The comparison between the infrastructures will be based upon how each system reacts from its steady-state operation. The faults to be investigated are loss of generation and load faults. The effects of faults upon the main bus of either system will be the primary focus with an examination of responses that propagate through the system. Voltages and real power for the loads and generation were monitored and presented for each case. All voltage measurements shown are peak values unless noted otherwise. A table of the different generation sources and loads is provided in Table 4-1.

Table 4-1. Generation Sources and Loads

Generation Sources	Load Entities
Utility	Three-phase AC Load
Wind	Simplified DC Storage Load
PV Array	

4.1 MVDC SYSTEM AT STEADY-STATE

The fault simulations are subsequently carried out after the system had reached a steady-state initial condition for at least 0.5 second and all outputs are relatively constant. The voltage start-up on the 20kV bus can be seen in Figure 4.1. A closer look between the time of 0.6s and 0.7s, after the system had reached a steady-state, is shown in Figure 4.2. There is a small ripple present on the voltage but, with the passive filters present on the generation, especially the utility connection, this appears acceptable and may be further improved with better filtering techniques.

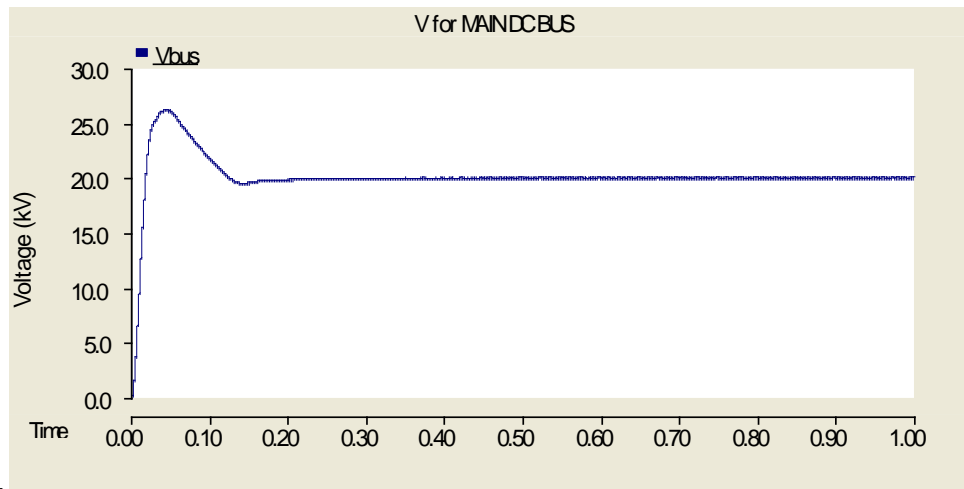


Figure 4.1. Voltage values on bus at steady-state

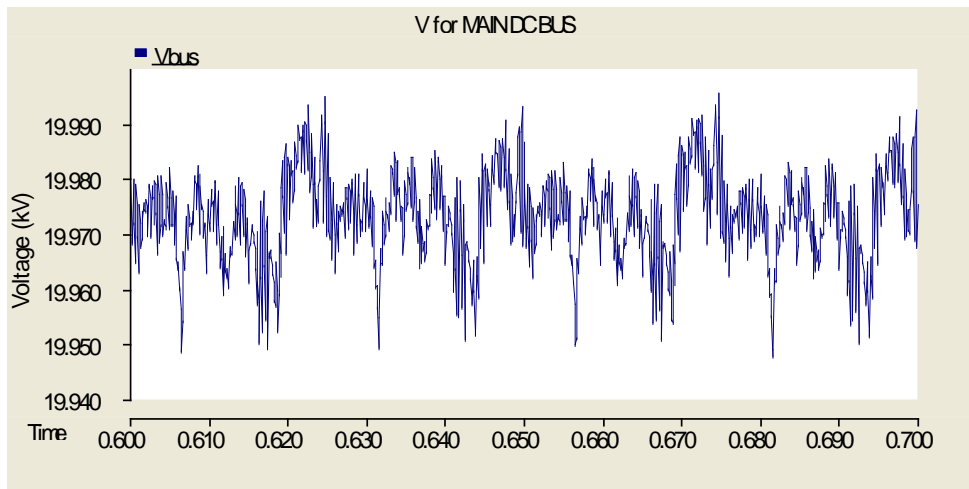


Figure 4.2. Zoomed-in version of steady-state voltage on the bus

The power flows for each element of the system can be seen on an individual basis in Figure 4.3. The curves entitled "Putil", "Pwind", and "Ppvarray" are supplying real power to the main bus. Loads "Pload" and "Pstorage" are consuming power. The responses shown in Figure 4.3 are helpful to observe the dynamics of each generation and load. The total generation at each source and load consumptions are shown in Figure 4.4. The power measurement for all of the generation sources was taken directly at the output of the source itself. That is, the utility was taken at the outputs of its block, the PV array at its output, and finally, the wind measurement at the inside of the wind block at the machine output. In a similar manner, the load power measurements were taken at the load itself. For an initial analysis and representation of the system with no faults, measurements were taken to show the total amount of generation being delivered to the bus and finally how much was actually consumed at the loads.

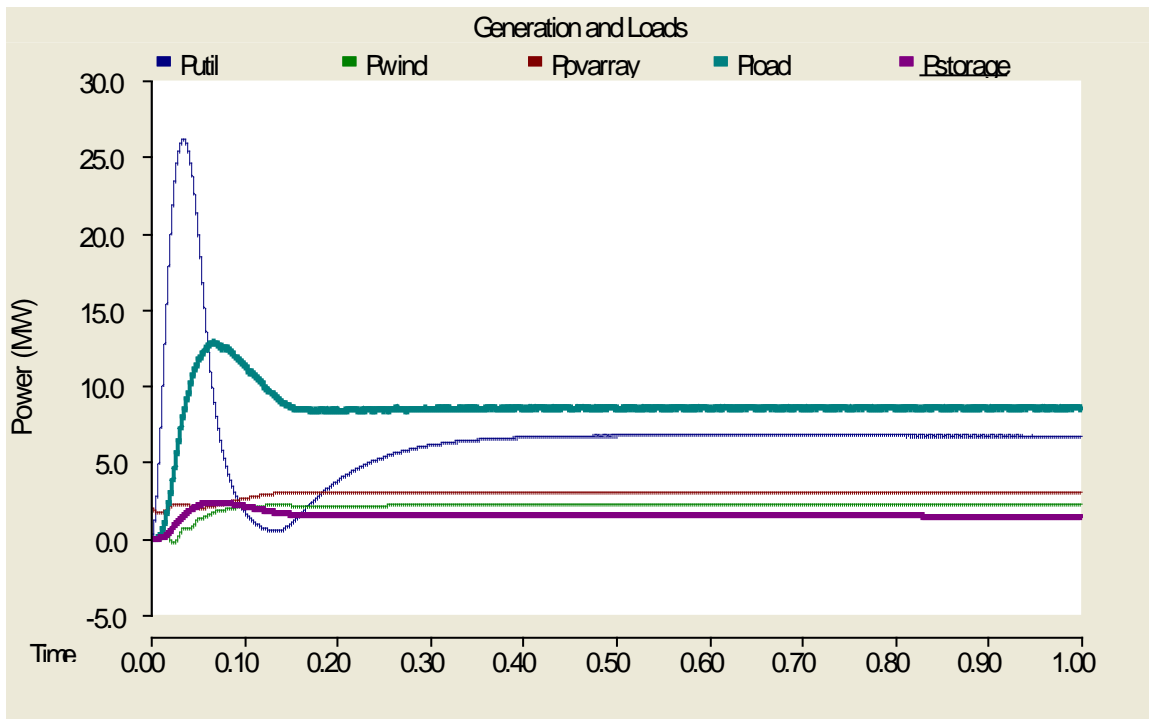


Figure 4.3. Real power flow for each section of the system

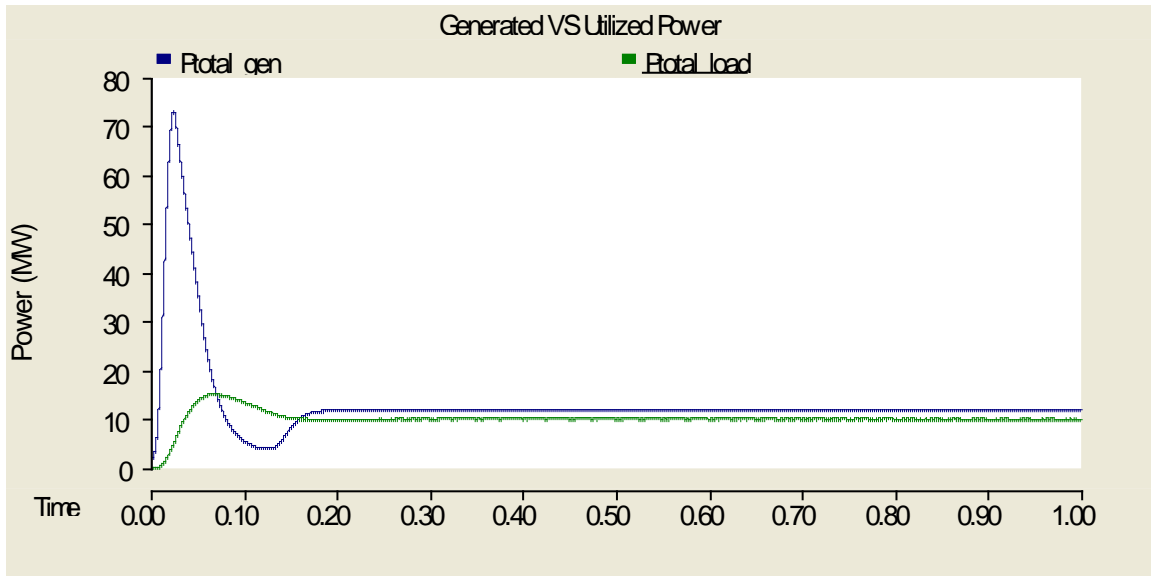


Figure 4.4. Total power generated and consumed at steady-state

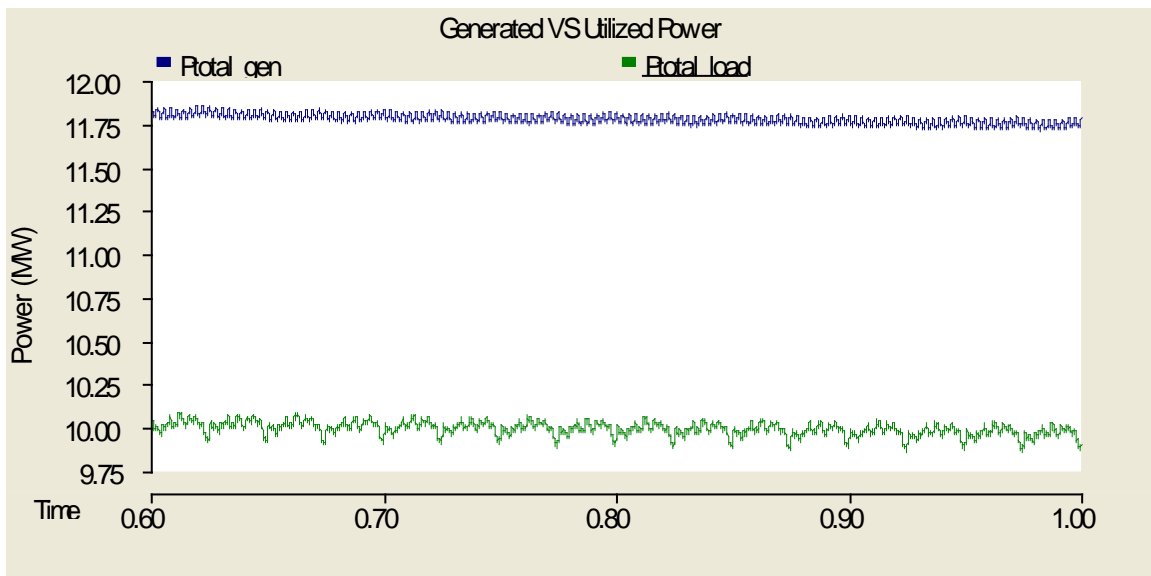


Figure 4.5. Closer look at steady-state duration in Figure 4.4

A closer look at each generation and load source will be taken again to discuss the losses and dynamics that occur going from the generation to the bus or from the bus to the load. The two loads will be discussed first. The curves in Figure 4.6 show the flow of power starting at the bus, entering the DCMLI, through the transformer, and ultimately at the load itself. It can be noted that during steady-state there was close to a 3MW loss of power going from the bus to the

load. Also, the load is rated for 10MW and was only delivered around 8.52MW. This is largely due to the unfiltered AC output from the DCMLI. The fundamental had a magnitude of about 11kV whereas an ideal value would be 14.14kV. Adjusting the transformer tap caused the load to be delivered the 10MW necessary, but the loss actually increased to 4MW and this solution is far from ideal. A more advanced control scheme to control the DCMLI as well as to balance the voltages across each of the input capacitors would very likely increase the efficiency a noticeable amount. An AC filter at the output would help as well to smooth the waveform and eliminate the harmonic content.

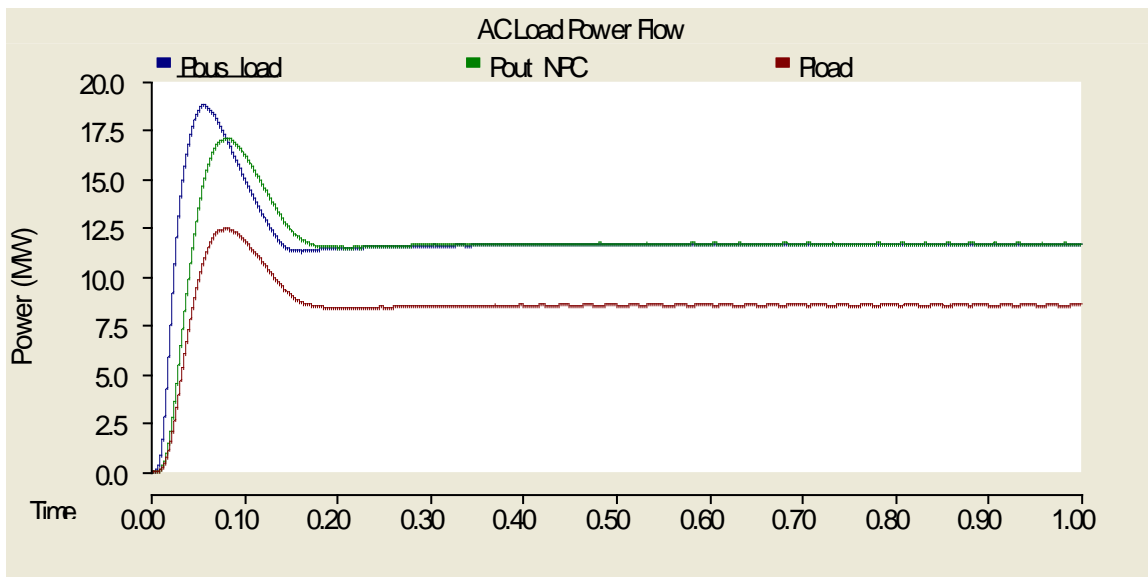


Figure 4.6. Measurement of power for the AC load from the bus to the load itself

The power flow from the bus to the storage load is shown in Figure 4.7. An initial spike in power was due to the charging of the input filter capacitor on the DC/DC converter followed by a bit of an overshoot causing power to be sent back to the bus where finally a steady-state was reached. The voltage measured at the storage load was as expected upon reaching steady-state and is shown in Figure 4.8.

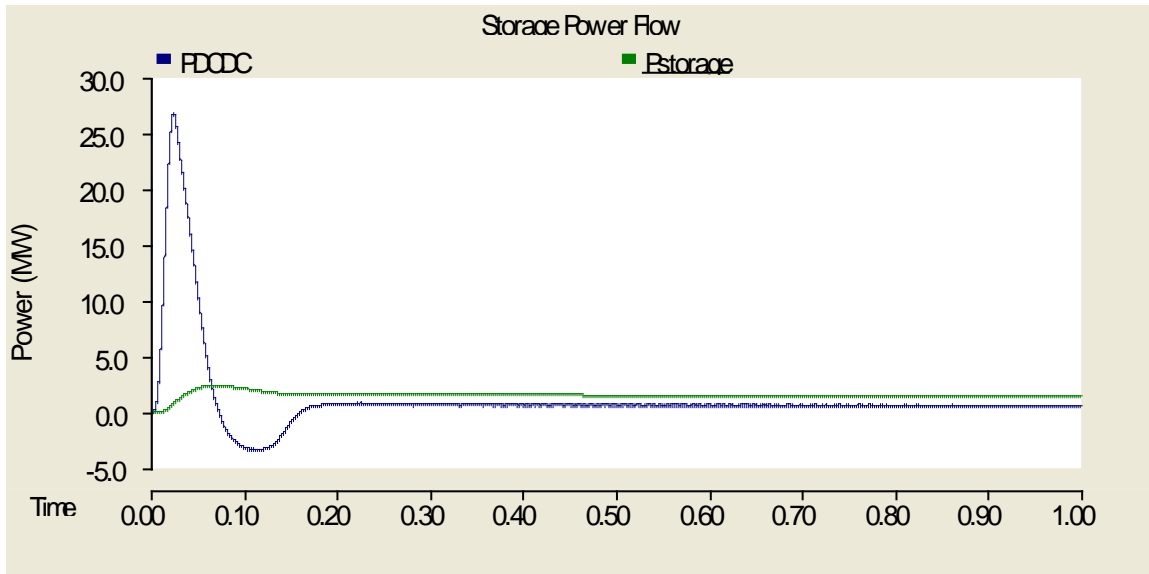


Figure 4.7. Total power flow from the main bus to the storage load

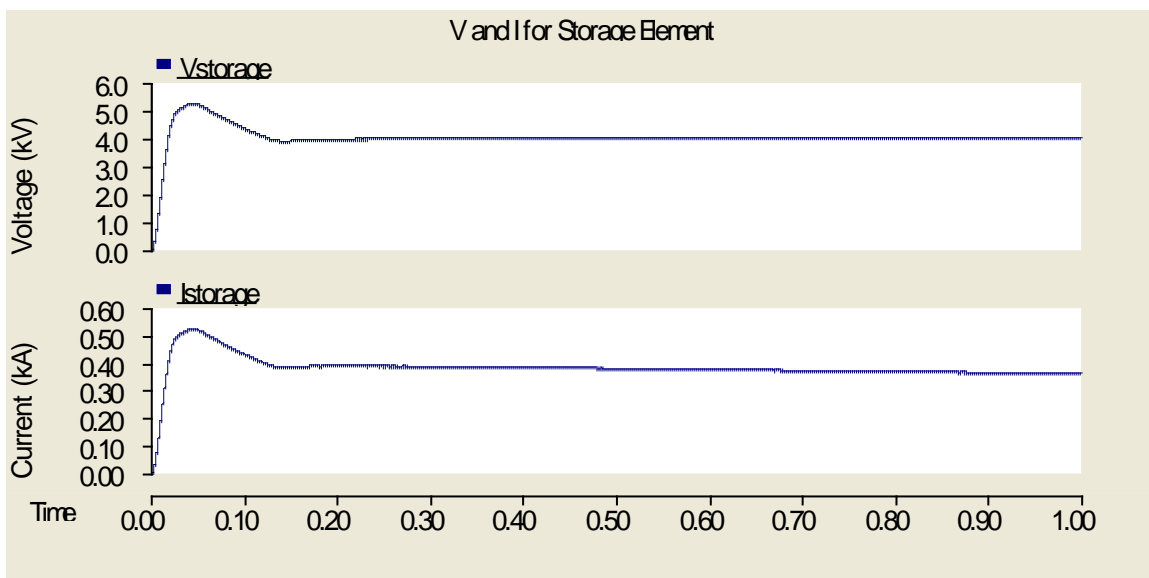


Figure 4.8. Voltage and current present at the storage load

Moving on to the power flows for each of the generation sources, the power supplied from the utility to the main DC bus appeared to have very little loss traveling through the transformer, being rectified, and finally reaching the bus as seen in Figure 4.9. Upon closer inspection in Figure 4.10 at steady-state between 0.6s and 1.0s, it seems as though the capacitance of the output filter for the rectifier is supplying a bit of power in the area of 30kW.

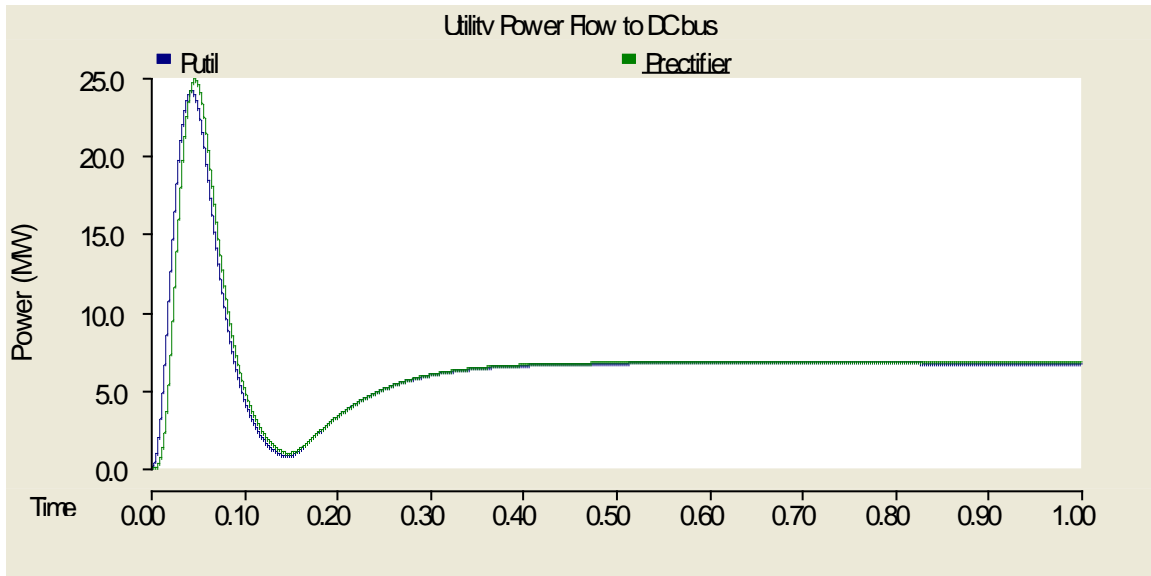


Figure 4.9. Power flow from utility to the DC bus

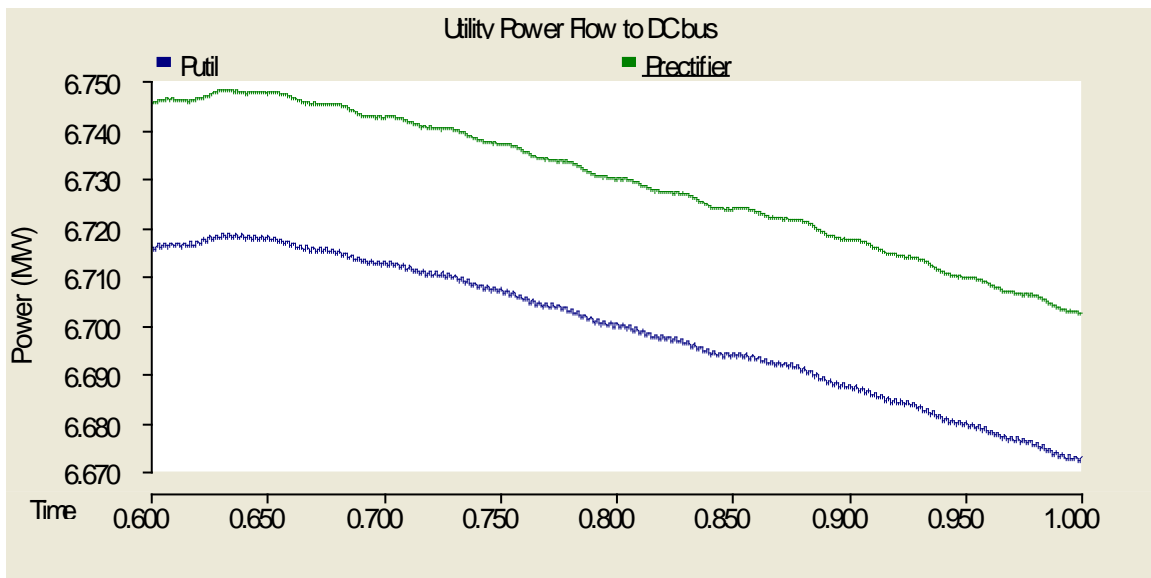


Figure 4.10. Close up of Figure 4.9 from 0.6s to 1.0s

As was already seen in the case of the DC/DC converter attached to the storage load, the DC/DC converter that connects the PV array to the bus experiences a supply of power from the bus to charge the output filter capacitor before finally reaching a steady-state value. This can be seen in Figure 4.11. The transient eventually settled and the power delivered to the bus was

slightly more than what the PV array actually produced, most likely due to the capacitance present.

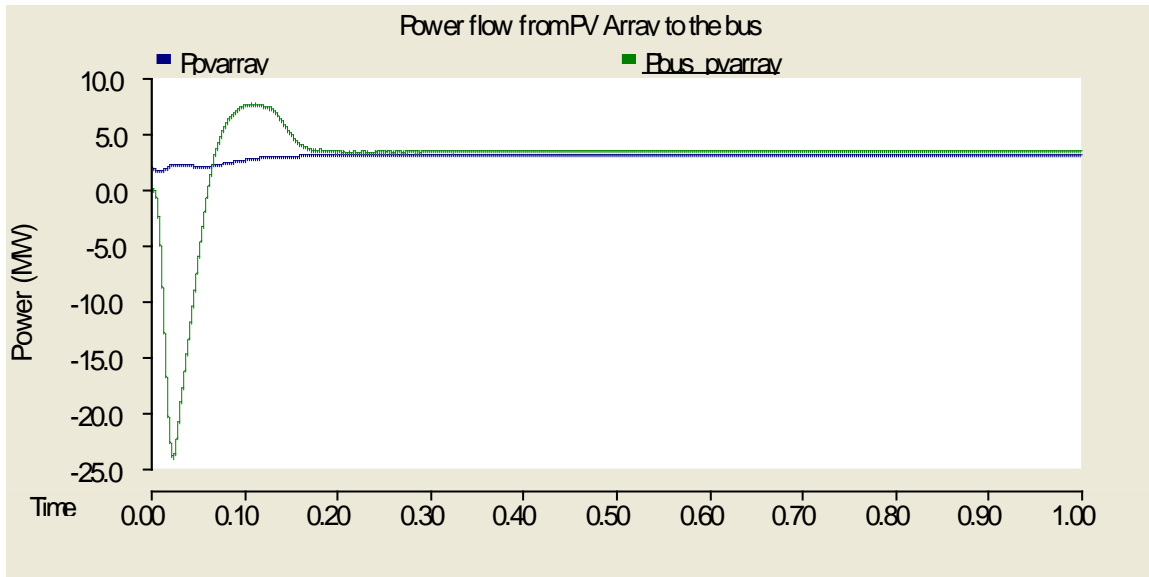


Figure 4.11. Power produced and delivered to the bus

Lastly, the dynamics of the wind source are presented in Figure 4.12. To clarify, the curve "Pwind" was measured at the output of the induction machine within the wind page module block, "Pwind_grid" was measured at the output of the source that was connected to the induction machine to provide it with reactive power, and "Pbus_wind" was measured after the rectifier where the main bus is connected. The summation of "Pwind" and "Pwind_grid" results in the curve of "Pbus_wind". At the start of the simulation, the source providing reactive power has an initial spike of power delivered, which has been seen in many other cases already. This spike was most likely due to capacitance and inductance throughout the system. After the transient subsides, it can be seen in Figure 4.13 that during steady-state operation the source actually draws a bit of power from the wind/induction machine resulting in about 2.075MW finally making it to the bus for use by the loads.

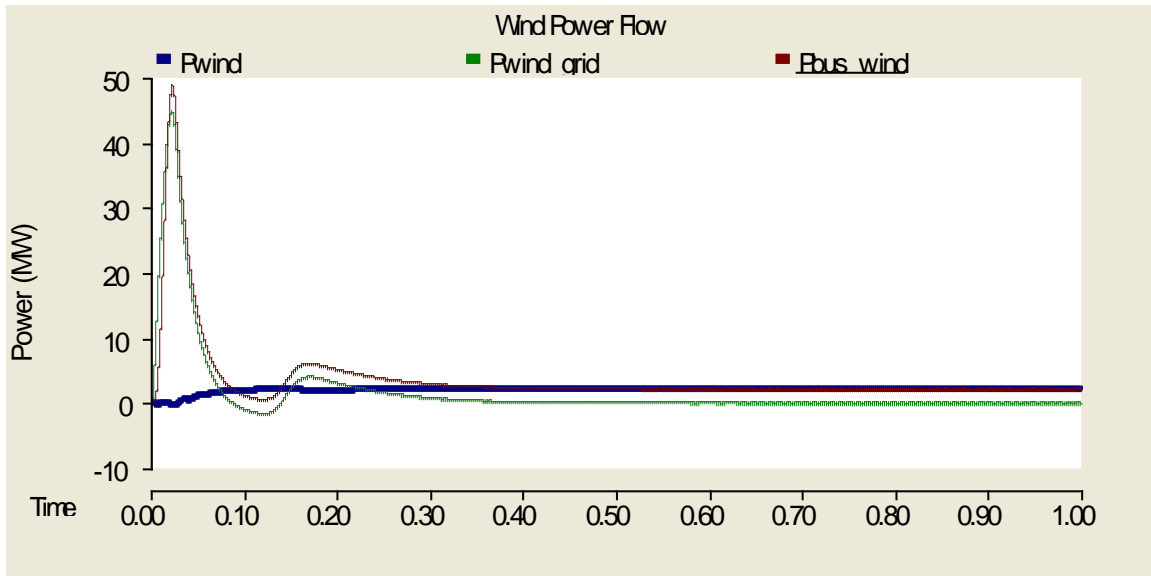


Figure 4.12. Power from wind delivered to the main DC bus

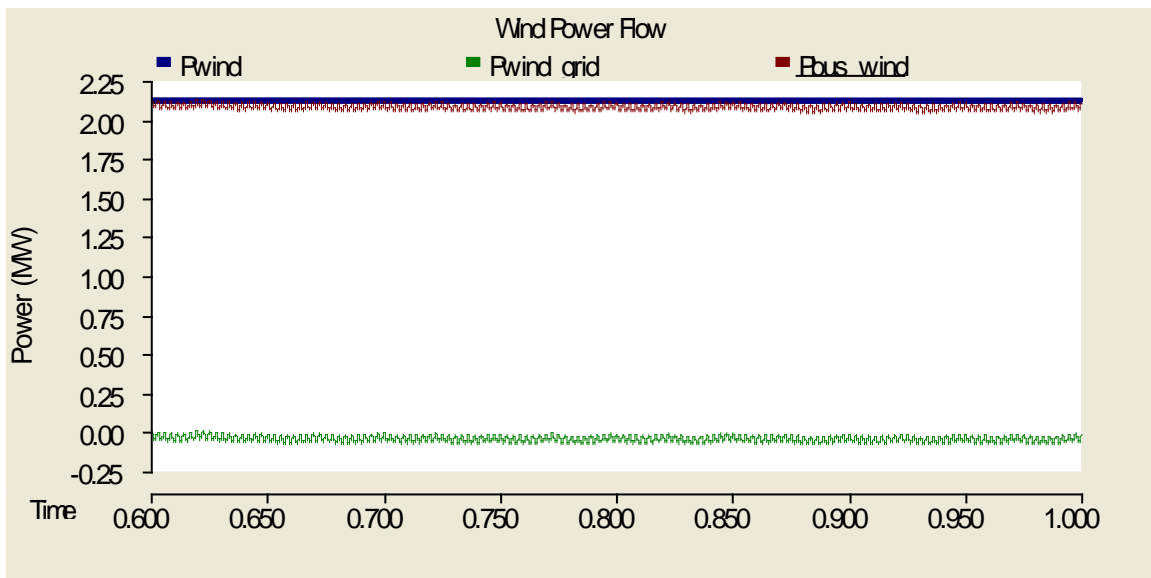


Figure 4.13. Closer look at steady-state portion of Figure 4.12

After looking through the power generated and power losses for each component of the entire MVDC system, a better understanding of the dynamics that occurred in Figure 4.3 and Figure 4.4 was made. It appears that the extra generation that was required in Figure 4.3 was due to the losses experienced while moving from the main DC bus to the AC load where about 3MW were lost. Coupling this with the power gains from capacitors in the case of the PV array and the

storage load, the overall loss balances out to around 1.8MW. The main contributors to this loss are the control schemes used for the converters throughout the circuit as well as simple passive filters at the input and output of most of the converters.

4.2 MVAC SYSTEM AT STEADY-STATE

With a steady-state case established for the MVDC system, the next step will be to do the same for the MVAC system. The same approach will be taken with plots of real power flow and any other important voltages and currents that are noteworthy. The power flow will be outlined for the two loads and then for each of the three generation sources.

Firstly, the peak, line-to-line voltages that appear on the main AC bus once the system has reached a point of steady-state operation are shown in Figure 4.14. The voltages appear slightly below ideal due to the ripple and overall jagged nature of the sine waves. A closer look at the imperfect peaks of each phase voltage can be seen in Figure 4.15.

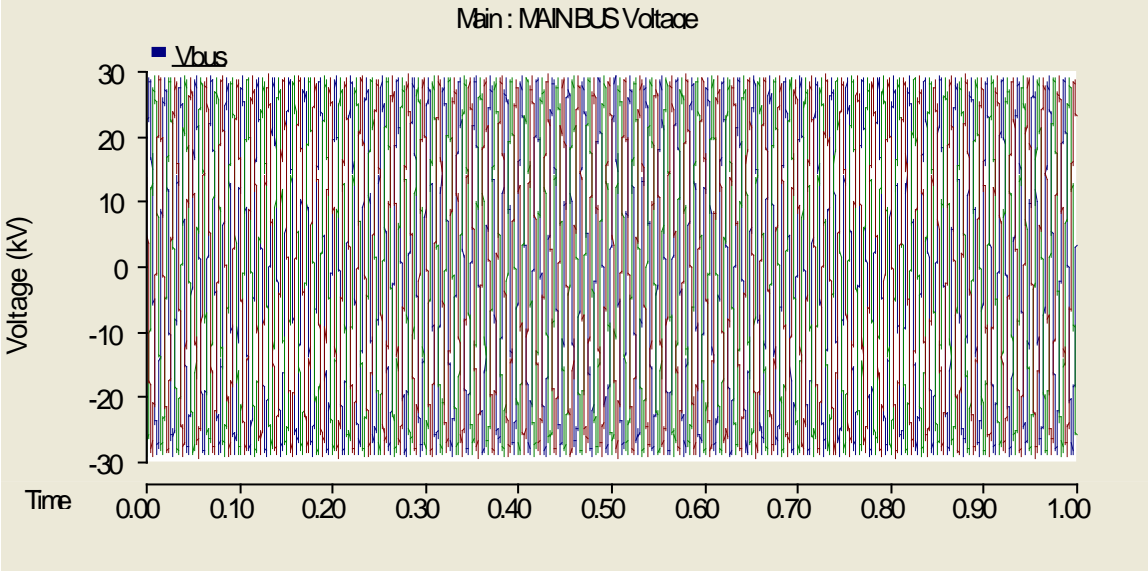


Figure 4.14. Voltage on the AC bus during steady-state

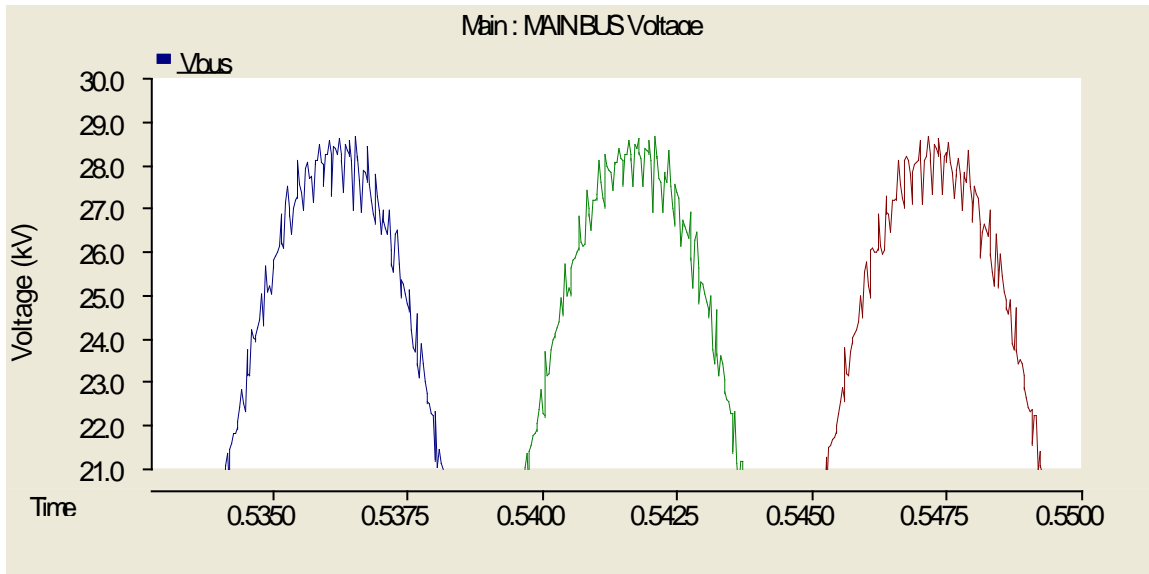


Figure 4.15. Closer look at the peaks appearing in Figure 4.14

The ripple present overtop the main AC bus voltage is caused by the diode clamped multilevel inverter connected to the PV array generation source. More specifically, the choppy, unfiltered output would then affect the voltage appearing on the main AC bus. A filter applied at the output in the future would very likely remedy this problem but, since the ripple was relatively small, it was ignored.

The power flow for the whole system on an individual basis for each source and load is shown in Figure 4.16 whereas the total generation from all sources and the total consumption from all loads are depicted in Figure 4.17. The generation measurements were all taken directly on the output terminals of the source itself. The same can be said for the loads. The measurements were taken directly before the loads. A quick look at Figure 4.17 shows that there was a loss during the transmission process going from the generation to their ultimate destinations at the loads. The specific causes and locations of these losses will be addressed later on in this section.

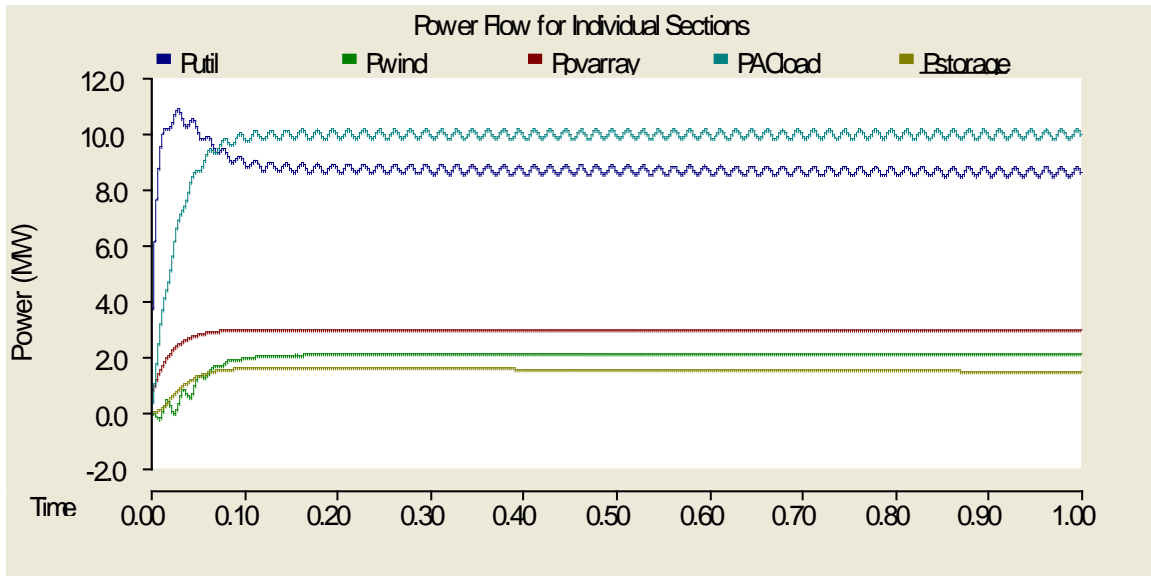


Figure 4.16. Power being supplied and consumed by the generation and loads individually

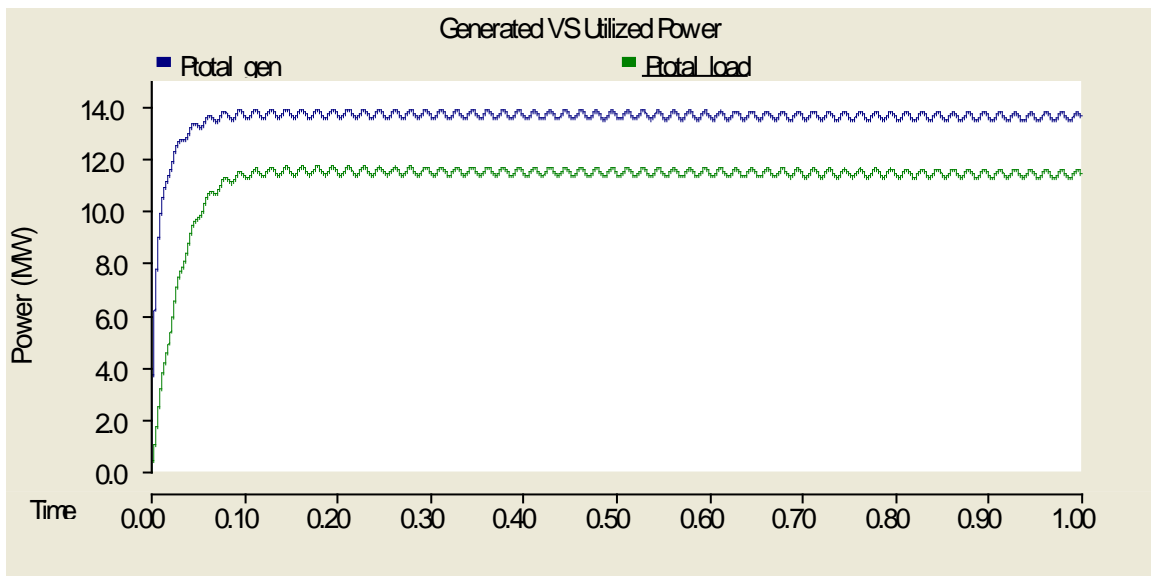


Figure 4.17. Total generation and load consumption for the system

Starting at the loads, the power delivered from the bus to the AC load is depicted in Figure 4.18. The only conversion that the AC load power experienced was going through a transformer to achieve the correct voltage level necessary. The losses were very small with the efficient transformer used in the system when going from the bus to the AC load. The curves

appear practically overlapping in Figure 4.18. To emphasize how small the losses were, a closer look at the curves during steady-state is shown in Figure 4.19.

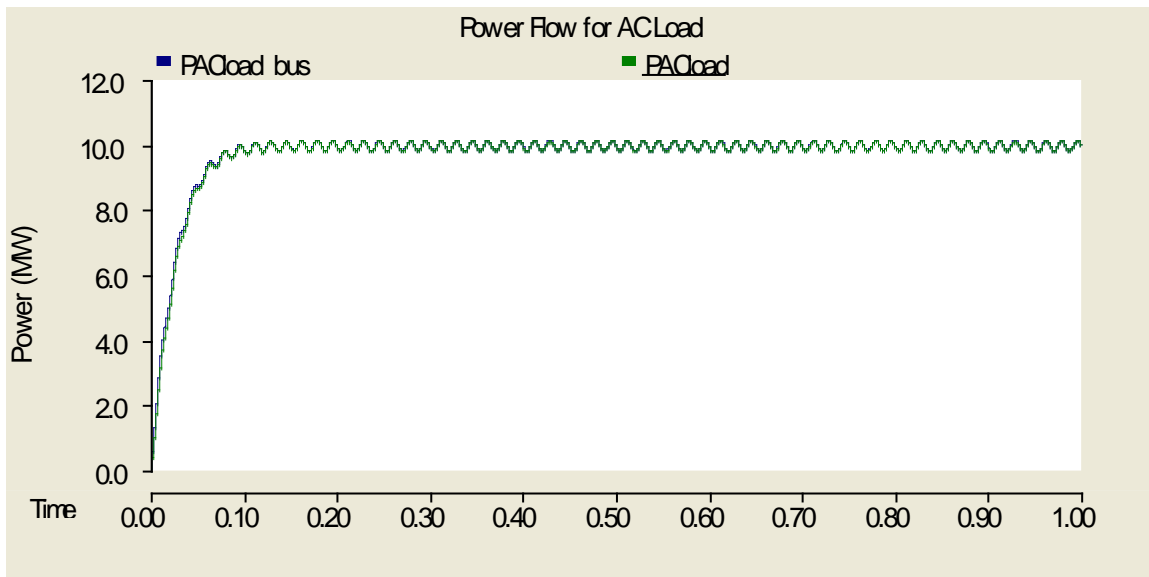


Figure 4.18. Power flow from the bus to the AC load

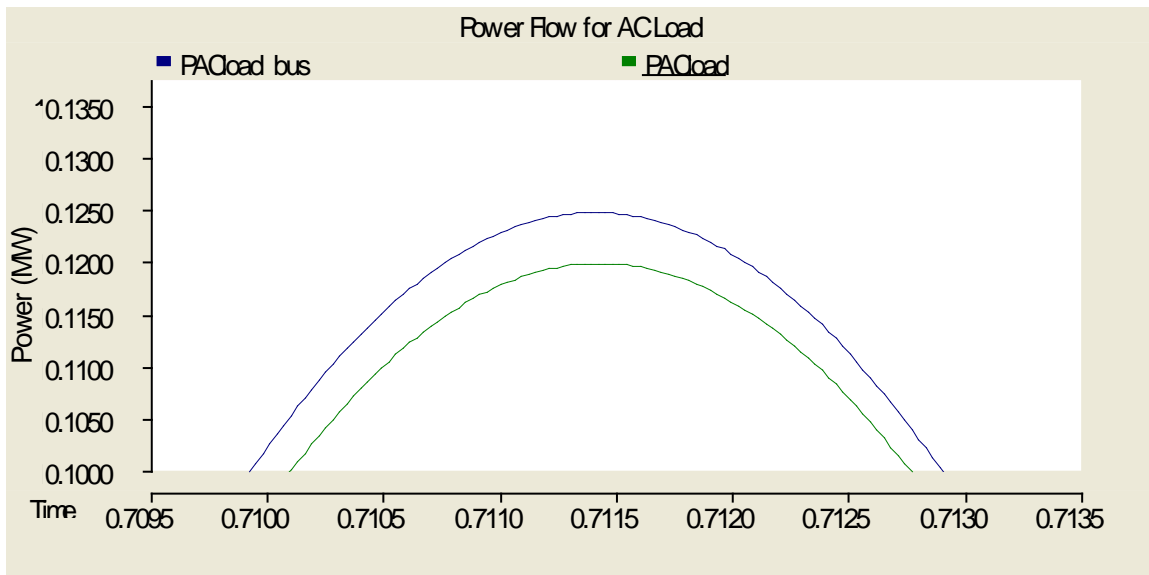


Figure 4.19. Closer look at Figure 4.18 to emphasize small losses of transformer

The other load, the simplified storage model, sees a similar transfer of power. The power flow from the bus and the power delivered to the storage load itself is shown in Figure 4.20. The power that appeared at the bus and after the transformer was virtually identical, so only the

power that was present on the bus is shown. As was the case with power flowing through the transformer, there was hardly any power lost through the rectifier circuitry. The voltage and current that was seen at the storage load is shown in Figure 4.21. A zoomed-in version to identify the ripple is shown in Figure 4.22. It can be seen that after going through the rectifier and the output filter, the voltage and current were relatively free of any large ripple and satisfactory.

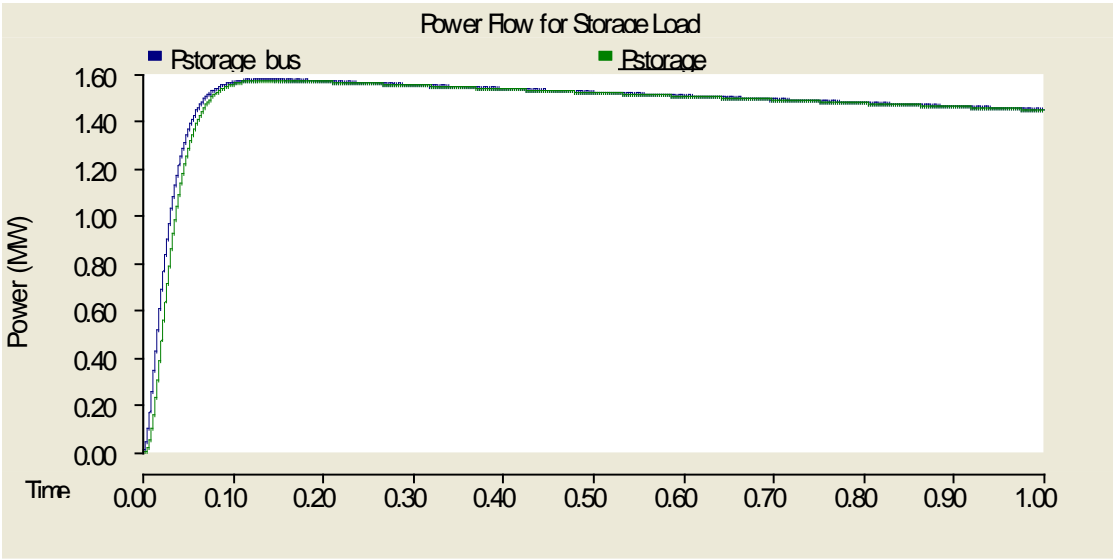


Figure 4.20. Power flow from the main bus to the storage load

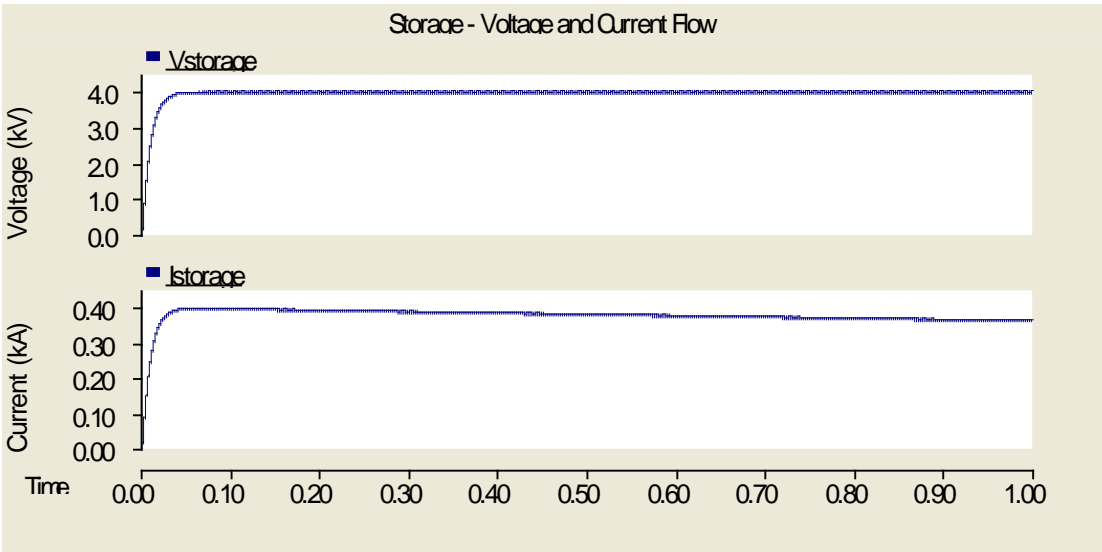


Figure 4.21. Voltage and current values appearing at the storage load

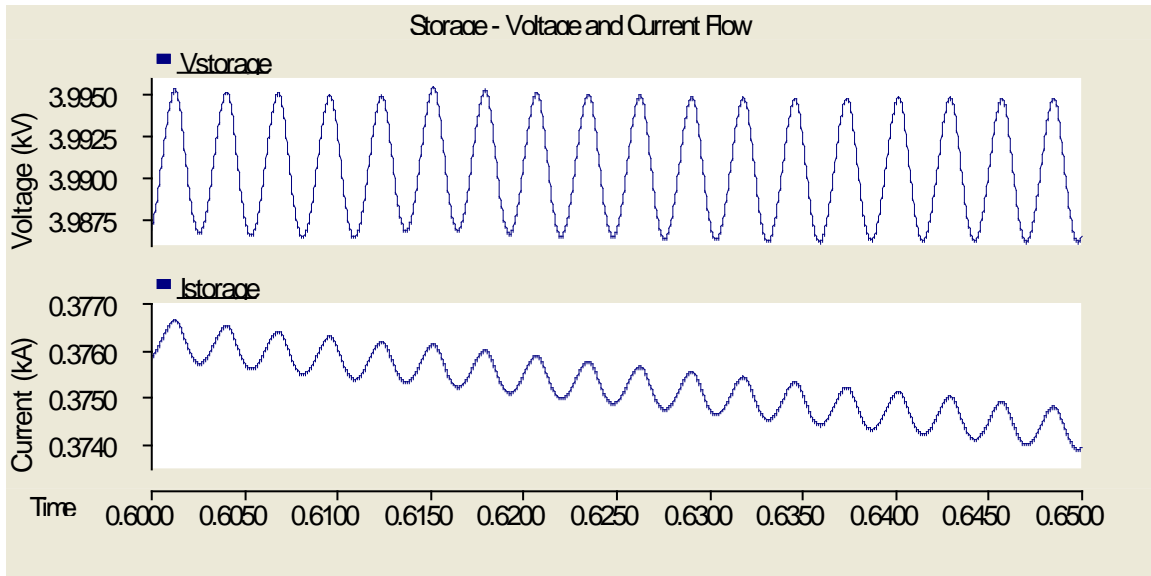


Figure 4.22. Closer look at the ripple present on the curves in Figure 4.21

The loads have been discussed and now the generation sources will receive the same treatment starting with the utility source. As discussed earlier with the AC load power transfer, a very small loss occurs across the transformer that connects the utility source to the main bus. The power at the terminals of the utility source and the power appearing at the bus are shown in Figure 4.23. Nothing further will be discussed on the utility generation.

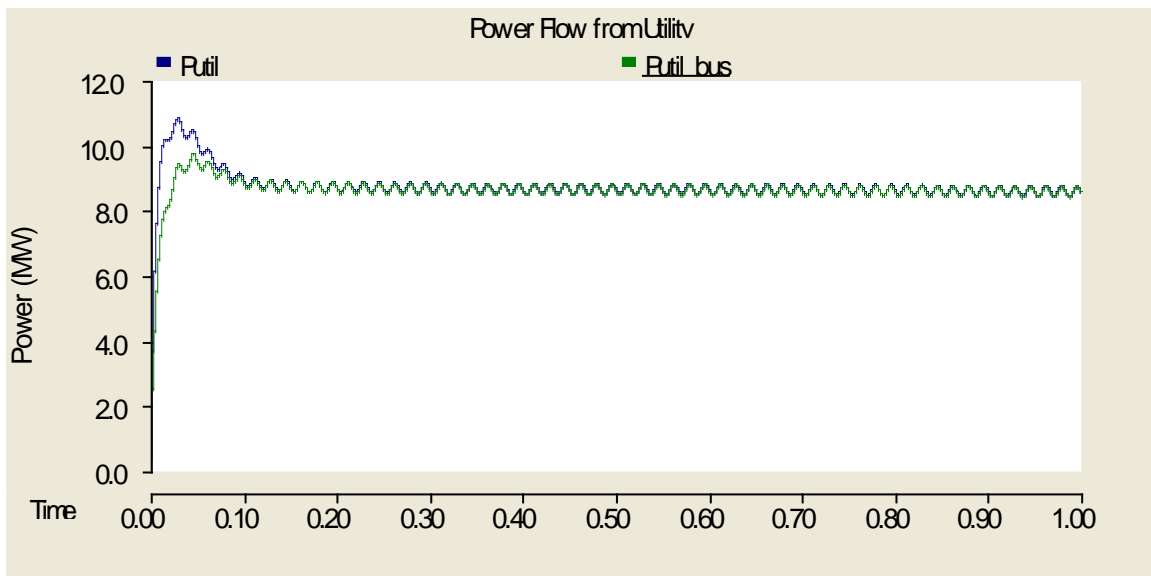


Figure 4.23. Power flow from the utility to the bus

The PV array source was the most interesting to observe since it involved power electronics and was the only DC power source being connected to the main AC bus. The power at important points starting at the output of the PV array and ending at the main bus can be seen in Figure 4.24.

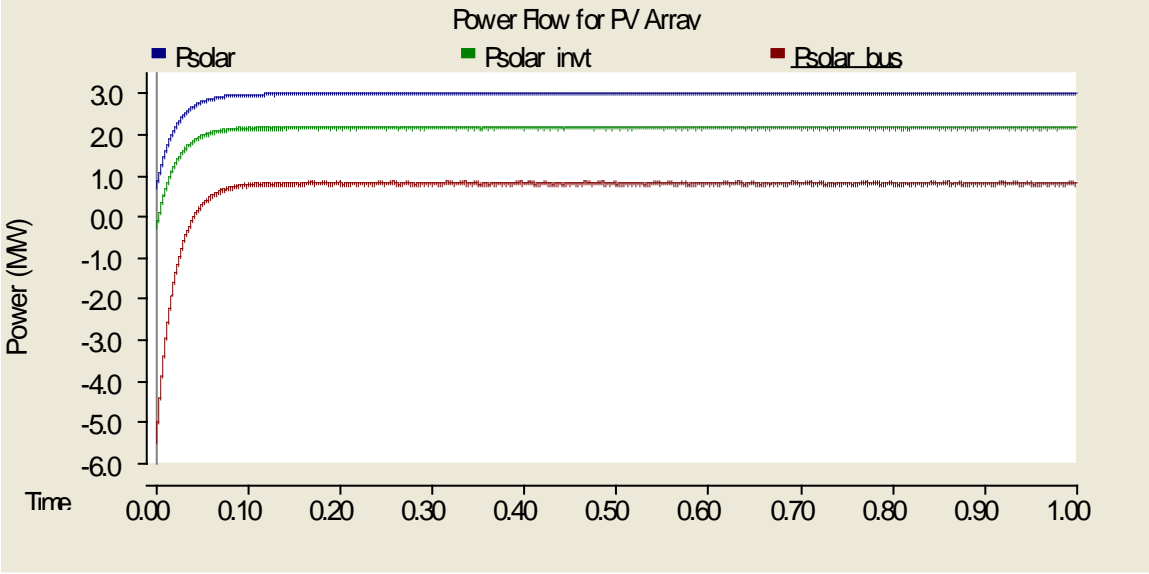


Figure 4.24. Power flow from the PV array to the bus

For clarification, "Ppvarray" was the measurement at the output of the PV array, "Ppvarray_invt" was at the input of the DCMLI, and "Ppvarray_bus" was the output of the transformer connected to the AC bus. At steady-state, it can be seen that the PV array was producing very close to the expected 3MW of power generation. However, the power that made it to the bus for use by the loads was only around 0.785MW. It can therefore be concluded that a large amount of loss was incurred going from the PV array to the bus. Starting with the 3MW generated from the PV array, there was about 1MW lost in the DC/DC converter, which left 2.13MW being sent to the DCMLI. Approximately 1.4MW was lost in the DCMLI resulting in the final value of 0.785MW. Looking at Figure 4.24, at the start of the simulation there was power being supplied to the DCMLI. This value eventually becomes positive, delivering power

from the PV array but it seems as though the output of the DCMLI was being affected by the AC voltage present on the bus. The power that was initially being supplied to the PV array section of the system from the main bus eventually becomes smaller than the 2MW coming from the DC/DC converter but still has a significant impact on the final power value coming from the PV array. In the future, different types of voltage converters will be investigated to better extract the maximum amount of power, with minimal losses, from the PV array.

Lastly, the wind generation source has a similar setup as the utility with only a transformer in place to convert the voltage level to the 20kV bus value. The power flow can be seen in Figure 4.25. The negative power being supplied to the wind was an effect of the induction machine starting transients and the power flow quickly arrived to a steady-state value with little loss across the transformer.

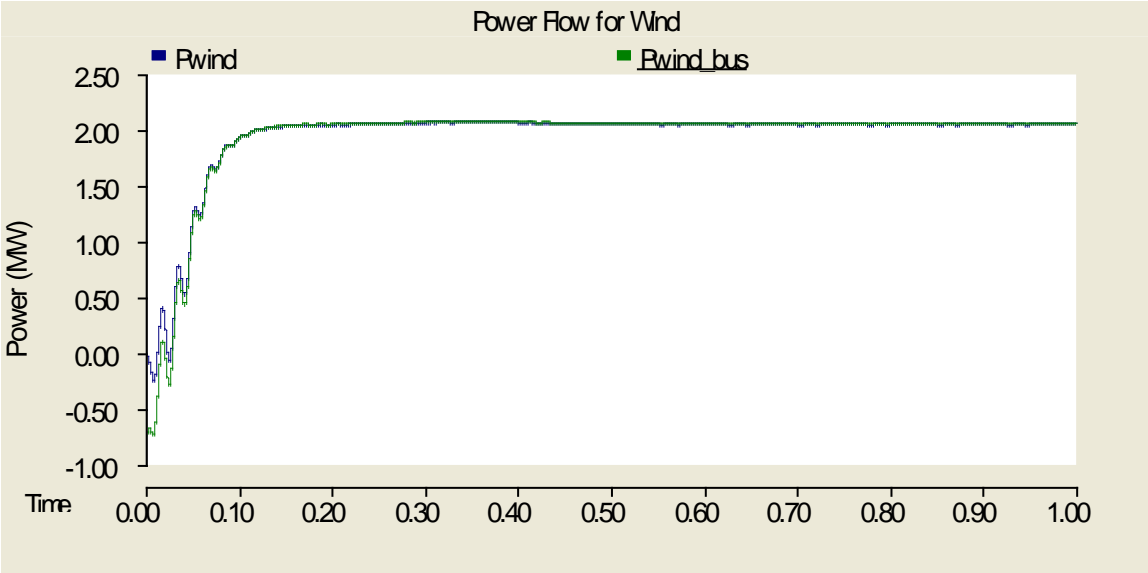


Figure 4.25. Power from wind source to the AC bus

With all of the power flow for the components presented and analyzed, it can be deduced that most of the loss that was originally shown in Figure 4.17 was from more than 2MW of loss from the PV array conversion process. These converters will be changed or altered in the future

to lessen these losses but for sake of a one-to-one comparison with the MVDC system, the converters were left alone instead of investigating better options.

4.3 COMPARISON OF SYSTEMS DURING FAULTS

The steady-state operation for the MVDC and MVAC systems has been discussed and analyzed in the previous section. A set of different faults can now be applied to determine whether each system is able to recover from the faults and also what transients occur. Before applying the respective fault, the systems were left alone to reach steady-state until the initial transients had passed. For both systems, this time was 0.6s. Two types of simple faults were chosen to investigate. These were loss of generation and load faults. Loss of generation implies simply that a specific generation source that been lost in some way and is now providing zero power to the system. The load fault was carried out by shorting both loads, one at a time, with a small resistance of 0.001Ω to ground. This was done with the components shown in Figure 4.26. Also, the "Fault ON resistance" used in PSCAD was $1.0e9\Omega$. A time was specified for when the fault would occur as well as how long it would take to clear it. A time of 0.2s was chosen for how long the fault would last for the cases and the fault was set to be able to clear any current that was present. For the most part, the goal was to determine whether or not the system could recover back to its original steady-state operation after the fault was cleared. A brief analysis will be given for each case pertaining to why certain changes occurred. Not all of the analysis may be spot-on since it was sometimes difficult to pinpoint exactly what caused specific transient responses.

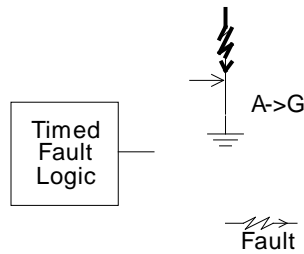


Figure 4.26. Components used to apply single and three-phase faults

4.3.1 Loss of Generation

Each source of power generation, one at a time, was removed from the system to observe what effects this had on the main bus and how the other components in the system reacted. Focus was placed on the voltage appearing on the main bus and how the flow of power altered depending on what source of generation was lost.

4.3.1.1 PV Array – MVDC System

The first case investigated was the loss of the PV array power generation source for 0.2s. The effects of the fault may be seen in Figure 4.27, Figure 4.28, Figure 4.29, and Figure 4.30. The fault caused no major instability to the voltage on the bus seen in Figure 4.27. It can be seen in Figure 4.28 that the generation from the PV array dissipated following an exponential curve due to the capacitor present on the output of the DC/DC converter. As shown in Figure 4.29, a drop in delivered power resulted at the start of the fault, then a short recovery period to balance power supplied to loads, and lastly the power saw a slight overshoot before finally resting close to its original steady-state operation. The utility produced more power to account for the loss of the PV system according to the waveforms in Figure 4.30. Once the PV was returned, the utility reverted to producing its original value.

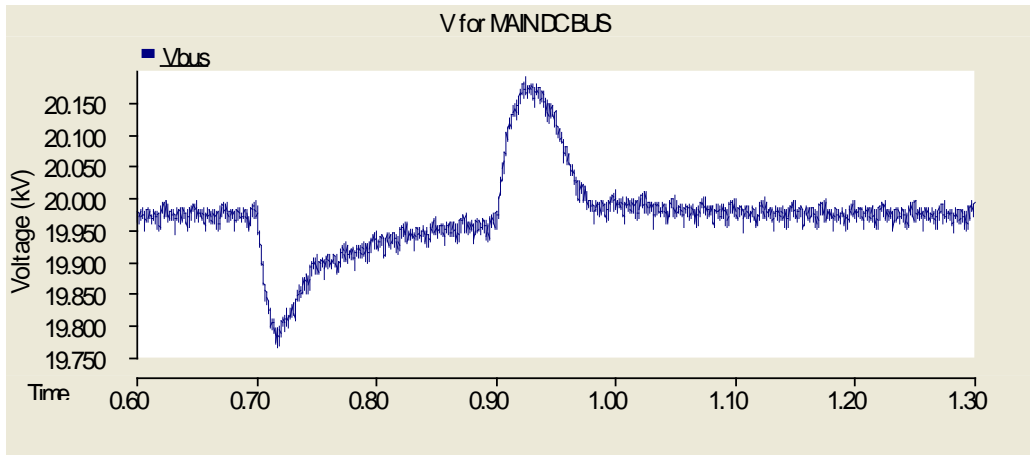


Figure 4.27. DC bus voltage during PV fault (MVDC)

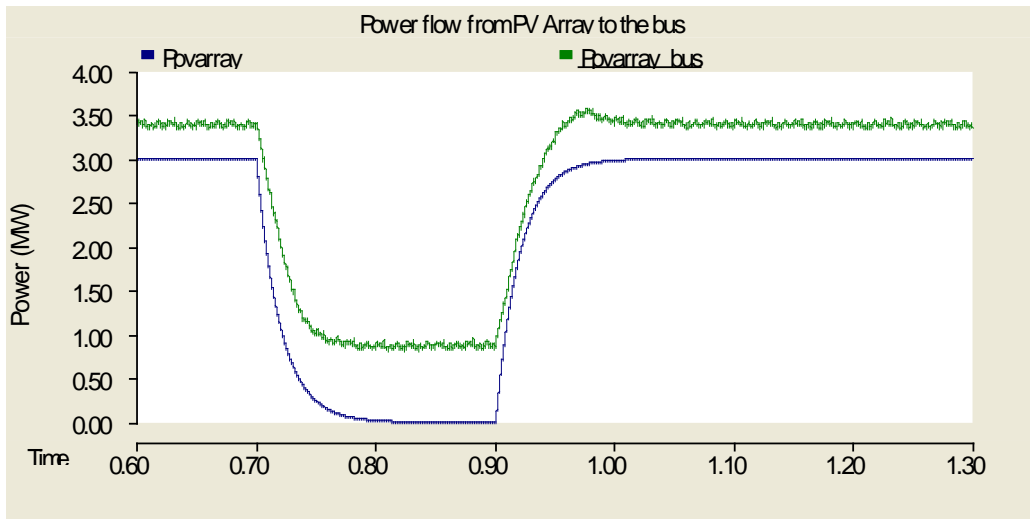


Figure 4.28. Power flow for PV array during PV fault (MVDC)

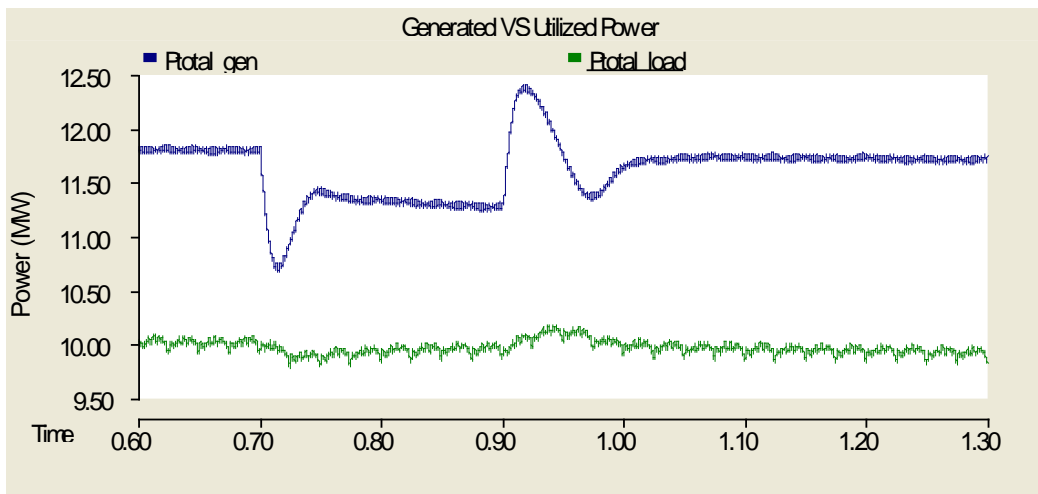


Figure 4.29. Power flow of the whole system during PV fault (MVDC)

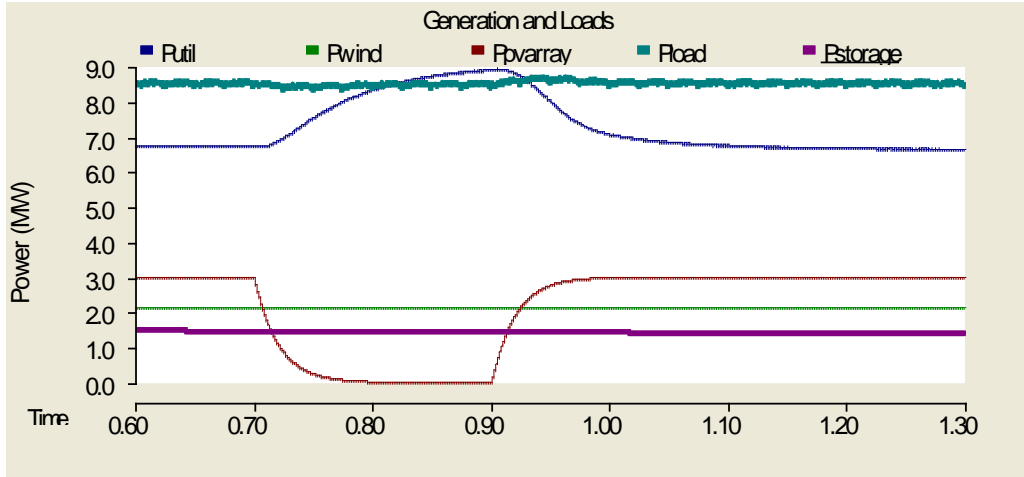


Figure 4.30. Power flow for loads and sources during PV fault (MVDC)

4.3.1.2 PV Array – MVAC System

The same fault to the PV array was applied in the MVAC infrastructure. The bus voltage, seen in Figure 4.31, was not affected by the fault. The power from the PV array reacted in the same way as in the MVDC case. There was an exponential charging and discharging of the PV array as seen in Figure 4.32. In Figure 4.34, the utility power generation increases to compensate for the loss of the PV array and then decreases once the PV array returned. The overall system returns to steady-state with relative ease and no large transients are present.

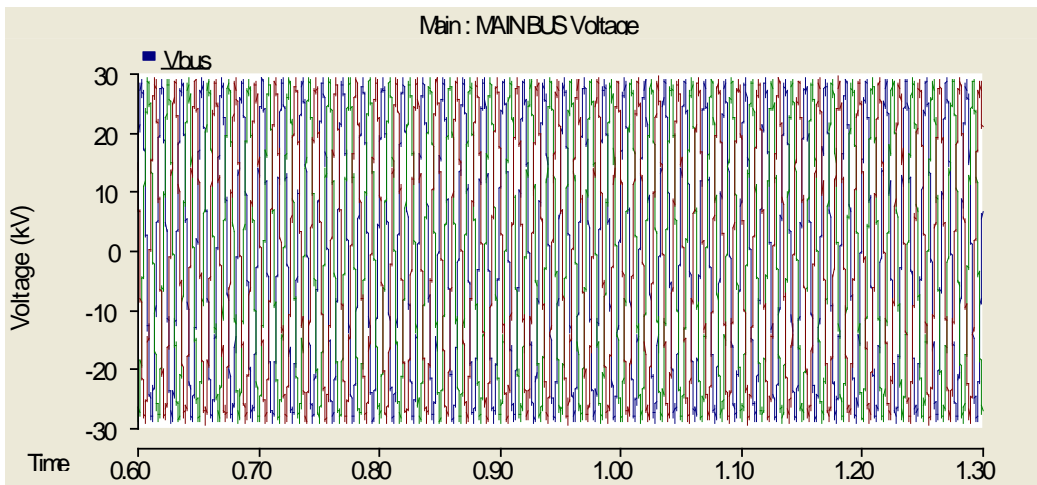


Figure 4.31. Voltage of the AC bus during PV fault (MVAC)

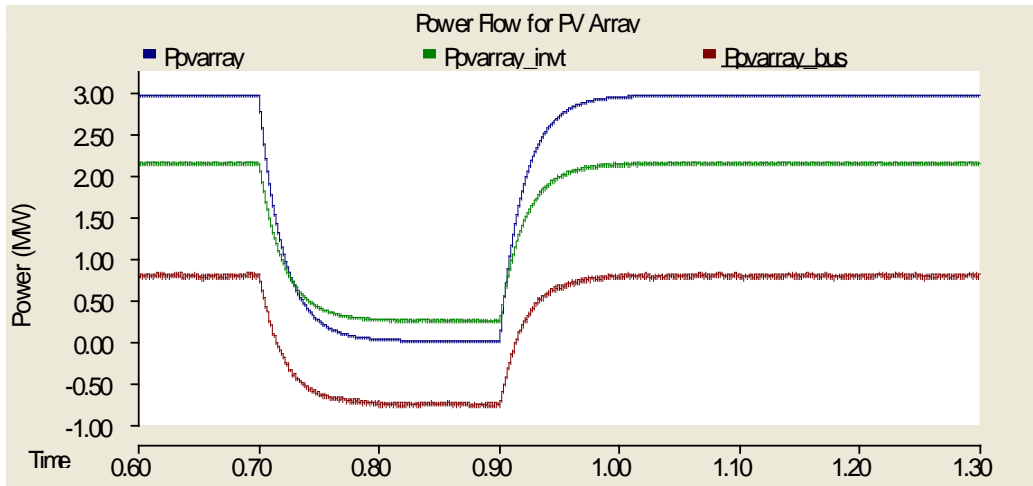


Figure 4.32. Power flow of PV array during PV fault (MVAC)

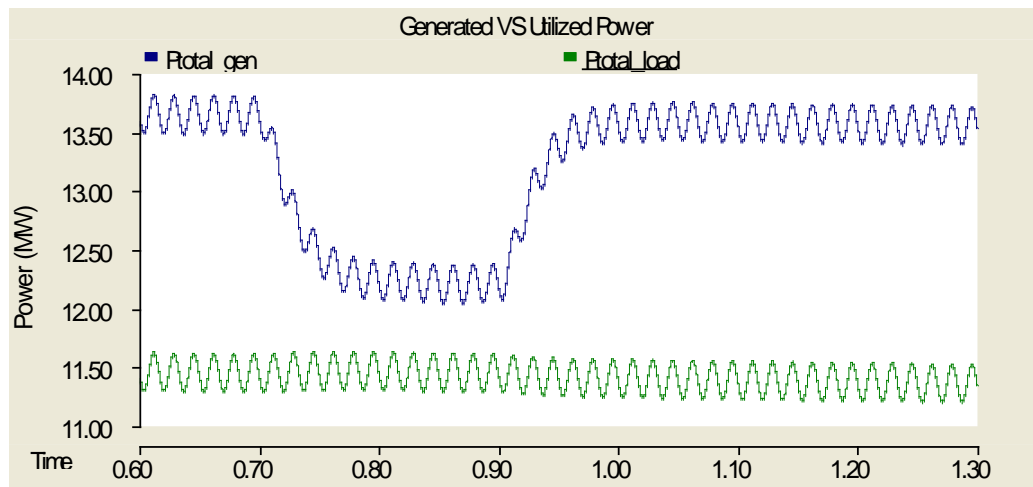


Figure 4.33. Total generation and load consumption during PV fault (MVAC)

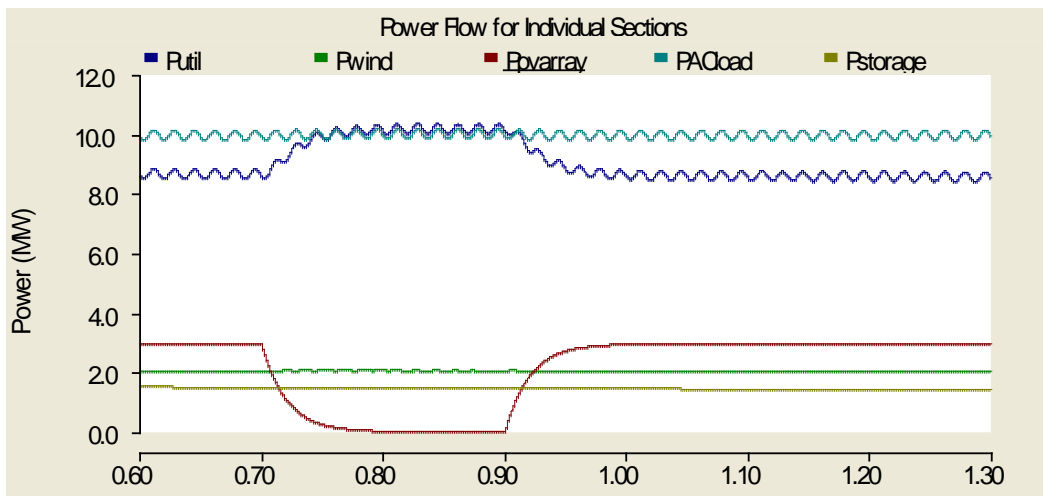


Figure 4.34. Power flow of each element during the PV fault (MVAC)

4.3.1.3 Wind Fault – MVDC System

The loss of the wind generation in the MVDC system causes a small oscillation on the main DC bus. This fluctuation in voltage has a direct effect on the AC load as well as the capacitors on the DC/DC converters that are connected to the bus. Following the voltage in Figure 4.35, when the wind was lost, the voltage saw a dip and was recovered by the utility source. However, as mentioned, the capacitors on the filters of the converters also saw a fluctuation and therefore the utility had to make up for not only the power that was being supplied by the wind generation but also account for power oscillations from the capacitors (Figure 4.38). The system was again able to reach a steady-state rapidly as depicted in Figure 4.37.

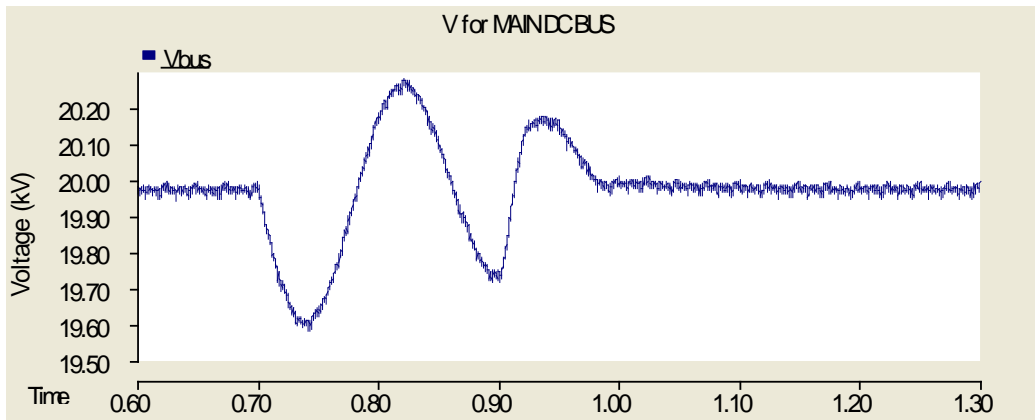


Figure 4.35. DC bus voltage during wind fault (MVDC)

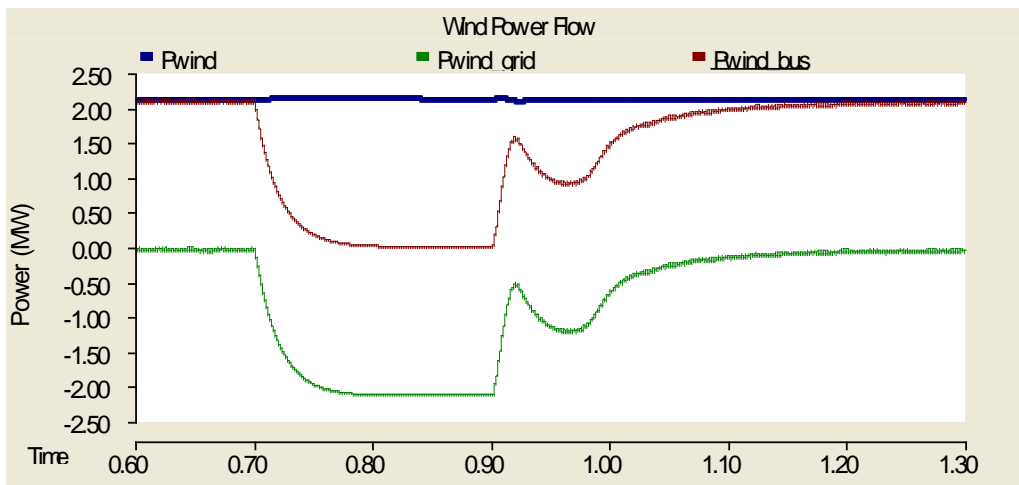


Figure 4.36. Power flow of wind source during wind fault (MVDC)

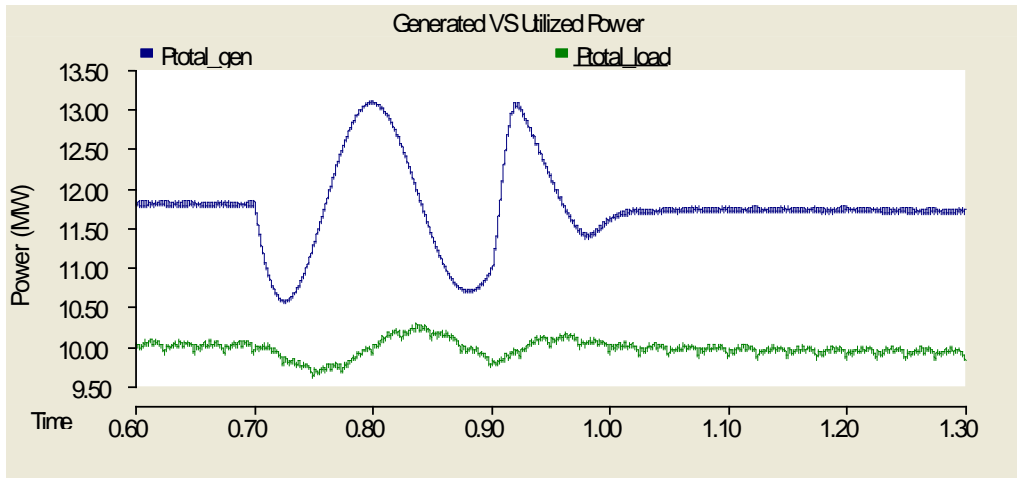


Figure 4.37. Total generation and load consumption during the wind fault (MVDC)

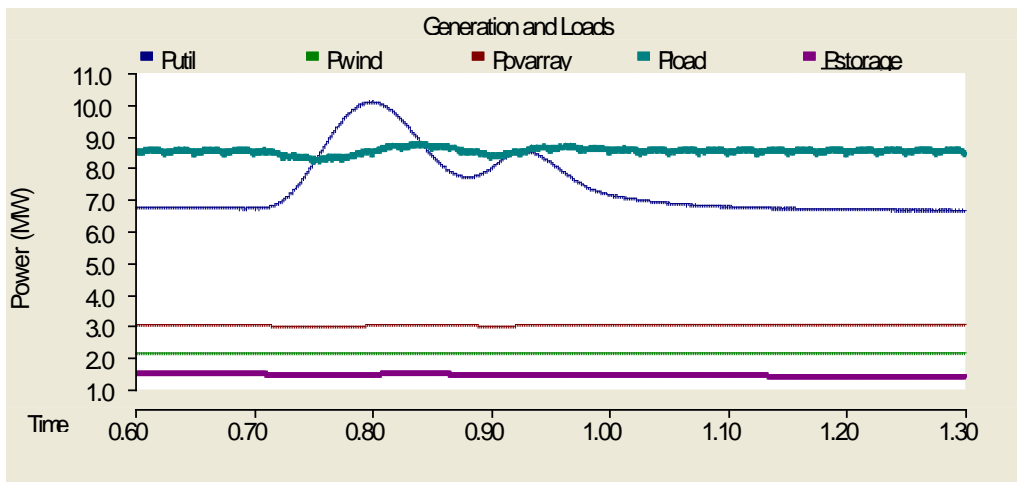


Figure 4.38. Individual power flows during wind fault (MVDC)

4.3.1.4 Wind Fault – MVAC System

The voltage on the AC bus remains solid throughout the entirety of the wind fault, seen in Figure 4.39, which can be attributed to the dominance of the utility source to withstand changes to the renewable generation sources. The curves in Figure 4.40 represent the generation coming from the induction machine, "Pwind", and the actual power being sent to the bus, "Pwind_bus". The "Pwind_bus" curve represents a more accurate curve for analysis of effects to the system. This curve first went to zero, as expected, and when the fault was cleared, a small transient occurred.

This transient was created because the induction machine went from seeing the loads on the system, to the "grid" (voltage source in Figure 3.23) attached to it, which has very little resistance, and finally back to seeing the system loads again. The effect this change in loads had on the machine can be seen from the electrical torque presented in Figure 4.41. As a conclusion once more, the utility compensated by providing power to the loads that was lost from the wind source since the PV was producing its maximum power. Other than the transient effect on the electrical torque of the induction machine, no other noteworthy electrical transients occurred on the system.

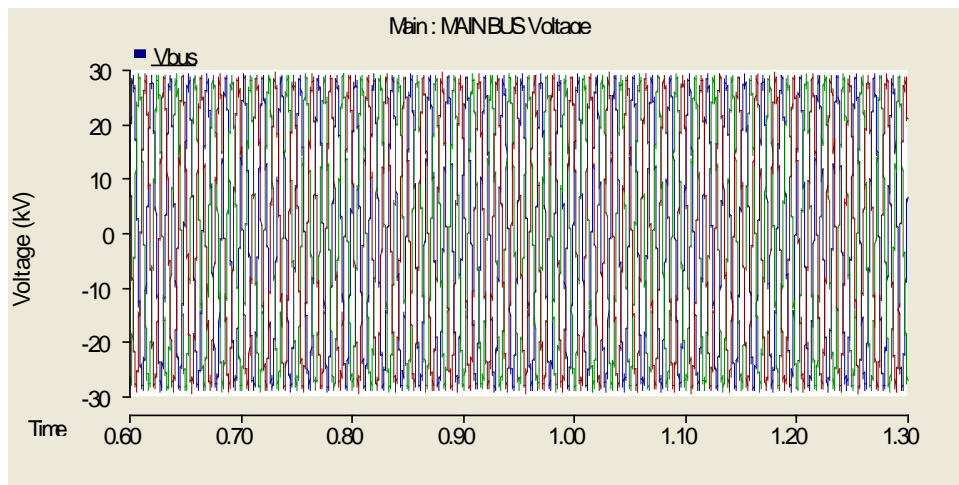


Figure 4.39. AC bus voltage during wind fault (MVAC)

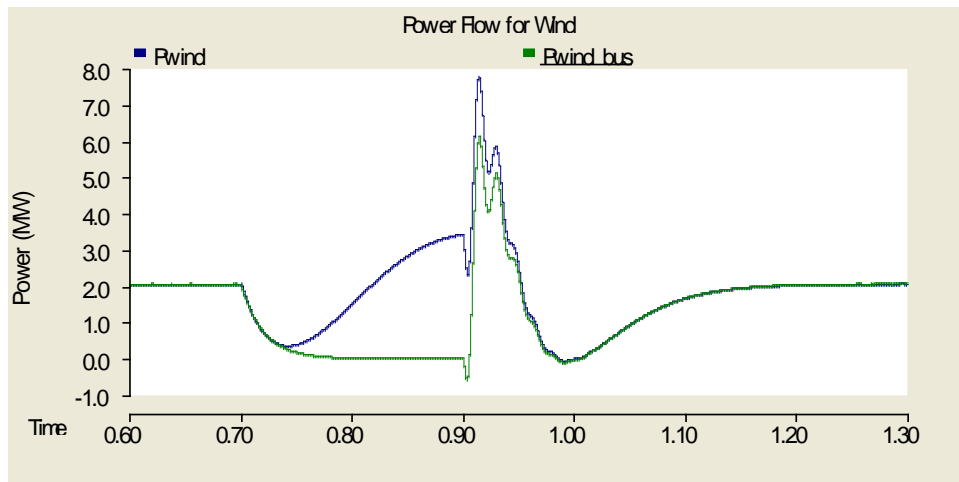


Figure 4.40. Power flow of the wind generation during wind fault (MVAC)

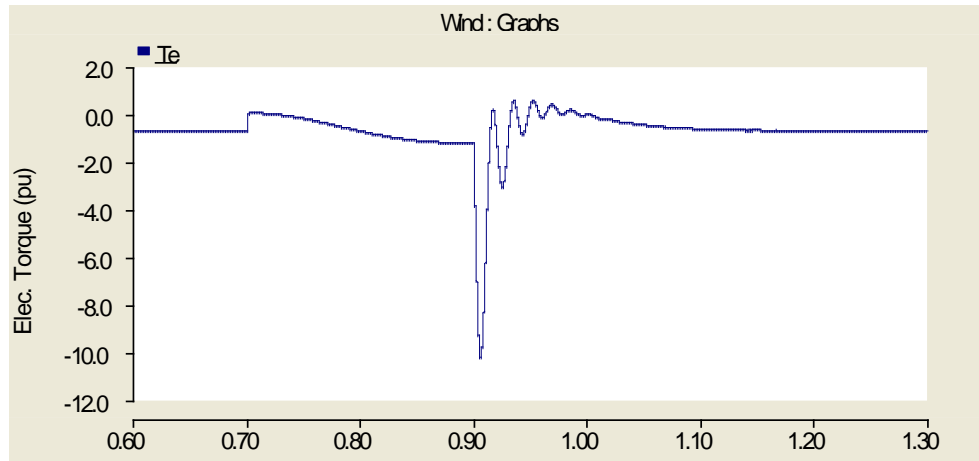


Figure 4.41. Electrical torque of the wind induction machine during wind fault (MVAC)

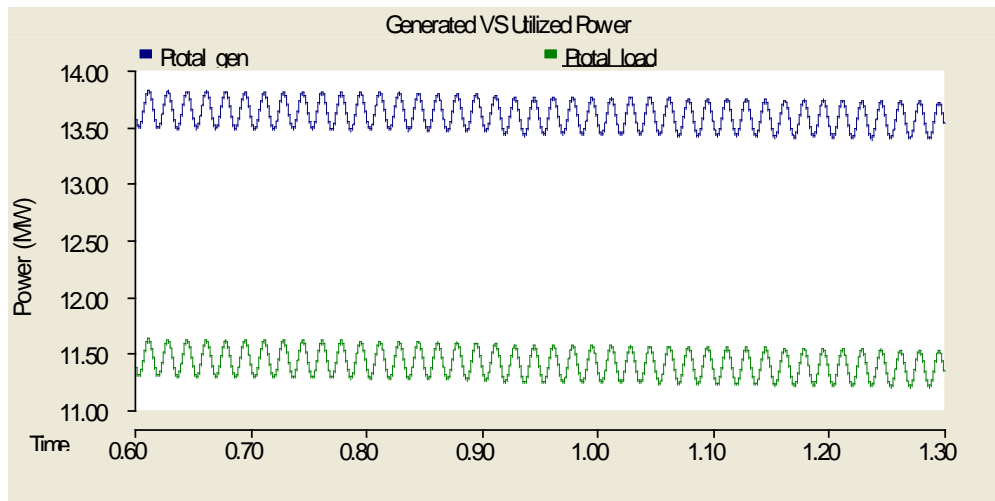


Figure 4.42. Total generation and power consumption during wind fault (MVAC)

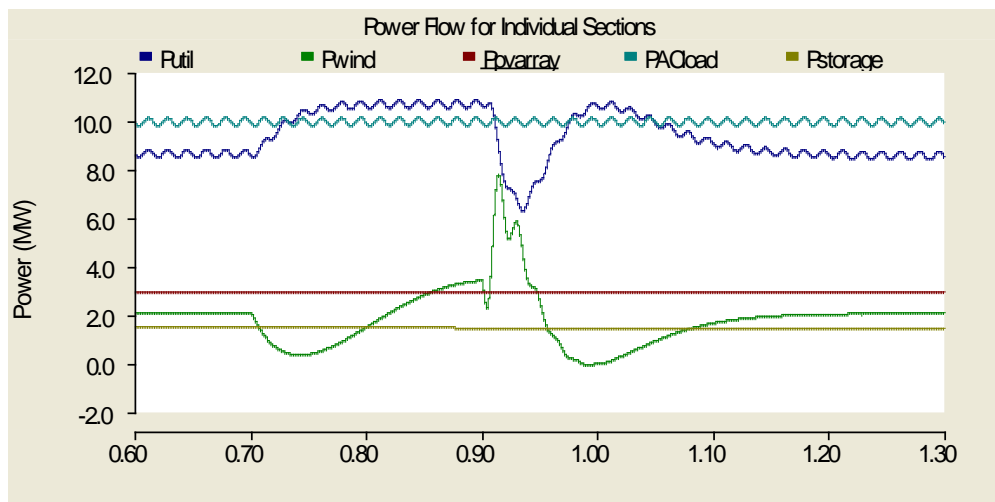


Figure 4.43. Individual power flows during wind fault (MVAC)

4.3.1.5 Utility Fault – MVDC System

Since the utility was the strongest source of generation, so to speak, the most drastic effects were caused when it was lost. With that said, the reaction of the system to the loss of the utility generation was still nothing substantial, as seen in Figure 4.47. The main DC bus voltage dropped about 500V, as seen in Figure 4.44, when the utility was taken out at 0.7s. The power flow from the utility source is depicted in Figure 4.45. The loss of the generation was compensated for by the "grid" connection on the induction machine of the wind generation, shown by the increase of power delivered in Figure 4.46 and Figure 4.48. The "grid" connection essentially represents another utility source capable of supplying any amount of power requested from it and therefore was not surprising to see that compensation occur. Since the wind and PV array were supplying their rated power output, the only source left to provide power was the "grid" source.

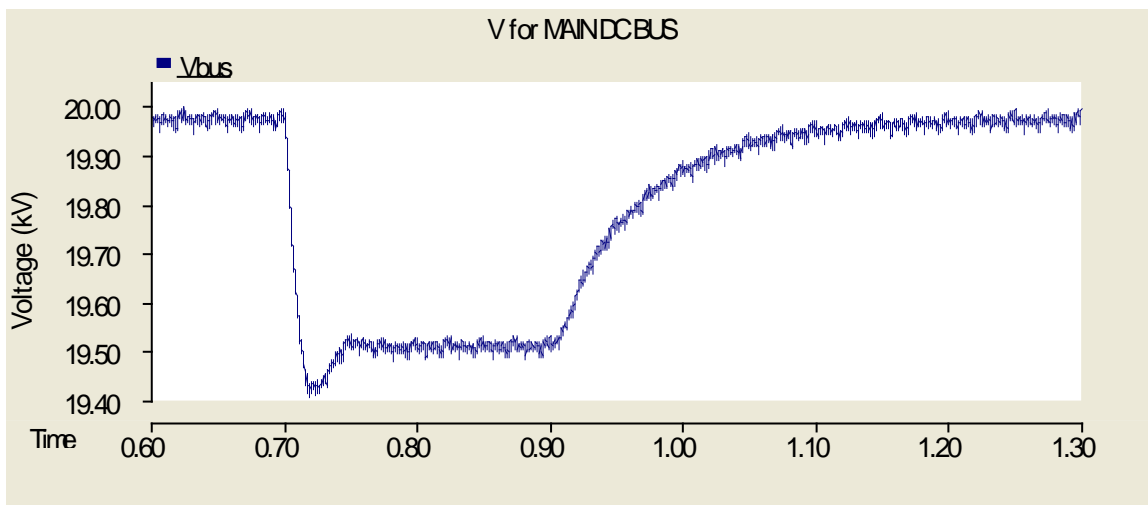


Figure 4.44. DC bus voltage and current during utility fault (MVDC)

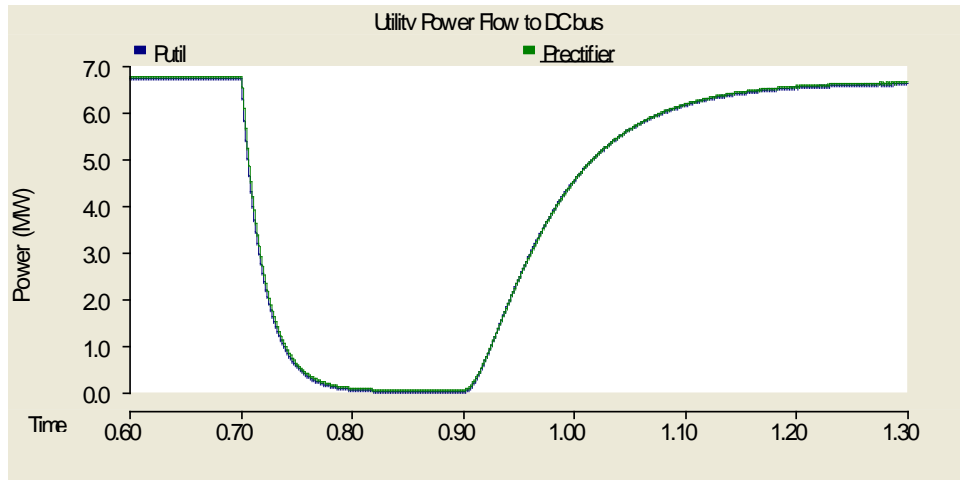


Figure 4.45. Utility power flow during utility power fault (MVDC)

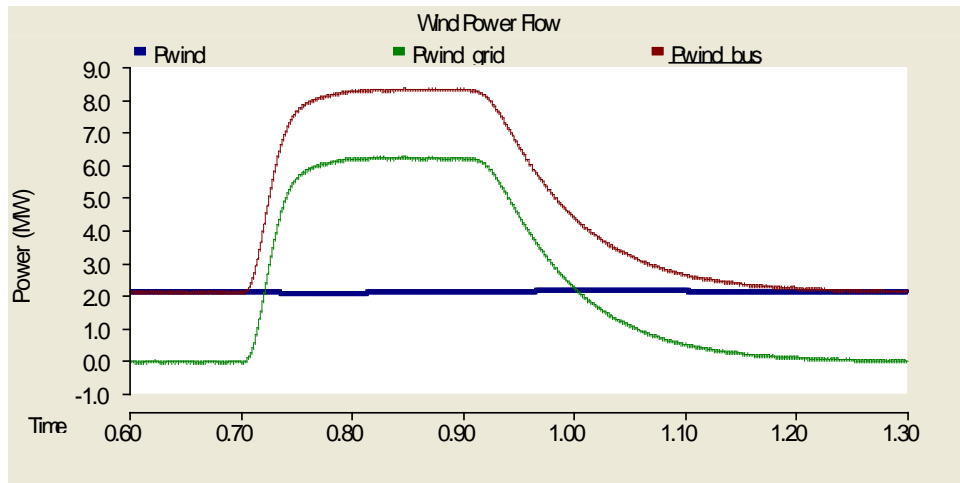


Figure 4.46. Wind power flow during utility fault (MVDC)

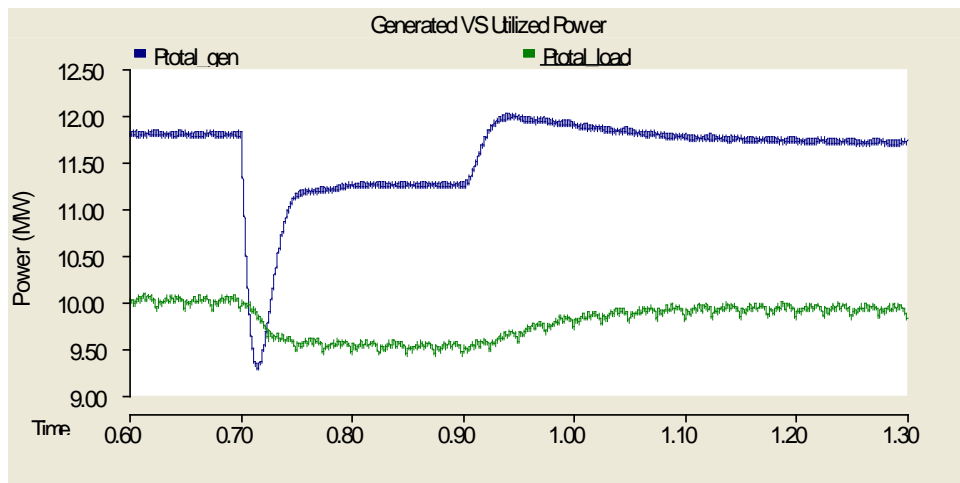


Figure 4.47. Total generation and power consumption during utility fault (MVDC)

The drop in main bus voltage results in the AC load being delivered less power than desired, shown in Figure 4.48, due to its dependence on the voltage that appears across the load. This demonstrates the importance of an intelligent control system to maintain the voltage being generated at the output of the inverter to insure delivery of power to the loads so they may operate properly.

As with the other generation losses analyzed so far, the only transient present was the drop of power from the utility and the corresponding voltage drop on the grid, which initiated the "grid" connection to provide more power to compensate for the lost generation.

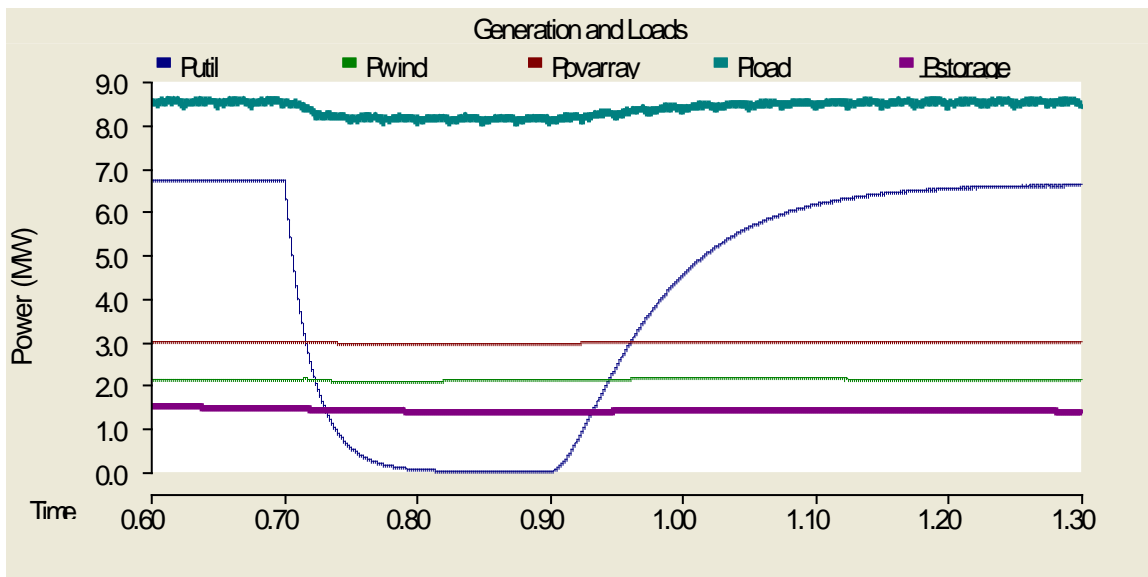


Figure 4.48. Individual power flows for the system during utility fault (MVDC)

4.3.1.6 Utility Fault – MVAC System

When the utility was lost in the MVAC system, the main effect on the system was an increase in bus voltage, shown in Figure 4.49, because the "grid" voltage source of the wind compensated for the loss of generation, as it did in the case for the MVDC system. Since the transformer connecting the wind generation to the bus was based on ideal situations, the small voltage

increase was a result of the "grid" source not being exactly 575V. The bus voltage again had a direct effect on the AC load. The load is dependent on the voltage that appears on the bus and therefore consumed less power during the fault than it did during steady-state, as depicted in Figure 4.50. The compensation from the "grid" of the wind generation and how it coincided with the loss of the utility source can be seen in Figure 4.51. The system was easily able to return to a steady-state despite the disturbance.

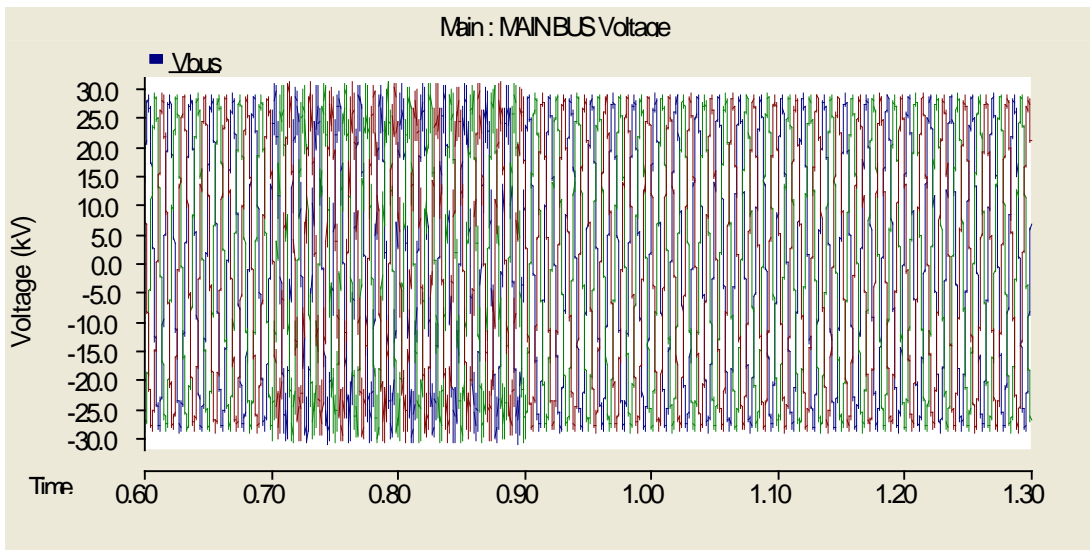


Figure 4.49. AC bus voltage during utility fault (MVAC)

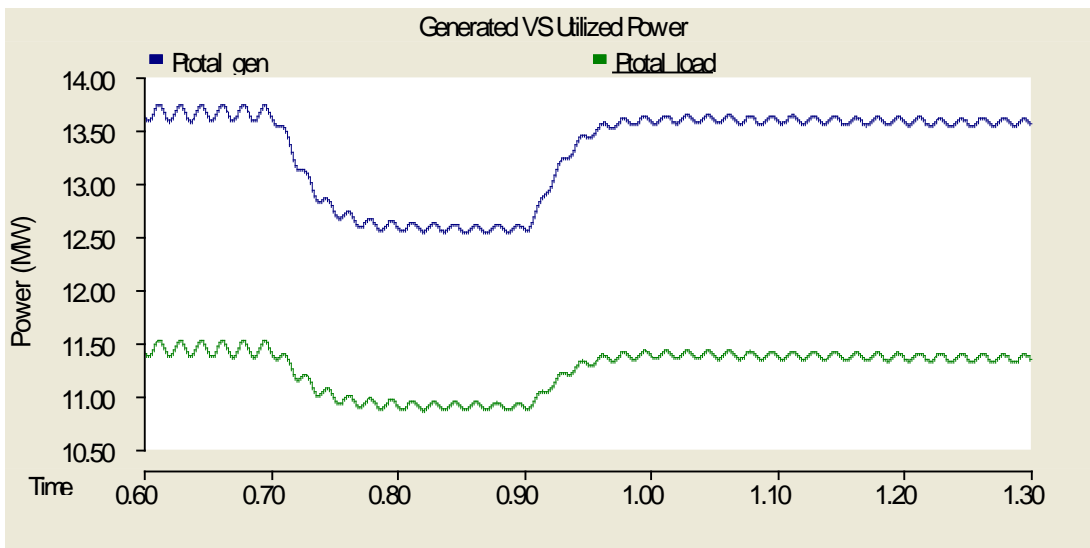


Figure 4.50. Total power generated and consumed during utility fault (MVAC)

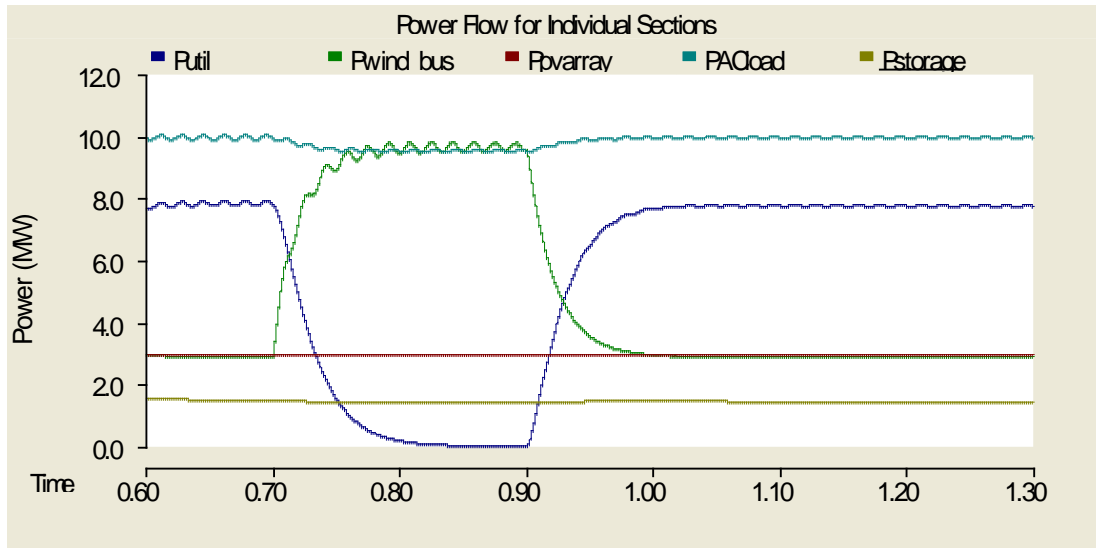


Figure 4.51. Individual power flows during utility fault (MVAC)

4.3.2 Load Faults

A fault was applied to each of the two loads connected to the main bus. These load faults were performed in order to observe how the two infrastructures reacted and also to identify weaknesses in the control systems and converter topologies chosen. For the three-phase AC load, a simple line-to-ground fault on Phase A was applied for 0.2s on both systems. The storage load received a fault by shorting the outputs of the DC/DC converter to ground using a 0.001Ω resistor also for 0.2s. The respective system was then run until it reached a new steady-state.

Despite the lack of feedback control in the model, half of a cycle ($833\mu\text{s}$) after the fault on the DC storage load was applied, the converter connecting the load to the bus isolated the fault by opening all of the switching devices contained within it, in the case on the MVDC system with the DC/DC converter. For the MVAC system, a circuit breaker was used to isolate the fault from the rest of the system. This simulates a primitive yet effective way to control the large amount of current that would begin to flow during the 0.2s fault duration, resulting in a

significant power spike through the system. This large amount of power would be unrealistic in a real system and so this protection scheme was implemented in order to have a better representation of a real fault and protection measures.

4.3.2.1 AC Load Fault – MVDC System

During the AC load fault on the MVDC system, the voltage on the bus saw an initial drop and then slowly began to recover as the power from the utility began to rise and accommodate the increased demand from the fault. Since both the PV array and wind were already at their maximum power output, it makes sense that the utility provided the extra power for the fault. Once the fault was cleared at 0.9s, the voltage rose by 1kV and then settled to a steady-state 0.1s later. This voltage jump was likely due to the load changing quickly and the inductor on the filter of the rectifier for the utility system not allowing an abrupt change in the current on the bus. The data for the voltage is shown in Figure 4.52 and the power flows in Figure 4.53 and Figure 4.54.

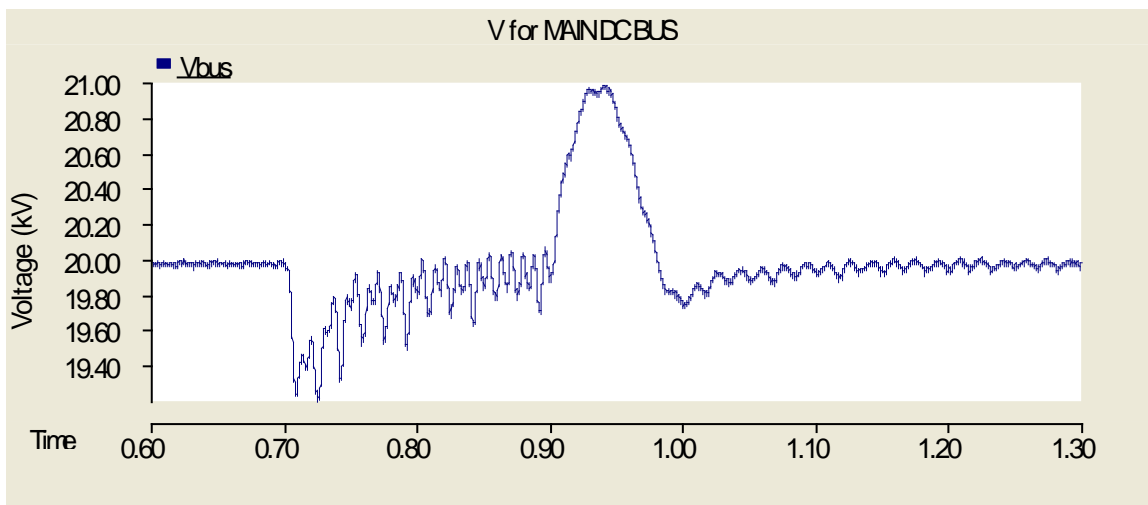


Figure 4.52. Bus voltage during the AC load fault (MVDC)

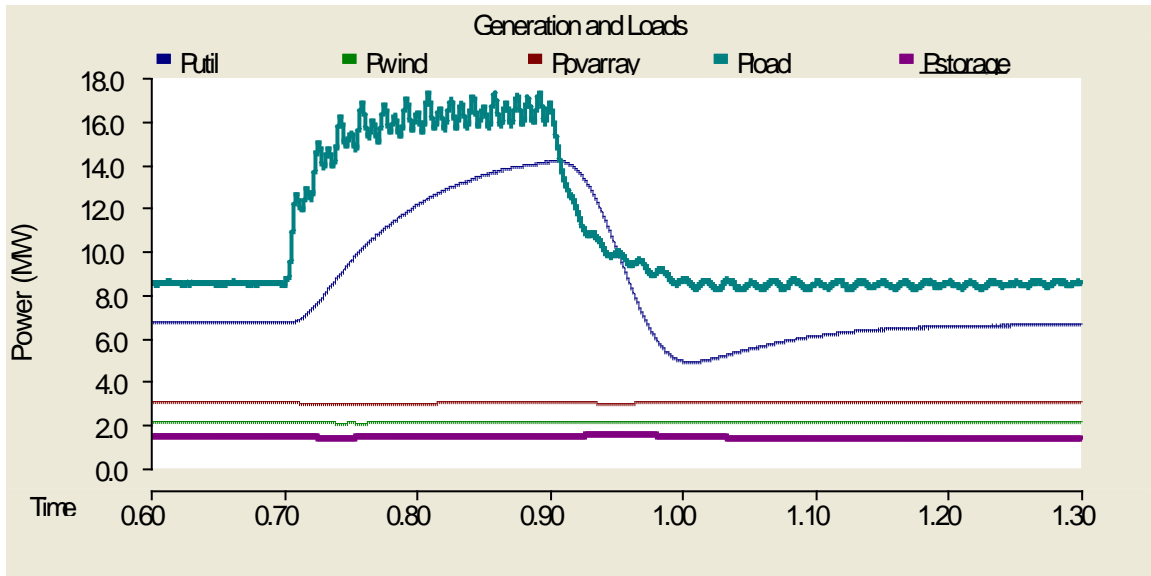


Figure 4.53. Individual power flows during AC load fault (MVDC)

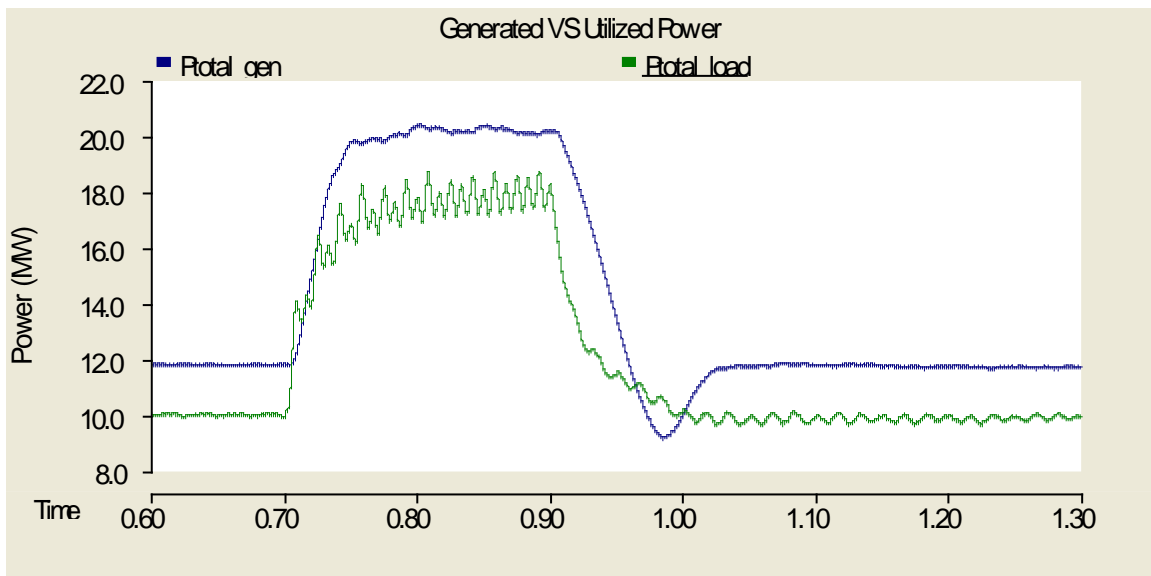


Figure 4.54. Total power generation and consumption during AC load fault (MVDC)

4.3.2.2 AC Load Fault – MVAC System

As can be seen in Figure 4.55, only the voltage on phase A, where the fault occurred, was affected between 0.7s and 0.9s. The utility initially changes drastically to meet the new power demand and then slowly decreases to match the power demand of the AC load. When the fault

was cleared, the system quickly went back to steady-state 0.1s later when the load and utility smoothly decreased to their original levels seen in Figure 4.56. A total of system power flow for the loads and generation can be seen in Figure 4.57.

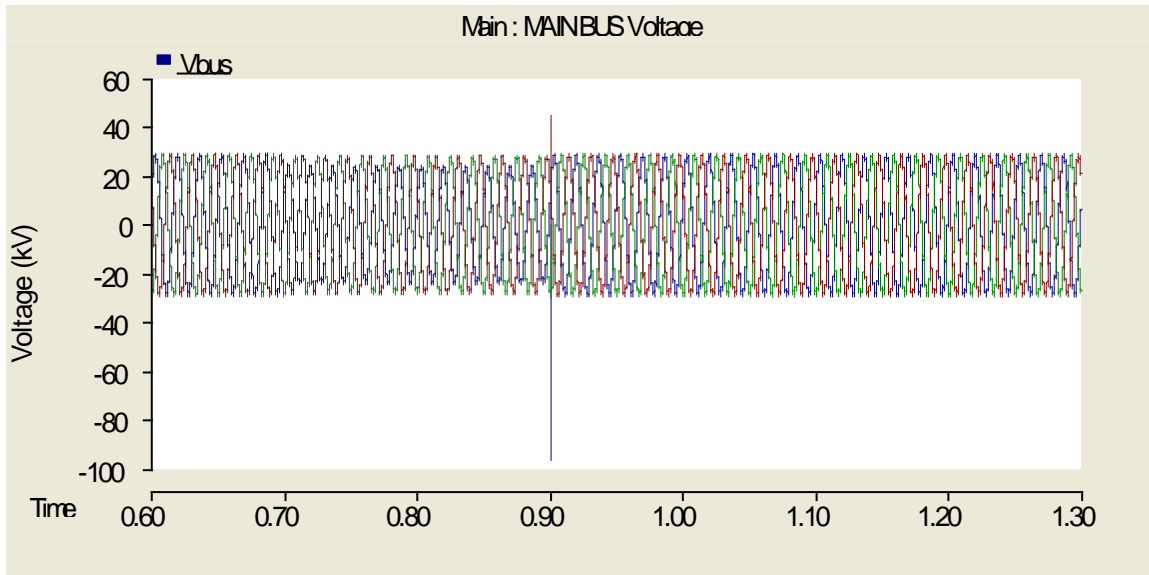


Figure 4.55. Voltage on the bus during the AC load fault (MVAC)

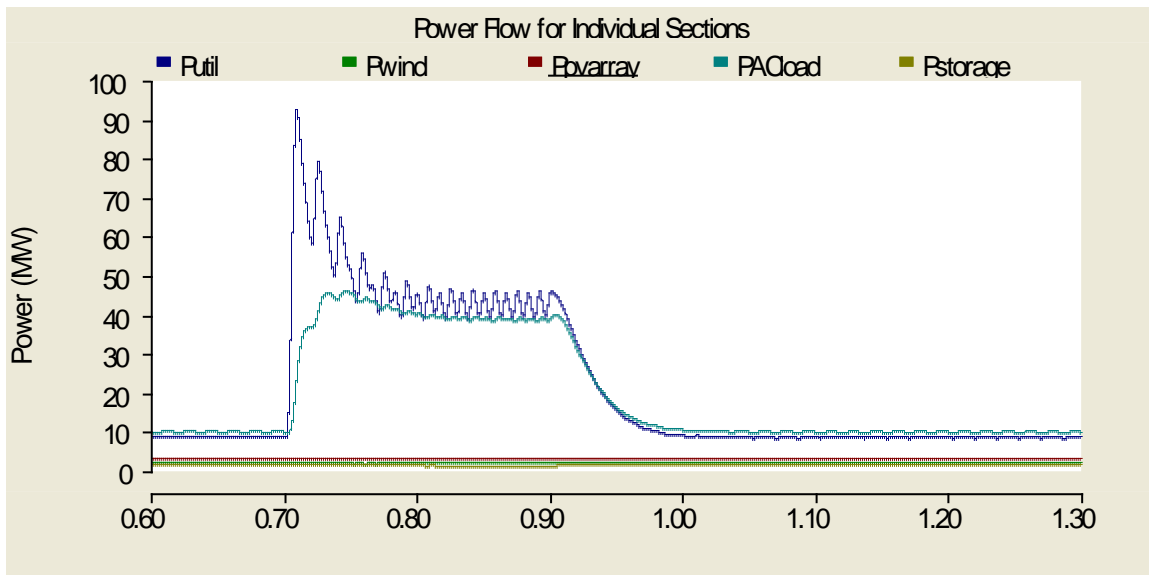


Figure 4.56. Individual power flows during the AC load fault (MVAC)

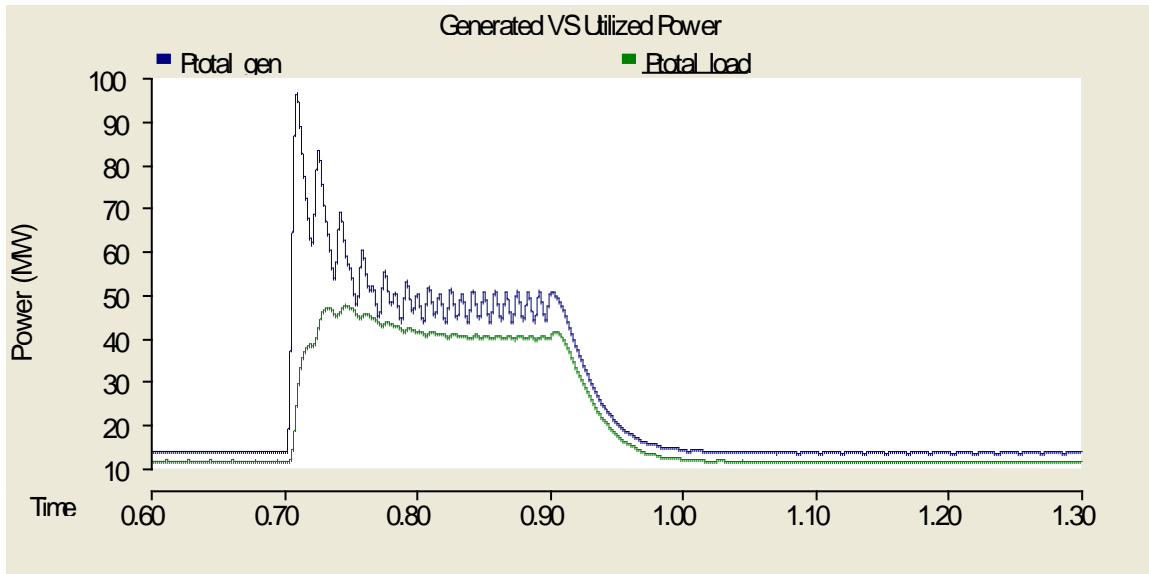


Figure 4.57. Total power generation and consumption during AC load fault (MVAC)

4.3.2.3 Storage Load Fault – MVDC System

The voltage on the bus during the storage load fault experienced an almost 75% drop from its steady-state value per Figure 4.58. After the fault was isolated by the converter at 0.7083s, the voltage began to quickly recover. An overshoot occurred before the system ultimately arrived close to its original steady-state value. When the load was connected back to the grid at 0.9s, only a very small voltage disturbance was seen on the bus.

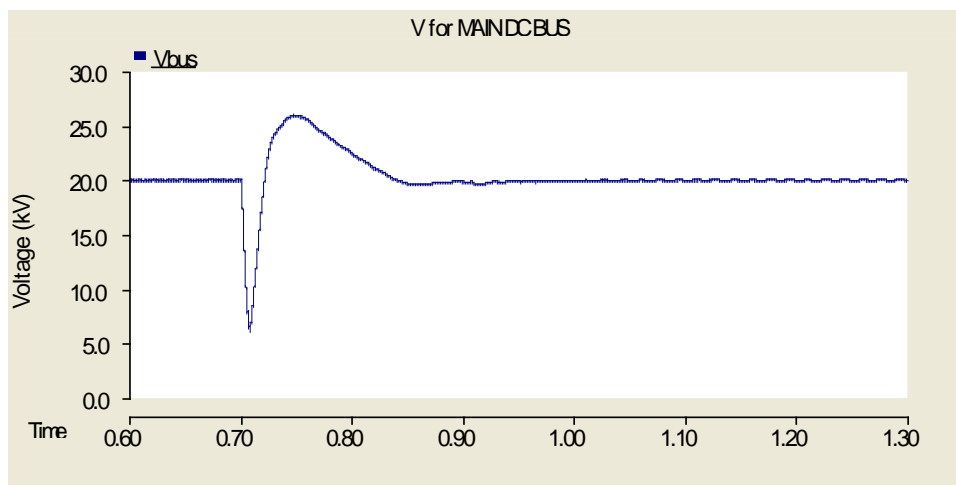


Figure 4.58. Voltage on the bus during the storage load fault (MVDC)

For a short period, the power through the system begins to increase because of the smaller resistance and larger power demand caused by the fault as seen in Figure 4.60. After the fault was isolated, the power decreased rapidly to compensate for the change again. The system finally reaches close to its original steady-state for each load and generation source with the exception of the power being delivered to the AC load ("Pload" on Figure 4.59). The ripple seen on the AC load was a result of the capacitors at the input of the DCMLI becoming unbalanced. The control system was not able to correctly rebalance the voltages with the algorithm utilized.

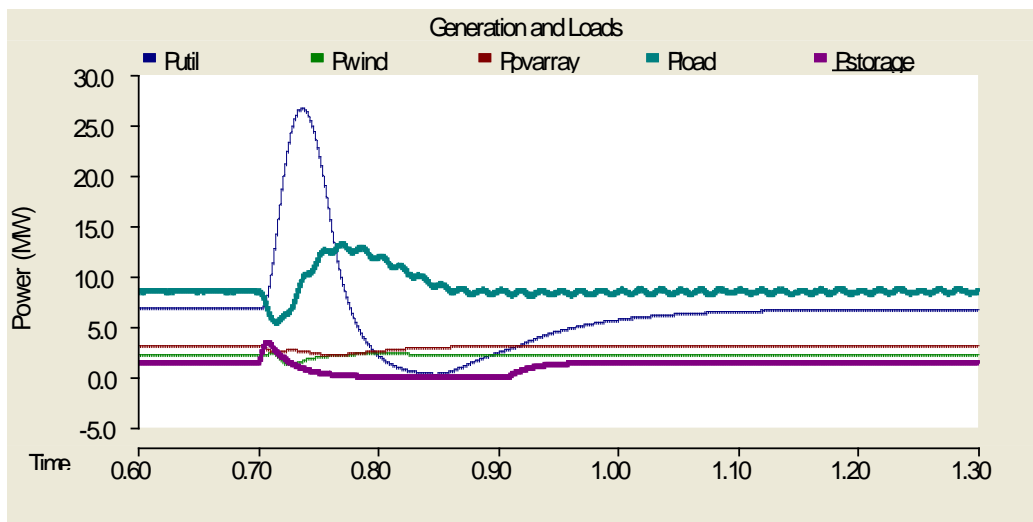


Figure 4.59. Individual power flows during storage load fault (MVDC)

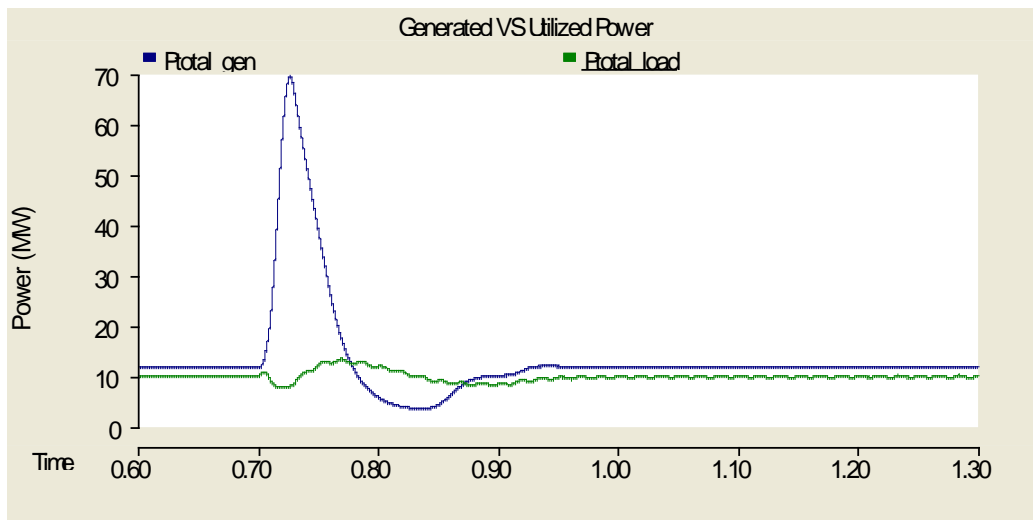


Figure 4.60. Total power generated and consumed during storage load fault (MVDC)

4.3.2.4 Storage Load Fault – MVAC System

In the case of the storage fault on the MVAC system, the voltage on the bus was unaffected throughout the whole duration of the fault as illustrated in Figure 4.61. As with the MVDC case, the fault was isolated from the rest of the system at the power converter. The power converter in this simulation used diodes but a very similar output could have been created using semiconductor switches with an appropriate control scheme. With this in mind, the fault was cleared by use of a circuit breaker at the converter output to simulate the fault being isolated by opening all the semiconductor switches. This action prevented large power spikes that would not as closely reflect a real system. Depicted in Figure 4.62, the utility lowered its total power output in order to compensate for the decrease in the total load when the fault was applied at 0.7s. The opposite then occurred where the utility ramped back to its previous value to account for the original load value being connected again to the system.

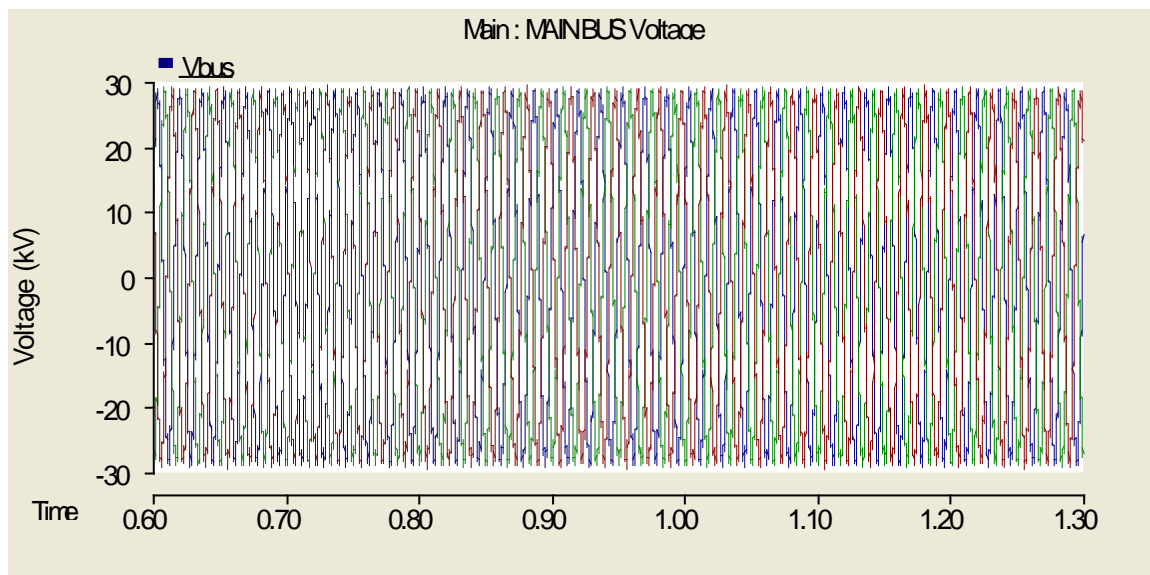


Figure 4.61. Voltage on the bus during storage load fault (MVAC)

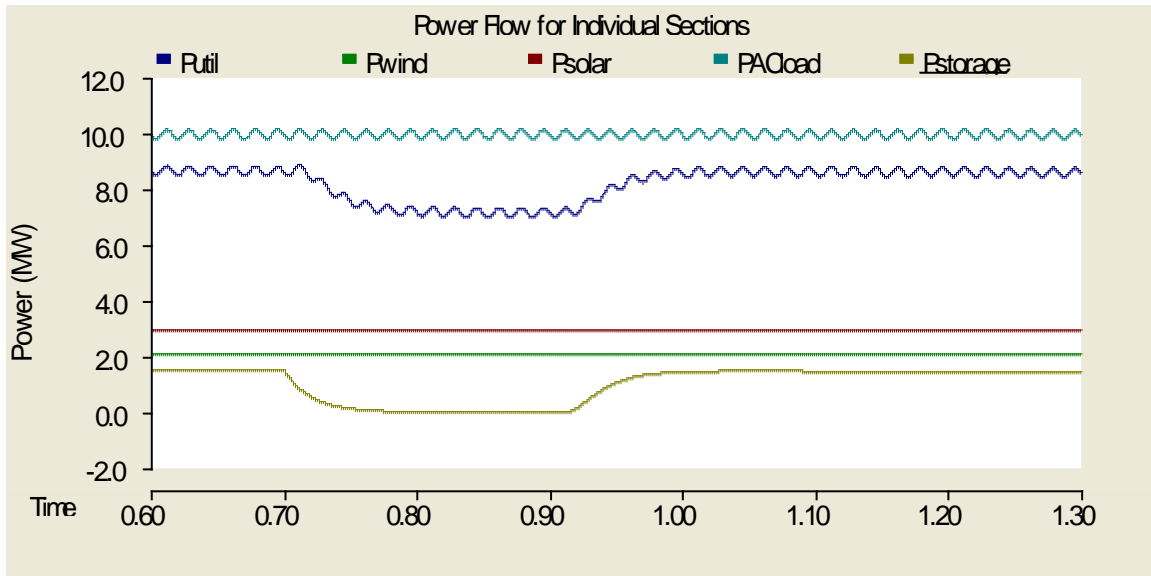


Figure 4.62. Individual power flows during storage load fault (MVAC)

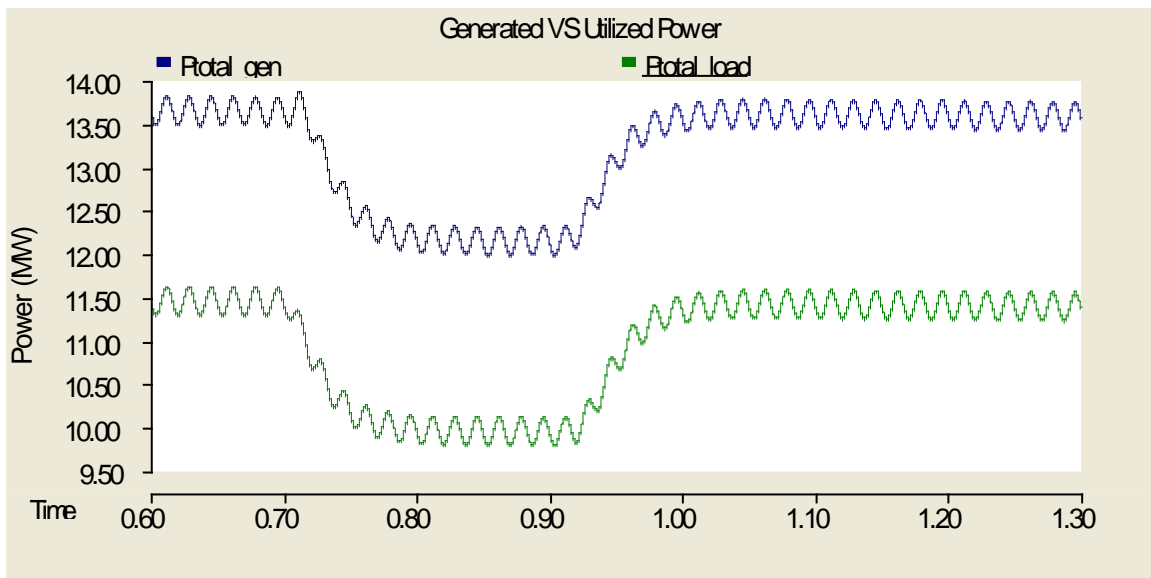


Figure 4.63. Total power generated and consumed during storage load fault (MVAC)

5.0 CONCLUSIONS

An increasing amount of consumer devices and end-use applications of electricity at the low voltage level that require a direct current (DC) power source have continued to advance in modern day society. At the same time the existing alternating current (AC) infrastructure that has served so well over the past century is beginning to show its age and vulnerability, leading to increased outages and reduced reliability. However, with the widespread development and maturation in recent years of low voltage DC devices and systems, as well as large scale HVDC systems, no DC-based infrastructure or delivery system exists to efficiently connect the two together. Such an infrastructure would be developed through a medium voltage DC (MVDC) architecture. In order to properly analyze the benefits of a MVDC infrastructure for power distribution networks, a comparison between MVDC and MVAC architectures is necessary, which would identify advantages and disadvantages of both approaches.

The MVDC and MVAC infrastructure models were constructed using the PSCAD software package, due to its transient capabilities and freedom to create larger models with smaller components, such as semiconductor switches, produce model transients of entire systems. Each medium voltage model system was constructed to be as similar as possible, with the exception that one was AC and the other was DC. The systems were chosen in such a way that at least one DC/DC converter, DC/AC inverter, and AC/DC rectifier were used. A series of faults were applied to determine how the converters, and especially the main bus, reacted to the

disturbances. The types of faults fell into two categories – 1) loss of generation and 2) load faults. The key measurements made were the voltage on the main bus for either system, as well as power flows to and from each generation source and load entity.

Before discussing the overall results from the fault tests, a few notes will be made about the components required for either system to operate properly. The MVAC system was much more simplistic in its design consisting largely of transformers to adjust AC voltage levels. The conversions were made knowing in advance what the voltage levels should be on the input and output of the different power converters. As realistic of an approach as possible was taken to insure credibility of the system, and, as a result, a transformer was utilized whenever an AC/AC conversion was necessary. The biggest challenge arose in connecting the PV array to the bus, since it produces power in DC versus the wind and utility, which used AC. A large loss was incurred during conversion from DC to the proper AC voltage level. In all other cases, the transitions were rather seamless involving only a transformer and, for the DC storage load an additional rectifier circuit. Since the rectifier chosen was composed of diodes rather than semiconductor switches, the conversion was similar in nature to the transformer. That is, it was passive and required no external control scheme to operate properly. This rectifier can easily be altered to incorporate switches rather than diodes and therefore a form of control may be introduced for voltage level control. The disadvantage to the overall simplistic, passive design and utilization of many transformers is that whatever large swings occurred on the bus translated directly to the loads and resulted in undesirable transients. The loads either received too much power or too little power and, without an external control scheme in place to control the voltage levels present throughout the system, it would be necessary to introduce more equipment than used in this initial MVAC design to function in an acceptable manner during faults.

In contrast, the MVDC infrastructure had a minimum requirement of using different dynamic power electronic conversion circuitry to carry out changes from DC to DC and from DC to AC. The compromise was the potential to have a fine tune control on power flow and voltage levels for every branch of the system. All of the connections made to and from the main DC bus were via power converters in the MVDC system. As an aside, this would also mean that any AC frequency signal could be connected to the MVDC bus. The same equipment currently implemented in the MVDC system would not need to be changed but only the control scheme used. The control algorithms necessary would further add to the complexity of the converters and the system as a whole.

The generation fault tests performed on the systems provided further insight to what the advantages and disadvantages were between the two approaches. Both the MVAC and MVDC systems showed an expected, favorable response to the loss of the PV array generation. The bus voltage for both systems dipped to a lower value when the utility connection was lost, but due to the extra "grid" connection on the wind generation a balance was maintained in the power flow to the loads. The chance that both the utility and "grid" connections would be lost simultaneously is somewhat improbably, and therefore was not investigated. During the loss of the wind generation, the MVDC bus experienced a short oscillatory response to the bus voltage, while the MVAC was unaffected. This small oscillation in the DC bus voltage was deemed to be based on the different filtering capacitors on the converters, as well as the reconnection of the induction machine to the system.

A similar response was seen in both systems during the two different load faults. The infrastructures recovered well during the line-to-ground fault placed on the AC load with little difficulty. However, the fault on the DC storage load would have resulted in a large spike in

power flow on both systems had a protection scheme not been implemented. In reality, this control scheme may have reacted to disturbances caused by the other faults but since most of the faults caused only minor changes to the system, the protection was utilized in only the DC storage load fault. Again, the protection scheme prevented a large, unrealistic power flow from occurring to better represent a real-world implementation of the MVDC and MVAC systems.

With the fault tests performed on both systems, an advantage of one system over the other cannot be determined easily, especially at this early stage of development. A proper control and protection system must be implemented in order to obtain more meaningful results to make a direct comparison. The MVAC and MVDC systems experienced similar alterations in power flow during faults and these responses can be improved with more advanced control and protection devices in place. Overall, it appears that there are specific advantages and disadvantages to each system approach for different electrical situations. Further development is necessary to gather more relevant data and to continue deeper investigations into the MVDC architecture.

6.0 FUTURE WORK

As discussed previously in the “Conclusions” section, a main focus toward future development of both models will be to implement a more robust control strategy used in the power electronic converters, as well as to integrate protection schemes and equipment to increase the dynamic response and realistic representation of the systems. The existing models for converters will be developed to be non-ideal and account for a wider range of losses and other inefficiencies. The storage load model will be made to function in a bidirectional manner and will consist of a much more accurate implementation than what is currently in place. Naturally, more loads and generation sources will be added on to the main bus of the structures, including a HVDC link, data center facility, and other forms of power plants such as fossil and nuclear.

The control will also be expanded to include a central controller that will govern over power flow for each branch of the system. This central control system will interact directly with the lower level, individual based control implemented for each of the converters. The objective would be to extract as much power from the renewable generation as possible, while only calling upon the rest of the grid to compensate for the remaining power needed.

A long term goal will be to ultimately connect the developed MVDC and MVAC systems to a more realistic grid representation. This would include machine generators in place of ideal voltage sources and loads that are external to the medium voltage infrastructure itself. A fault

occurring on the grid may have direct effects upon the medium voltage systems, and tests can be performed on the protection schemes and control algorithms for the entire system.

Future areas of development for the MVDC and MVAC models include:

- Increased complexity of source and load models
- More diversity in generation and load types
- Dynamic control for each converter, as well as a robust communication between them to control power flows
- Implementation of protection equipment and protection schemes, also making use of the isolation capabilities of the converters
- Take into account the economics and footprint for each system

APPENDIX A

MATLAB SCRIPT FOR PHOTOVOLTAIC V-I CURVE

```
%% PV Array Calculation

q = 1.6022e-19;
k = 1.3807e-23;
Tc = 25+273;           % In Kelvin

Rs = 0.138;
Rsh = 86.85;
Ns_base = 36;
Ns = 1;
Np = 1;
A = 1.37;

Isc = 8.0;
Voc = 21.7*Ns;

I = 0;
V = 0;
Irs = Isc/(exp(q*Voc/(A*Ns_base*Ns*k*Tc))-1);

Vsave = 0;
Isave = 0;
Rsave = 0;
i = 1;

for V=0:0.005:Voc

    I = Np*Isc - Np*Irs*(exp(q*(V+I*Rs*Ns/Np)/(Ns_base*Ns*A*k*Tc))-1) -
    (V+I*Rs*Ns/Np)/(Rsh*(Ns/Np));

    if I < 0
        I = 0;
    end

    Vsave(i) = V;
```

```
    Isave(i) = I;  
  
    i = i + 1;  
end  
allsave = [Vsave;Isave];  
  
P = (Vsave.*Isave);  
plot(Vsave,Isave)
```

BIBLIOGRAPHY

- [1] EPRI. "DC Power Production, Delivery and Utilization." *EPRI*. Web. <http://mydocs.epri.com/docs/CorporateDocuments/WhitePapers/EPRI_DCpower_June2006.pdf>.
- [2] Ericson, T., "The ship power electronic revolution: Issues and answers," *Petroleum and Chemical Industry Technical Conference, 2008. PCIC 2008. 55th IEEE*, vol., no., pp.1-11, 22-24 Sept. 2008
- [3] Woodford, Dennis, A., "Basic Principles of HVDC" *Manitoba HVDC Research Centre*. Web. <<https://psc.ad.com/resource/File/Library/BasisPrinciplesofHVDC.pdf>>.
- [4] Maxim. "Source Resistance: The Efficiency Killer in DC-DC Converter Circuits - Maxim." *Analog, Linear, and Mixed-signal Devices from Maxim/Dallas Semiconductor*. Web. <<http://www.maxim-ic.com/app-notes/index.mvp/id/3166>>.
- [5] EPRI. "Energy Efficiency Opportunities." *Power Supply Efficiency in Active Mode*. Web. <http://www.efficientpowersupplies.org/efficiency_opportunities.html>.
- [6] ABB. "What Is a Variable Frequency Drive (VFD)? How Does a VFD Work?" *Variable Frequency Drives, Variable Speed Drive Systems and Controls*. Web. <http://www.joliettech.com/what_is_a_variable_frequency_drive.htm>
- [7] Glover, J. Duncan., Mulukutla S. Sarma, and Thomas J. Overbye. *Power System Analysis and Design*. Australia: Thomson, 2008. Print.
- [8] Wu, Bin. *High-power Converters and AC Drives*. Hoboken, NJ: Wiley-Interscience, 2006. Print.
- [9] Kundur, P., Neal J. Balu, and Mark G. Lauby. *Power System Stability and Control*. New York: McGraw-Hill, 1994. Print.
- [10] Erickson, Robert W., and Dragan Maksimovic. *Fundamentals of Power Electronics*. Norwell, MA: Kluwer Academic, 2001. Print.

- [11] Il-Yop Chung; Wenxin Liu; Andrus, M.; Schoder, K.; Siyu Leng; Cartes, D.A.; Steurer, M., "Integration of a bi-directional dc-dc converter model into a large-scale system simulation of a shipboard MVDC power system," *Electric Ship Technologies Symposium, 2009. ESTS 2009. IEEE* , vol., no., pp.318-325, 20-22 April 2009
- [12] Severns, Rudolf P., and Gordon Bloom. *Modern DC-to-DC Switchmode Power Converter Circuits*. New York: Van Nostrand Reinhold, 1985. Print.
- [13] Rashid, M. H. *Power Electronics: Circuits, Devices, and Applications*. Upper Saddle River, NJ: Pearson/Prentice Hall, 2004. Print.
- [14] Mohan, Ned, William P. Robbins, and Tore M. Undeland. *Power Electronics: Converters, Applications, and Design*. Hoboken, NJ: Wiley, 2007. Print.
- [15] Newton, C.; Sumner, M., "Novel technique for maintaining balanced internal DC link voltages in diode clamped five-level inverters," *Electric Power Applications, IEE Proceedings -* , vol.146, no.3, pp.341-349, May 1999
- [16] Anderson, P.M.; Bose, A., "Stability Simulation Of Wind Turbine Systems," *Power Apparatus and Systems, IEEE Transactions on* , vol.PAS-102, no.12, pp.3791-3795, Dec. 1983
- [17] Manitoba HVDC Research Centre, *Equations adapted for wind turbine parameters for the wind turbine PSCAD simulation file*, Received upon request.
- [18] Campbell, R.C., "A Circuit-based Photovoltaic Array Model for Power System Studies," *Power Symposium, 2007. NAPS '07. 39th North American* , vol., no., pp.97-101, Sept. 30 2007-Oct. 2 2007
- [19] Phang, J.C.H.; Chan, D.S.H.; Phillips, J.R., "Accurate analytical method for the extraction of solar cell model parameters," *Electronics Letters* , vol.20, no.10, pp.406-408, May 10 1984
- [20] Gow, J.A.; Manning, C.D., "Development of a photovoltaic array model for use in power-electronics simulation studies," *Electric Power Applications, IEE Proceedings -* , vol.146, no.2, pp.193-200, Mar 1999
- [21] Tsai, Huan-Liang; Tu, Ci-Siang; Su, Yi-Jie, "Development of Generalized Photovoltaic Model Using MATLAB/SIMULINK," *Proceedings of the World Congress on Engineering and Computer Science 2008WCECS 2008 on*, October 22 - 24, 2008, San Francisco, USA, <<http://citeseerx.ist.psu.edu/viewdoc/download?doi=10.1.1.148.8225&rep=rep1&type=pdf>>
- [22] King, D. L., Boyson, W. E., & Kratochvil, J. A. (2004). *Photovoltaic Array Performance Model*. Received upon request from Sandia National Laboratories.
- [23] Sandia National Laboratories. *Sandia's Photovoltaic Research & Development Database*. Received upon request from Sandia National Laboratories.

- [24] Srikanthan, S.; Mishra, M.K., "DC Capacitor Voltage Equalization in Neutral Clamped Inverters for DSTATCOM Application," *Industrial Electronics, IEEE Transactions on* , vol.57, no.8, pp.2768-2775, Aug. 2010
- [25] PSCAD Software, *Ind. Generator driven by a wind turbine*, Accessed with file windfarm_indmac.psc, Example file packaged with software.
- [26] Chapman, Stephen J. *Electric Machinery Fundamentals*. New York, NY: McGraw-Hill Higher Education, 2005. Print.
- [27] General Electric. "2.5 MW Series Wind Turbine." *GE Energy*. Web. <http://www.gepower.com/prod_serv/products/wind_turbines/en/downloads/GEA17007A-Wind25Brochure.pdf>.